ANGIOGENIC GENE SIGNATURE IN HUMAN PANCREATIC CANCER CORRELATES WITH TGF-BETA AND INFLAMMATORY TRANSCRIPTOMES

Kelly E. Craven

Submitted to the faculty of the University Graduate School
in partial fulfillment of the requirements
for the degree
Doctor of Philosophy
in the Department of Biochemistry and Molecular Biology,
Indiana University

August 2016

Accepted by the Graduate Faculty, Indiana University, in partial fulfillment of the requirements for the degree of Doctor of Philosophy.

Doctoral Committee

Murray Korc, MD, Chair

Yunlong Liu, PhD

Amber L. Mosley, PhD

April 11, 2016

Lawrence A. Quilliam, PhD

Dedication

I dedicate this dissertation to my parents, Pat and Beth Gallagher, and to my husband, Andrew Craven, as without their continued love and support, this would not have been possible.

Acknowledgments

I want to thank my advisor, Murray Korc, and my committee, Yunlong Liu, Amber L. Mosley, and Lawrence A. Quilliam for their guidance and support during my graduate studies. I would like to thank Jesse Gore for his collaborative work on the mouse models and 3-dimensional (3D) cultures, as this story is more complete with that work included, and I would like to thank both Jesse Gore and Sudha Savant for their day to day guidance in the lab. Additionally, I would like to thank the National Cancer Institute of the National Institutes of Health for providing funding for this project under award number F30CA200301.

Kelly E. Craven

ANGIOGENIC GENE SIGNATURE IN HUMAN PANCREATIC CANCER CORRELATES WITH TGF-BETA AND INFLAMMATORY TRANSCRIPTOMES

Pancreatic ductal adenocarcinoma (PDAC), which comprises 85% of pancreatic cancers, is the 4th leading cause of cancer death in the United States with a 5-year survival rate of 8%. While human PDACs (hPDACs) are hypovascular, they also overexpress a number of angiogenic growth factors and receptors. Additionally, the use of anti-angiogenic agents in murine models of PDAC leads to reduced tumor volume, tumor spread, and microvessel density (MVD), and improved survival. Nonetheless, clinical trials using anti-angiogenic therapy have been overwhelmingly unsuccessful in hPDAC. On the other hand, pancreatic neuroendocrine tumors (PNETs) account for only 2% of pancreatic tumors, yet they are very vascular and classically angiogenic, respond to anti-angiogenic therapy, and confer a better prognosis than PDAC even in the metastatic setting.

In an effort to compare and contrast the angiogenic transcriptomes of these two tumor types, we analyzed RNA-Sequencing (RNA-Seq) data from The Cancer Genome Atlas (TCGA) and found that a pro-angiogenic gene signature is present in 35% of PDACs and that it is mostly distinct from the angiogenic signature present in PNETs. The pro-angiogenic PDAC subgroup also exhibits a transcriptome that reflects active TGF-β signaling, less frequent SMAD4 inactivation than PDACs without the signature, and up-regulation of several pro-inflammatory genes, including members of JAK signaling pathways. Consequently, targeting the TGF-β receptor type-1 kinase with SB505124 and JAK1/2 with ruxolitinib blocks proliferative crosstalk between human pancreatic cancer cells (PCCs) and human endothelial cells (ECs). Additionally, treatment of the KRC (oncogenic Kras, homozygous deletion of Rb1) and KPC (oncogenic Kras, mutated Trp53) genetically engineered PDAC mouse models with ruxolitinib suppresses murine PDAC (mPDAC) progression only in the KRC model, which shows superior enrichment and differential expression of the human pro-angiogenic gene signature as compared to KPC tumors. These findings suggest that targeting both TGF-β and JAK signaling in the 35% of PDAC patients whose cancers exhibit an pro-angiogenic gene signature should be explored in a clinical trial.

Murray Korc, MD, Chair

Contents

List of Tables

List of Figures

Abbreviations

3D 3-dimensional. v, ix, xi, 39, 41–46, 53, 54, 56, 65, 66, 76, 78
Actb murine actin, beta. 80
ACTH adrenocorticotropic hormone (gene: POMC). 17
ACVRL1 activin A receptor type IL. 26, 35, 64
ADM acinar-to-ductal metaplasia. 57–59, 65
angiostatin angiostatin (gene: PLG). 61
ANGPT angiopoietin. 61
ANGPT1 angiopoietin 1. 26, 30, 64
ANGPTL3 angiopoietin like 3. 31
ANOVA analysis of variance. 22
APOLD1 apolipoprotein L domain containing 1. 26, 64, 68
ATCC American Type Culture Collection. 75, 76
ATRX alpha thalassemia/mental retardation syndrome X-linked. 18, 62
BMPER BMP binding endothelial regulator. 26, 64
BRAF serine/threonine-protein kinase B-raf. 11–16
C3AR1 complement component 3a receptor 1. 26, 35
CAF cancer associated fibroblast. 6
CCK cholecystokinin. 2
CCR2 chemokine (C-C motif) receptor 2. 27, 35
CCR7 chemokine (C-C motif) receptor 7. 37, 88
CD28 CD28 molecule. 37, 88
CD31 murine cluster of differentiation 31 (gene: Pecam1). 44, 47, 57–60, 69
CD31 human cluster of differentiation 31 (gene: PECAM1). xi, xii, 20–23, 37–39, 43, 61, 62, 65, 69, 74, 76, 95–97
CDKN2A cyclin-dependent kinase inhibitor 2A. 32, 34, 62
cDNA complementary DNA. 80
CI confidence interval. 11–16
CK19 murine keratin 19 (gene: Krt19). 44, 47, 69
CK19 keratin 19 (gene: KRT19). 43
CLIC4 chloride intracellular channel 4. 27, 35
CM conditioned media. viii, xi, xii, 41, 43, 44, 51–55, 65, 66, 75–77, 80, 81
COL15A1 collagen type XV alpha 1. 27, 30, 64
COL4A3 collagen type IV alpha 3. 27, 30, 64
CPTAC Clinical Proteomic Tumor Analysis Consortium. 62

Cripto-1 teratocarcinoma-derived growth factor 1 (gene: TDGF1). 64

CSF1R macrophage colony-stimulating factor 1 receptor. 9, 11–13, 17, 83

CTGF connective tissue growth factor. 36, 83

Ctgf murine connective tissue growth factor. 46, 50, 53, 66

CUL3 cullin 3. 32

CXCL1 Growth-regulated alpha protein. 53, 66

CXCL5 C-X-C motif chemokine 5. 53, 66

Cyr61 murine cysteine rich protein 61. 46, 50, 53, 66

DAVID Database for Annotation, Visualization and Integrated Discovery. 79, 80

DAXX death-domain associated protein. 18, 62

DLL4 delta-like protein 4. 5, 6

DMEM Dulbecco's Modified Eagle Medium. 75, 76

DNA deoxyribonucleic acid. 39

DNA-Seq DNA-Sequencing. 62

EC endothelial cell. vi–viii, xi, xii, 4–6, 17, 20, 30, 37, 38, 41–45, 47, 51–56, 58–61, 64–66, 75–77, 80, 81

ECM extracellular matrix. 6

EGFR epidermal growth factor receptor. x, 15–17, 88

Egfr murine epidermal growth factor receptor. 46, 50, 66

ELISA enzyme-linked immunosorbent assay. ix, 53, 55, 81

ELK3 ELK3, ETS transcription factor. 27, 35

endostatin endostatin (gene: COL18A1). 61

EPAS1 endothelial PAS domain protein 1 (protein: HIF-2α). 26, 27, 64

ERK2 murine mitogen-activated protein kinase 1 (gene: Mapk1). 45, 55

ERK2 mitogen-activated protein kinase 1 (gene: MAPK1). 43, 76

FBS fetal bovine serum. 75, 76

FC Fold Change. 24–30, 36–38, 40, 48–50, 53, 63, 64, 71, 72, 74, 75, 78–80, 82–94

FDA Food and Drug Administration. 18, 68

FDR False Discovery Rate. 24–30, 36, 38, 40, 50, 53, 63, 64, 71, 72, 74, 75, 78, 79, 82–94

FGF fibroblast growth factor. 61, 64

FGF9 fibroblast growth factor 9. 27, 31, 64

FGFR-1 fibroblast growth factor receptor 1 (gene: FGFR1). 9

FGFR1 fibroblast growth factor receptor 1. 27, 30, 35, 64

FGFR2 fibroblast growth factor receptor 2. 27, 64

FLT1 fms related tyrosine kinase 1 (protein: VEGFR-1). 26, 27, 35, 64

FLT4 fms related tyrosine kinase 4 (protein: VEGFR-3). 26, 27, 35, 64
FOA Funding Opportunity Announcement. 62
FOLFIRINOX fluorouracil plus leucovorin, irinotecan, and oxaliplatin. 7, 24
FTP File Transfer Protocol. 71
FWER family-wise error rate. 39, 50–52
gastrin gastrin (gene: GAST). 3, 17
GEF guanine exchange factor. 32
GEMM Genetically Engineered Mouse Model. viii, 19, 52, 58, 74, 75
GHRH growth hormone releasing hormone (gene: GHRH). 17
glucagon glucagon (gene: GCG). 3, 4, 17
GM-CSF granulocyte-macrophage colony-stimulating factor (gene: Csf2). 53, 66
GNA13 guanine nucleotide binding protein (G protein), alpha 13. 27, 35
GO Gene Ontology. ix, xi, 20, 23, 46, 48, 49, 70, 71, 78–80
GPI glycosylphosphatidylinositol. 64
GPLD1 glycosylphosphatidylinositol specific phospholipase D1. 27, 64, 68
GPR124 adhesion G protein-coupled receptor A2 (gene: ADGRA2). 27, 64
GREM1 gremlin 1, DAN family BMP antagonist. 27, 35
GSC genome sequencing center. 73
GSEA Gene Set Enrichment Analysis. viii, 35, 37, 39, 47, 50–52, 71, 74, 75
HGNC HUGO Gene Nomenclature Committee. 71
HIF-1α hypoxia inducible factor 1, alpha subunit (gene: HIF1A). 6
HIF1A hypoxia inducible factor 1 alpha subunit. 26, 28, 30, 31, 35, 64
hPDAC human PDAC. vi, xii, 8–10, 15, 19–21, 37, 38, 44, 54, 69, 95–97
HPMC hydroxypropyl methylcellulose. 77
HR Hazard Ratio. 11–16, 18, 19
HSPG heparan sulfate proteogylycan. 8
HUGO Human Genome Organisation. 71, 74, 75
HUVEC human vascular endothelial cell. xii, 39, 41–45, 64, 66, 75, 76
I immune cell. 6
IFN interferon. 61
IHC immunohistochemistry. viii, 8, 9, 69
IL-8 C-X-C motif chemokine ligand 8 (gene: CXCL8). 61
IL2RA interleukin 2 receptor subunit alpha. 37, 91, 93
IL6 murine interleukin-6 (gene: Il6). 54
IL6 interleukin 6. 37, 38, 89, 94
IL6R interleukin 6 receptor. 38, 94

IL6ST interleukin 6 signal transducer. 38, 89, 94
INSM1 insulinoma associated 1. 63
insulin insulin (gene: INS). 3, 4, 17
IPA Ingenuity Pathway Analysis. viii, 74
IRB Institutional Review Board. 69
ISL1 ISL LIM homeobox 1. 26, 28, 64, 68
ITGA5 integrin subunit alpha 5. 36, 84
ITGAV integrin subunit alpha V. 28, 30, 35, 64
ITGB1 integrin subunit beta 1. 28, 30, 35, 64
JAK janus kinase. vi–viii, x, xi, 38–41, 65, 68, 75, 93
JAK1 janus kinase 1 (gene: JAK1). vii, xi, 41, 43–45, 66, 76
JAK1 janus kinase 1. 38, 39, 42, 44, 45, 66, 76, 94
JAK1/2 murine janus kinase 1/2. 54, 56, 58
JAK1/2 janus kinase 1/2. vi, 65, 67
JAK2 janus kinase 2 (gene: JAK2). xi, 41, 44, 76
JAK2 janus kinase 2. 37–39, 42, 89, 94
JAK3 janus kinase 3. 38, 94
KBTBD6 kelch repeat and BTB domain containing 6. 32, 34
KC **K**ras$^{\text{LSL-G12D/+}}$; Pdx-1-**C**re. viii, ix, 7, 46, 49, 50, 52, 53, 75, 79, 80
KDR kinase insert domain receptor (protein: VEGFR-2). 26, 28, 64
Ki67 antigen identified by monoclonal antibody Ki 67 (gene: Mki67). 53
KIC **K**ras$^{\text{LSL-G12D/+}}$; Cdkn2a$^{\text{LoxP/LoxP}}$; Pdx-1-**C**re. 52
KMT2D lysine methyltransferase 2D. 34, 62
KPC **K**ras$^{\text{LSL-G12D/+}}$; Tr**p**53$^{\text{LSL-R172H/+}}$; Pdx-1-**C**re. vi, viii, ix, xii, 7, 47, 50–53, 58, 60, 65, 67, 69, 74, 75, 77–79
KRAS human kirsten rat sarcoma viral oncogene homolog. 32, 34, 39, 62, 67, 75
Kras murine kirsten rat sarcoma viral oncogene homolog. vi, 7, 44, 46, 47, 67
KRC **K**ras$^{\text{LSL-G12D/+}}$; **R**b1$^{\text{-/-}}$; Pdx-1-**C**re. vi–ix, xi, xii, 44, 46–59, 65–67, 69, 74–81
LTA lymphotoxin alpha. 37, 89
MAF mutation annotation format. 73
MCP-1 C-C motif chemokine 2 (gene: Ccl2). 53, 66
MEF mouse embryonic fibroblasts. 75
MEFV mediterranean fever. 37, 92
MEN-1 multiple endocrine neoplasia type-1. 18
MEN1 menin 1. 18, 62
MGI Mouse Genome Informatics. 79, 80

mPDAC murine PDAC. vi, xi, 44, 47, 53, 54, 57–60, 65, 67
mRNA messenger RNA. 9, 46, 50, 53, 54, 62, 80
MSigDB Molecular Signatures Database. 35
mTOR mechanistic target of rapamycin (gene: MTOR). 18, 62
MTT 3-(4,5-dimethylthiazol-2-yl)-2,5-diphenyltetrazolium bromide. 45, 80
MVD microvessel density. vi, vii, 8, 9, 20, 61
NCBI National Center for Biotechnology Information. 71
NES normalized enrichment score. 50–52
NICD notch intracellular domain. 5, 6
NOTCH notch. 5, 6
NRP1 neuropilin 1. 4–6, 28, 35
Nrp2 murine neuropilin 2. 46, 50, 66
NRXN1 neurexin 1. 28, 64
NRXN3 neurexin 3. 28, 64
ORR objective response rate. 10–16
OS overall survival. 10–17, 25
OSMR oncostatin M receptor. 37, 38, 89, 94
P P-value. 19, 22, 24–30, 36, 38, 42, 43, 45, 48–50, 52, 54–57, 59, 65, 73, 78–80, 82–94
p-Histone H3 phosphorylated Histone H3. 58–60, 69
p-JAK1 phosphorylated JAK1. 41, 43, 44, 65, 66, 76
p-JAK2 phosphorylated JAK2. 43, 76
p-SMAD phosphorylated SMAD. 43, 65
p-SMAD2 murine phosphorylated SMAD2. 52, 53, 66, 77
p-SMAD2 phosphorylated SMAD2. 36
p-SMAD2/3 phosphorylated SMAD2/3. 44, 66
p-SMAD3 murine phosphorylated SMAD3. 52, 53, 66, 77
p-STAT3 murine phosphorylated STAT3. 55, 58, 59, 65, 66, 69, 77
pancreatic polypeptide pancreatic polypeptide (gene: PPY). 3, 4
PanIN pancreatic intraepithelial neoplasia. 44, 57, 58, 65
PARP poly (ADP-ribose) polymerase family, member 1 (gene: PARP1). 41, 43, 76
PC principal component. 26, 72
PCA Principal Component Analysis. viii, 25, 26, 72
PCC pancreatic cancer cell. vi–viii, xi, xii, 6, 36–39, 41–46, 51–54, 56, 57, 63, 65, 66, 75, 76
PCSK2 proprotein convertase subtilisin/kexin type 2. 63

PDAC pancreatic ductal adenocarcinoma. vi–viii, x–xii, 6–17, 19–40, 51–53, 57, 59, 61–65, 67, 68, 70–75, 78, 79, 82–97

PDGF platelet derived growth factor. 61

PDGFA platelet derived growth factor subunit A. 53, 85

Pdgfa murine platelet derived growth factor, alpha. 53

PDGFR platelet-derived growth factor receptor. 9, 11–13, 15, 17

PDGFRB platelet-derived growth factor receptor beta. 11–16

PFS progression free survival. 10–19

PIAS2 protein inhibitor of activated STAT 2. 38, 94

PlGF placenta growth factor (gene: PGF). 6, 14, 17

PNET pancreatic neuroendocrine tumor. vi, vii, x, xi, 17–19, 22–34, 36, 38, 40, 62–64, 68, 71–74, 82–87

PTPRB protein tyrosine phosphatase, receptor type B. 29, 30

PTPRN2 protein tyrosine phosphatase, receptor type N2. 63

qPCR quantitative Polymerase Chain Reaction. ix, xi, 46, 50, 80

QPCT glutaminyl-peptide cyclotransferase. 63

RAC1 ras-related C3 botulinum toxin substrate 1 (rho family, small GTP binding protein Rac1). 32

RAMP2 receptor (G protein-coupled) activity modifying protein 2. 29, 35

RB1 retinoblastoma 1. 44

Rb1 murine retinoblastoma 1. vi, 44, 46, 65

RNA ribonucleic acid. 46, 78–80

RNA-Seq RNA-Sequencing. vi, 9, 19, 20, 22–24, 36, 40, 62, 68, 70–72

ROBO4 roundabout guidance receptor 4. 29, 64

RORA RAR related orphan receptor A. 29, 35

RPPA reverse phase protein array. 20, 74

Rps6 murine ribosomal protein S6. 80

S1P sphingosine-1-phosphate. 30

S1PR1 sphingosine-1-phosphate receptor 1. 29, 30

SAM Significance Analysis of Microarrays. 24, 63

SCFR mast/stem cell growth factor receptor Kit (gene: KIT). 9, 11–13, 15, 17

SCG2 secretogranin II. 26, 29, 63, 64, 68

SCID severe combined immunodeficiency. 9

SD standard deviation. 55

secretin secretin (gene: SCT). 3

SEM standard error of the mean. 42, 43, 45, 50, 52, 54–56, 69, 76

SEMA3E semaphorin 3E. 29, 64

Serpine1 murine serine (or cysteine) peptidase inhibitor, clade E, member 1. 46, 50, 66

SFRP1 secreted frizzled-related protein 1. 29, 64, 68

shRNA small hairpin RNA. 44, 45, 54, 55, 66, 76, 77, 80, 81

SLIT2 slit guidance ligand 2. 29, 64

SMAD murine SMAD. 53

SMAD SMAD. 41, 76

SMAD2 murine SMAD family member 2 (gene: Smad2). 53, 66

SMAD2/3 murine SMAD2/3. 77

SMAD2/3/4 murine SMAD complex. 53

SMAD3 murine SMAD family member 3 (gene: Smad3). 53

SMAD4 SMAD family member 4 (gene: SMAD4). xi, 36–39, 65, 69, 74

SMAD4 SMAD family member 4. vi, xi, 32, 34, 36, 39, 62, 64, 65, 73, 75

SMI small molecule inhibitor. 11–14, 16

SOCS suppressor of cytokine signaling. 38

SOCS3 suppressor of cytokine signaling 3. 37, 92, 94

somatostatin somatostatin (gene: SST). 3, 4, 17–19

SSTR somatostatin receptor. 18

SSTR2 somatostatin receptor 2. 18

STAT signal transducer and activator of transcription. viii, x, xi, 38, 40, 65, 68, 75, 93

STAT1 signal transducer and activator of transcription 1. 38, 94

STAT3 murine signal transducer and activator of transcription 3 (gene: Stat3). viii, xii, 53–55, 77, 81

STAT3 signal transducer and activator of transcription 3 (acute-phase response factor). 38

Stat3 murine signal transducer and activator of transcription 3. 54, 55, 66, 77, 80, 81

STAT4 signal transducer and activator of transcription 4. 38, 94

TCGA The Cancer Genome Atlas. vi, viii, xi, 9, 19, 20, 22, 23, 25, 31, 32, 36–38, 40, 47, 51, 62, 63, 65, 67, 68, 70–74, 78, 79

TEK TEK receptor tyrosine kinase. 26, 29, 64

TGF-β murine transforming growth factor beta. viii, xi, 51–53, 55, 66, 75

TGF-β transforming growth factor beta. vi–viii, x, xi, 31, 32, 35, 36, 39, 41, 51, 61, 64, 65, 68, 71, 74, 82

TGF-β receptor type-1 murine TGF-β receptor type-1 (gene: Tgfbr1). xii, 53, 54, 56, 57

TGF-β receptor type-1 TGF-β receptor type-1 (gene: TGFBR1). vi, vii, xi, 39, 41, 42, 44, 65, 67

TGF-β1 murine transforming growth factor, beta 1 (gene: Tgfb1). 81

TGF-β1 transforming growth factor beta 1 (gene: TGFB1). 71, 75

TGFB1 transforming growth factor beta 1. 36

Tgfb1 murine transforming growth factor, beta 1. 53

TGFB2 transforming growth factor beta 2. 36

Tgfb2 murine transforming growth factor, beta 2. 53

TGFB3 transforming growth factor beta 3. 36, 53

Tgfb3 murine transforming growth factor, beta 3. 53

TGFBR1 transforming growth factor beta receptor I. 26, 29, 30, 35, 64

Tgfbr1 murine transforming growth factor, beta receptor I. 46, 50, 66

TGFBR2 transforming growth factor beta receptor II. 26, 29, 30, 35, 64

TIAM1 T-cell lymphoma invasion and metastasis 1. 32

TIE1 tyrosine kinase with immunoglobulin like and EGF like domains 1. 26, 29, 64

TLR2 toll like receptor 2. 37, 89

TMA tissue microarray. viii, 37, 38, 65, 69

TME tumor microenvironment. 53, 54

TP53 tumor protein p53. 32, 34, 62, 67

TRITC tetramethylrhodamine. 46, 77

Trp53 murine transformation related protein 53. vi, 7, 47, 67

TSP thrombospondin. 61

TTN titin. 32, 34

TTP time to progression. 11–13, 16

TTR transthyretin. 63

VE-caderin cadherin 5 (gene: Cdh5). 59

VEGF vascular endothelial growth factor. vii, 6, 9, 10, 17, 18, 20, 26, 30, 31, 61, 62, 64, 68

VEGF-A murine vascular endothelial growth factor A (gene: Vegfa). 53, 66

VEGF-A vascular endothelial growth factor A (gene: VEGFA). vii, 4–6, 8–18, 68

VEGF-B vascular endothelial growth factor B (gene: VEGFB). 6, 14, 17

VEGF-C murine vascular endothelial growth factor C (gene: Vegfc). 53, 66

VEGFA vascular endothelial growth factor A. 8, 9

Vegfa murine vascular endothelial growth factor A. 46

Vegfc murine vascular endothelial growth factor C. 46, 50, 53, 66

VEGFR vascular endothelial growth factor receptor. 6, 9, 11–15, 17

VEGFR-1 vascular endothelial growth factor receptor 1 (gene: FLT1). 5, 6, 9, 17

VEGFR-2 vascular endothelial growth factor receptor 2 (gene: KDR). 4–6, 9, 11–18

VEGFR-3 vascular endothelial growth factor receptor 3 (gene: FLT4). 6

VERGE vascular early response gene. 64

VIP vasoactive intestinal peptide (gene: VIP). 3, 17

Wisp1 murine WNT1 inducible signaling pathway protein 1. 53

WT wild type. viii, xi, 33, 36, 37, 46, 48, 50, 74, 75, 79

1 Introduction

1.1 Pancreas

The pancreas is located dorsally to the stomach at the L2 vertebral level in the upper abdomen (Figure 1.1). It is a retroperitoneal organ that sits in the "C" loop of the duodenum and slopes upwards towards the splenic hilum (Figure 1.1) [1, 2]. It functions both as an exocrine organ to support digestion and as an endocrine organ to control blood glucose levels [1–5]. The exocrine parenchyma, acini and ducts, makes up ∼85% of the pancreas while the endocrine parenchyma, the islets of Langerhans, constitute only 1-2% of the pancreas [1].

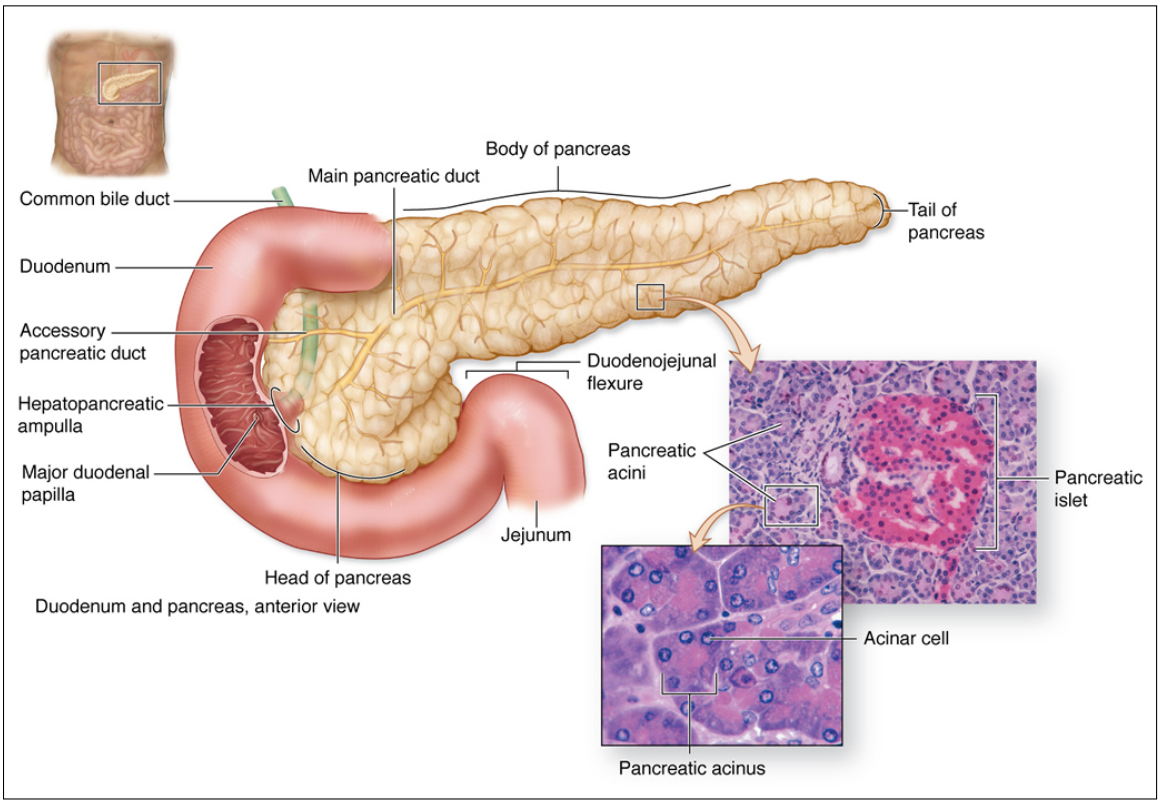

Figure 1.1: Pancreas. The main anatomical structures of the pancreas. The hepatopancreatic ampulla is also known as the ampulla of Vater. The micrographs highlight a pancreatic islet and acinus. Image reproduced from [5].

1.2 Exocrine pancreas

The exocrine pancreas is a secretory organ that secretes a pancreatic juice rich in HCO_3^- and digestive enzymes into a ductal system leading to the duodenum to help neutralize and digest the gastric contents being emptied from the stomach [4]. The

secretory unit of the pancreas consists of an acinus made up of 15 to 100 acinar cells that secrete digestive zymogens into an intercalated duct (Figure 1.2A) [4]. Multiple acini make up a larger unit called a lobule, and the intercalated ducts of the lobule drain into an intralobular duct, and the intralobular ducts from different lobules then drain into an interlobular duct (Figure 1.2B) [4]. The interlobular ducts drain into the main pancreatic duct, and this duct joins with the common bile duct immediately proximal to the duodenum to form the ampulla of Vater (Figure 1.1) [4]. This ampulla then drains bile and pancreatic juice via the greater duodenal papilla (also known as the major duodenal papilla) into the duodenum (Figure 1.1) [4]. There is also an accessory pancreatic duct that fuses with the main pancreatic duct during development and drains separately into the duodenum through the lesser duodenal papilla (Figure 1.1), though it can also end blindly in the pancreas in 30% of patients [2]. In an even a smaller percentage of patients (10%), these ducts fail to fuse, and the majority of the pancreas is then drained through the lesser duodenal papilla [2].

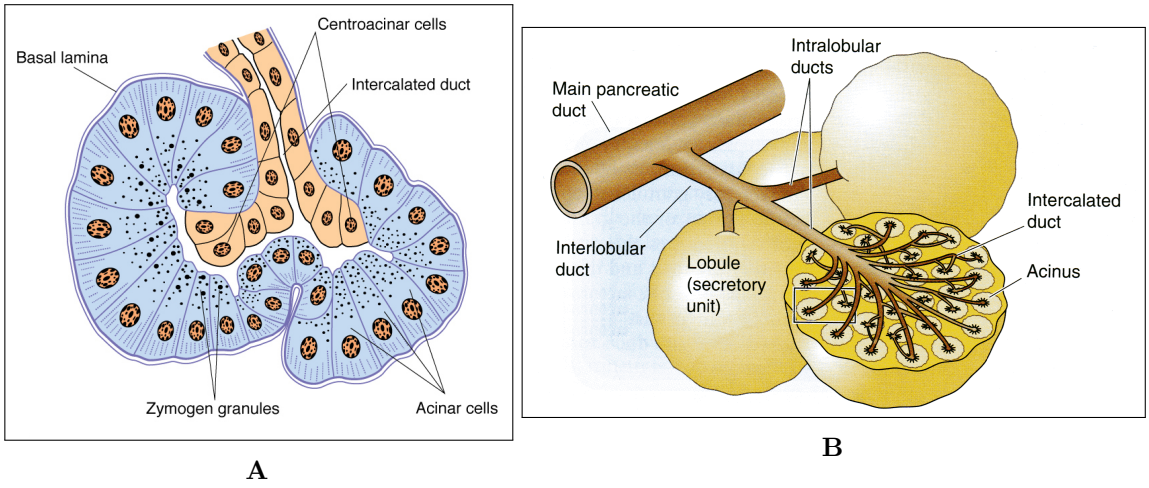

Figure 1.2: Acinar and ductal morphology of the pancreas. (A) The basic secretory unit of the pancreas consists of many acinar cells surrounding an intercalated duct. Acinar cells are specialized secretory cells with many zymogen granules present on their apical side posed for release into the duct upon neurohumoral stimulation by cholecystokinin (CCK) or the neurotransmitter acetylcholine. Image reproduced from [5]. **(B)** Intercalated ducts within a lobule of acini will coalesce into a larger intralobular duct and multiple intralobular ducts come together to form an interlobular duct. Interlobular ducts then drain into the main pancreatic duct. Image reproduced from [4].

Acinar cells are polarized epithelial cells that synthesize digestive enzymes that are packaged into zymogen granules on the apical side facing the duct lumen (Figure 1.2A) [4]. When lipid and protein digestive products enter the duodenum from the stomach, they stimulate the release of cholecystokinin (CCK) from I cells in the duodenal mucosa, and they stimulate afferent pathways that initiate a vagovagal reflex [4]. CCK will circulate and bind to CCK receptors on acinar cells to stimulate the

secretion of the zymogen granules' contents into the pancreatic ductal system [4]. Postganglionic parasympathetic neurons in the pancreas also release acetylcholine and exert the same effect through muscarinic cholinergic receptors on the acinar cells [4]. In a similar manner, gastric acid in the duodenum will stimulate duodenal S cells to release secretin (gene: SCT), and secretin will circulate and then act on the ductal cells to stimulate the secretion of HCO_3^- rich fluid into the ducts [4].

1.3 Endocrine pancreas

The normal human pancreas contains 500,000 to several million islets of Langerhans [6]. Islets are oval or spherical in shape and contain four types of secretory cells, α, β, δ, and F cells (Figure 1.3) [6]. α cells secrete glucagon (gene: GCG), β cells secrete insulin (gene: INS), δ cells secrete somatostatin (gene: SST), and F cells secrete pancreatic polypeptide (gene: PPY) (Figure 1.3) [6]. Insulin stimulates target tissues like the liver, muscle, and adipose tissue to take up carbohydrates, lipids, and amino acids during the fed state [6]. Insulin maintains glucose levels in the plasma within narrow limits, and both hypo- or hyperglycemia can produce characteristic symptoms in patients [6]. The hallmark of the diabetic state is hyperglycemia, and diabetes can be caused either by destruction of the β cells via immune mediated mechanisms (type 1 diabetes) or by impaired insulin secretion and tissue response (type 2 diabetes) [6]. Insulin release is triggered by glucose, neural, or incretin stimulation of the β cells [6].

Glucagon release is stimulated by protein ingestion and its main actions are to regulate carbohydrate and lipid metabolism in the liver [6]. In many respects, it antagonizes the actions of insulin by stimulating glycogenolysis, gluconeogenesis, and ketogenesis in the liver [6]. In contrast, insulin promotes glycogen synthesis, glycolysis, and the synthesis of fats in the liver. While somewhat confounding, glucagon would prevent hypoglycemia during ingestion of a protein rich meal without a carbohydrate. Its role in the production of glucose and ketone bodies is also important in the fasting state when insulin is low [6]. During fasting, the brain can utilize ketone bodies but not fatty acids as fuel [6].

Somatostatin inhibits the growth of many different types of hormones, including growth hormone, insulin, glucagon, gastrin (gene: GAST), vasoactive intestinal peptide (gene: VIP) (VIP), and thyroid-stimulating hormone [6]. Pancreatic polypeptide has unknown functions in mammalian metabolism [6].

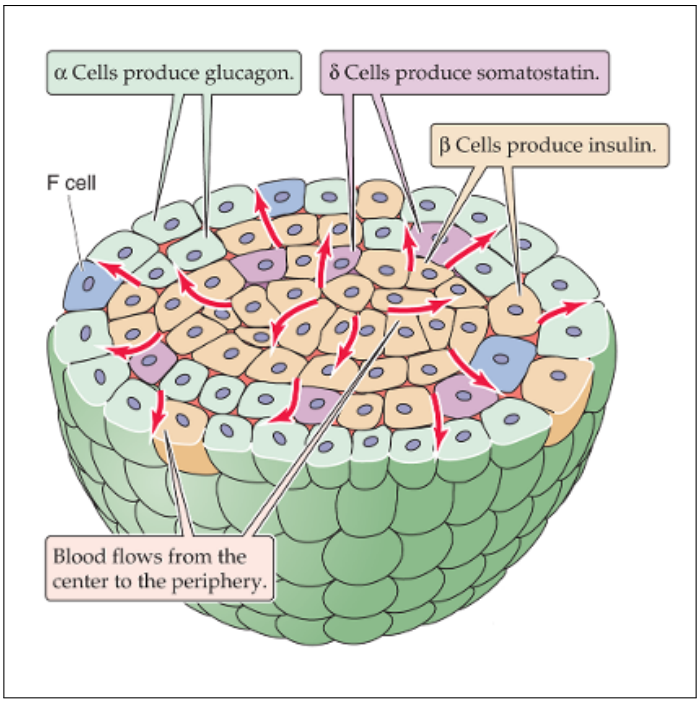

Figure 1.3: Islet of Langerhan. Pancreatic islets contain four types of secretory cells, α, β, δ, and F cells, that secrete insulin (gene: INS), glucagon (gene: GCG), somatostatin (gene: SST), and pancreatic polypeptide (gene: PPY) into the bloodstream, respectively. Image reproduced from [6].

1.4 Angiogenesis

Blood vessel growth throughout adult life is primarily achieved via angiogenesis [7–13]. However, the adult vasculature is mostly quiescent as only 0.01% of the endothelium undergoes cell division at any time [7, 8, 10, 12, 13]. Examples of physiologic angiogenesis in the adult include wound healing, tissues undergoing growth, exercise induced angiogenesis in heart and skeletal muscle, the hair cycle, skeletal growth, and female reproductive processes. Pathologic examples include intraocular neovascular disorders, infantile haemangiomas, immunogenic rheumatoid arthritis, psoriasis, and tumorigenesis [7, 8, 11–15].

Through the use of models like the mouse retina, which becomes vascularized postnatally, we now understand many of the key players and processes involved in physiologic angiogenesis [16]. In general, activation of endothelial cells (ECs) by pro-angiogenic molecules leads to the detachment of pericytes from the endothelium and remodeling of the basement membrane and cell-to-cell junctions (Figure 1.4) [17]. The best known pro-angiogenic molecule is VEGF-A (gene: VEGFA). VEGF-A binds to VEGFR-2 (gene: KDR) on ECs, and its signaling is enhanced by the NRP1 co-receptor, which facilitates complex internalization (Figure 1.4) [17]. Downstream

signaling results in increased expression of the NOTCH ligand DLL4, which binds to NOTCH receptors on neighboring ECs (Figure 1.4) [17]. This releases the notch intracellular domain (NICD) in these cells, which down-regulates VEGFR-2 and NRP1, and up-regulates VEGFR-1 (gene: FLT1), a decoy receptor for VEGF-A (Figure 1.4) [17].

The goal of this process is to isolate one cell that will migrate toward the pro-angiogenic gradient (called the tip cell), while de-sensitizing neighboring cells to the same signal. It is believed that DLL4 and NOTCH signaling are balanced in the quiescent vasculature, and that tip cells will offset the balance in response to pro-angiogenic signals [9]. The cells adjacent to the tip cell are called stalk cells, and they proliferate behind the tip cell to elongate the sprout and form a lumen (Figure 1.4) [17]. Once two tip cells on different sprouts meet, they will anastomose to form a perfused branch (Figure 1.4) [17]. Basement membrane then forms, and pericytes are recruited to cover the vessel (Figure 1.4) [17]. The process is dynamic in that ECs will compete for the tip position with different cells displaying the phenotype over time.

1.5 Tumor angiogenesis

Whereas physiologic angiogenesis is tightly controlled and comes to a resolution, pathologic angiogenesis is abnormal and does not resolve [8, 11, 12, 15, 16]. Because cells need nutrients and oxygen from nearby capillaries to function and survive, early tumor growth is often restricted to a volume of only a few cubic millimeters until the tumor is able to switch to an angiogenic phenotype [8, 11, 12, 14, 15, 18, 19]. Activation of angiogenesis occurs when pro-angiogenic molecules predominate over anti-angiogenic molecules, whereas, inactivation occurs when the anti-angiogenic molecules dominate [7, 8, 20]. In tumorigenesis, the observed activation from a quiescent state is often described as an "angiogenic switch" [7, 8, 20].

The vessels formed during tumor angiogenesis are tortuous or disorganized, immature, and convoluted with excessive vessel branching that lacks pericyte coverage rendering them fragile and leaky with bleeding and exudation of plasma proteins [10–13, 16, 17, 19, 21]. The distribution of new vessels in the tumor is also heterogeneous with some areas demonstrating intense neovascularization [10, 14, 15, 17, 21]. The vessels are often functionally defective with low blood flow and reduced oxygen delivery due to high interstitial pressure [10, 13, 17, 21]. The resulting hypoxic environment exacerbates the pathologic condition by further up-regulating pro-angiogenic molecules [10, 17, 21]. While one might assume that neovascularization would improve delivery

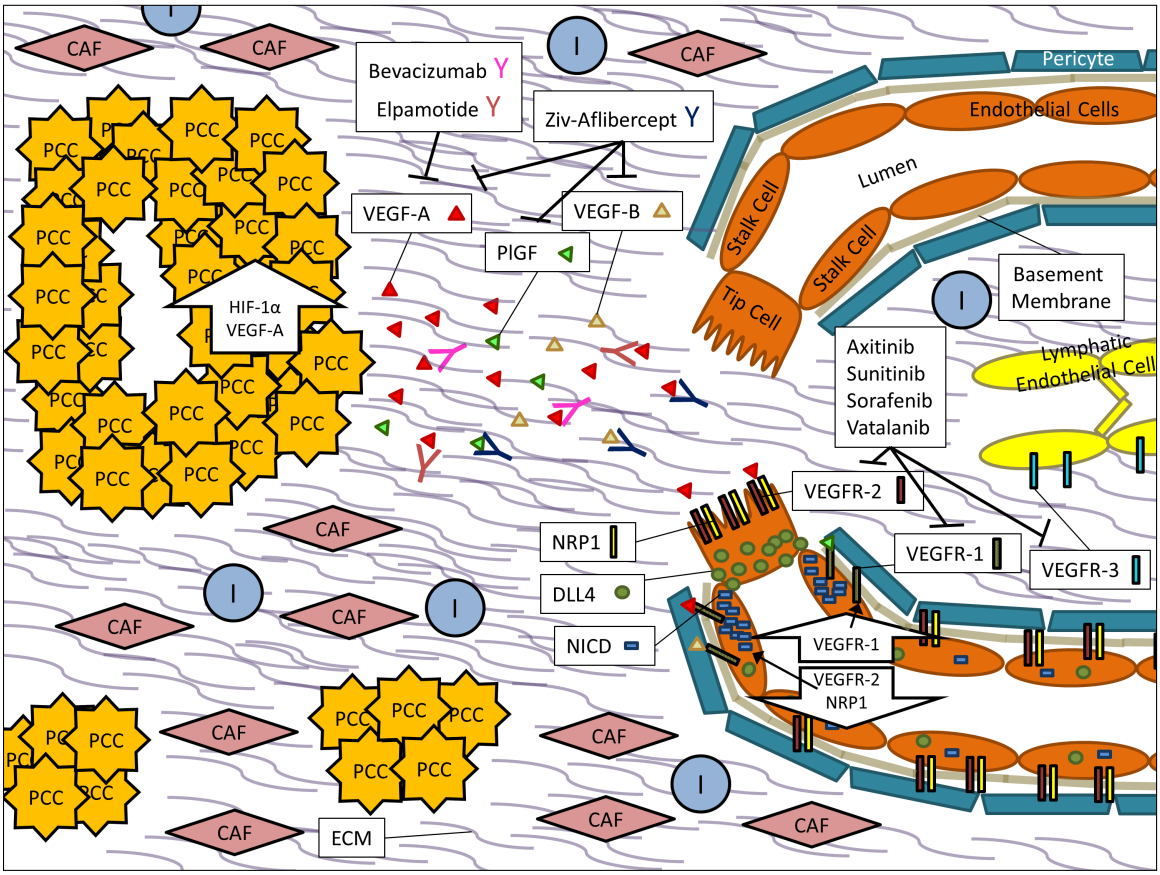

Figure 1.4: Pancreatic ductal adenocarcinoma (PDAC) angiogenesis. In PDAC, pancreatic cancer cells (PCCs) proliferate within a desmoplastic stroma that consists of both cellular components such as cancer associated fibroblasts (CAFs), immune cells (Is), and endothelial cells (ECs) as well as extracellular matrix (ECM) components like soluble growth factors, cytokines, collagens, fibronectin, laminin, glycoproteins, and proteoglycans.

Up-regulation of HIF-1α (gene: HIF1A) and the pro-angiogenic molecule VEGF-A (gene: VEGFA) within PCCs results in secretion of VEGF-A molecules into the tumor microenvironment. When VEGF-A signals through VEGFR-2 (gene: KDR) and its NRP1 co-receptor on ECs, downstream signaling results in increased expression of DLL4. DLL4 will bind to NOTCH receptors on neighboring cells, subsequently releasing notch intracellular domain (NICD), which then down-regulates VEGFR-2 and NRP1 expression and up-regulates expression of the VEGFR-1 (gene: FLT1) decoy receptor. This favors migration of a tip cell towards the VEGF-A gradient while the neighboring stalk cells become de-sensitized to the signal. In the quiescent vasculature, DLL4 and NOTCH signaling are balanced.

Small molecule inhibitors of angiogenesis, such as Axitinib, Sunitinib, Sorafenib, and Vatalanib primarily act on the vascular endothelial growth factor receptor (VEGFR) complexes (VEGFR-1, VEGFR-2, and VEGFR-3 (gene: FLT4)) while recombinant protein inhibitors of angiogenesis like Bevacizumab, Elpamotide, and Ziv-Aflibercept act on VEGF ligands like VEGF-A, VEGF-B (gene: VEGFB), and/or PlGF (gene: PGF).

of chemotherapeutic agents to the tumor, the poor perfusion and compression of the vascular supply actually impedes drug delivery [10, 11, 13, 15, 17]. Therefore, in addition to inhibiting angiogenesis and causing vessel regression, anti-angiogenic agents can enhance the effects of simultaneously administered chemotherapeutic drugs by normalizing the remaining vasculature [10, 11, 13, 15–17, 21].

1.6 Pancreatic ductal adenocarcinoma (PDAC)

Pancreatic ductal adenocarcinoma (PDAC) is a pancreatic tumor which arises from the exocrine pancreas and comprises >85% of pancreatic cancers [22–24]. PDAC is the 4th leading cause of cancer death in the United States with a 5-year relative survival rate of 8% [22–24]. These statistics are largely due to advanced stage at clinical presentation, a high frequency of major driver mutations, marked resistance to chemotherapy and radiation, and extensive desmoplasia that impedes drug delivery [25–29]. Because advances in screening, prevention, and treatment are limited compared to other cancers, PDAC is now projected to surpass breast, prostate, and colorectal cancers to become the second leading cause of cancer death by 2030 [30].

At presentation, only 15–20% of patients are eligible for surgical resection, the only chance for cure [22, 31, 32]. Even then, outcomes are poor, with a 5 year survival between 20–25% post-resection, since most of these patients develop disease recurrence [33]. Therefore, chemotherapy is recommended as adjuvant treatment for those undergoing surgical resection and is the mainstay of treatment for patients with locally advanced or metastatic disease [31]. The current standard of care for patients with metastatic disease includes gemcitabine plus nab-paclitaxel or fluorouracil plus leucovorin, irinotecan, and oxaliplatin (FOLFIRINOX) [31, 34].

1.7 PDAC is hypovascular

Using the **K**ras$^{\text{LSL-G12D/+}}$; Tr**p**53$^{\text{LSL-R172H/+}}$; Pdx-1-**C**re (KPC) PDAC mouse model, which has oncogenic Kras and mutated Trp53 in the pancreas due to Cre-mediated recombination, Olive et al. showed that KPC tumors are poorly vascularized, poorly perfused, and have impaired drug delivery when compared to KPC transplant models or normal mouse pancreas [35]. Likewise, using both **K**ras$^{\text{LSL-G12D/+}}$; Pdx-1-**C**re (KC) mice, which have oncogenic Kras in the pancreas due to Cre-mediated recombination, and KPC mice, Provenzano et al. reported that in addition to having reduced vascularity, KC and KPC tumors have a paucity of large diameter (>10 um) vessels when compared to normal mouse pancreas [36]. This is likely due to

vascular collapse caused by the presence of very high interstitial fluid pressures in these tumors, in the range of 75–130 mm Hg, compared to 8–13 mm Hg in normal mouse pancreas [36]. This observation also offers an explanation for the poor perfusion and drug delivery observed by Olive et al. [35]. Human PDAC (hPDAC) samples were also shown to be poorly vascularized compared to normal human pancreas or adjacent normal human pancreas, and to have fewer large diameter vessels compared to adjacent normal human pancreas [35, 36].

Because PDAC is inherently hypovascular, it might be assumed that this cancer either does not demonstrate significant angiogenesis or that it is not likely to benefit from anti-angiogenic agents. However, both concepts have been disproven in other cancers [37]. All tumor types need sufficient levels of nutrients and oxygen and are growth limited unless they are able to induce angiogenesis. This is also true of hypoxic tumors, which likely have increased requirements to drain away toxic by-products released by cancer cells. Instead of measuring angiogenesis, microvessel density (MVD) rather reflects the metabolic burden of the supported tumor cells [37]. In fact, because the oxygen consumption rate is often lower in tumors compared to the corresponding normal tissue, it is not uncommon for tumors to have lower MVDs as we see in PDAC [37]. This is also the case for renal cell carcinoma, a cancer known clinically to respond to anti-angiogenic therapy [37]. Both poorly and highly vascularized cancers have been shown to respond to anti-angiogenic therapy [37].

1.8 Correlation of VEGF-A expression or microvessel density (MVD) with health outcomes in PDAC

VEGF-A, a potent inducer of angiogenesis, was first discovered as a secreted protein that can enhance vascular permeability [7]. Many different isoforms exist, and their different binding affinities for heparan sulfate proteogylycans (HSPGs) function to create a gradient for guiding vessels during vascular development [11]. In recent years, more insight into the alternative splicing and translation of the gene has revealed that anti-angiogenic forms and a translational read through can also be produced [38, 39].

Using immunohistochemistry (IHC), several groups found that between 60–65% of hPDAC samples have a substantial amount of VEGF-A immunoreactivity [40–42]. In terms of gene expression, Ikeda et al. found that 27/40 (67.5%) hPDAC samples overexpress VEGFA compared to a colon cancer cell line while Itakura et al. found a 5.2 fold increase in VEGFA expression in hPDAC samples (n=7) compared to normal human pancreas samples (n=4) [40, 42].

MVD has not been shown to be an accurate measure of angiogenesis in other cancers [37]; nonetheless, three [40–42] of four [43] studies of hPDAC samples have shown an association between VEGFA mRNA or VEGF-A protein (IHC) expression and the amount of vascularity seen in the tumor. Patients with high levels of VEGFA mRNA or VEGF-A protein (IHC) also had increased liver metastasis [41], larger tumors [42], enhanced local spread [42], and decreased survival in two [40, 41] out of four [42, 43] studies. Lastly, one [40] out of two [43] studies reported that increased vascularity was associated with decreased patient survival. More recently, by RNA-Sequencing (RNA-Seq), The Cancer Genome Atlas (TCGA) dataset shows that only 8 out of 178 (4%) hPDAC samples overexpress VEGFA (2 z-scores above the mean, according to criteria established by Memorial Sloan Kettering Cancer Center), suggesting that this molecule may not be as important in PDAC as was first surmised [29, 44, 45].

1.9 Pre-clinical studies targeting VEGF signaling in PDAC

Many studies have examined the potential role of targeting VEGF signaling using subcutaneous or orthotopic nude mouse models of hPDAC. Injection of hPDAC cells expressing an anti-sense VEGFA into the flanks of nude mice led to an 80% reduction in tumor size compared to controls [46]. When diphtheria toxin, which inhibits protein synthesis in target cells, was fused with VEGF-A to target it to the vasculature in orthotopic nude mouse models of hPDAC, it led to reduced tumor volume, tumor spread, and MVD, and improvement in survival in 1 of 2 models [47]. Injection of adenovirus vectors encoding the soluble form of the decoy receptor VEGFR-1 into subcutaneous tumor xenografts of hPDAC in severe combined immunodeficiency (SCID) mice also resulted in reduced tumor growth and MVD [48]. Additionally, injection of adenovirus vectors encoding soluble VEGFR-1 or soluble VEGFR-1 plus a soluble FGFR-1 (gene: FGFR1) into subcutaneous tumor xenografts of hPDAC in nude mice resulted in reduced tumor growth [49].

The tyrosine kinase inhibitor PTK 787/ZK222584 (vatalanib) targets vascular endothelial growth factor receptors (VEGFRs), the platelet-derived growth factor receptors (PDGFRs), SCFR (gene: KIT), and CSF1R. Use of this compound in an orthotopic nude mouse model of hPDAC led to reduced tumor volume and MVD, and increased survival [50]. Moreover, use of VEGF-Trap (ziv-aflibercept), which is a recombinant fusion protein of the extracellular portions of VEGFR-1 and VEGFR-2 and the Fc fragment of human immunoglobulin IgG1, resulted in reduced tumor growth and MVD in subcutaneous tumor xenografts of hPDAC and reduced tumor

growth and metastasis in an orthotopic nude mouse model of hPDAC [51]. These promising results provide support for the testing of anti-VEGF agents in hPDAC clinical trials.

1.10 Clinical studies using anti-angiogenic agents in PDAC

To date, many phase II and phase III hPDAC clinical trials using different anti-angiogenic agents have been completed. Several of these involved bevacizumab, an anti-VEGF-A monoclonal antibody, that has already been FDA approved for the treatment of several other cancer types, including persistent, recurrent, or metastatic cervical cancer, metastatic colorectal cancer, or non-small cell lung cancer in combination with chemotherapy; metastatic renal cell carcinoma in combination with interferon alpha; or in glioblastoma as a second-line therapy.

An initial Phase II trial of bevacizumab plus gemcitabine in untreated advanced PDAC patients showed a 21% objective response rate (ORR), a 6-month survival rate of 77%, and a median survival of 8.8 months (Table 1.1) [52]. Because these were favorable numbers compared to the pivotal trial for gemcitabine approval [53], which observed an ORR of 5%, a 6-month survival rate of 46%, and a median survival of 5.7 months, several other Phase II and Phase III studies were launched.

Several Phase II trials added bevacizumab to any existing regimen that had previously shown any sort of modest activity in PDAC. These regimens included: cisplatin and gemcitabine [54]; capecitabine and gemcitabine [55]; capecitabine, radiation, and gemcitabine [56]; oxaliplatin and gemcitabine [57]; gemcitabine and radiation [58, 59], and docetaxel [60] (Table 1.1). However, results from the Phase III trial directly comparing bevacizumab plus gemcitabine to placebo plus gemcitabine in advanced PDAC patients showed that the addition of bevacizumab does not result in an improvement in overall survival (OS) or progression free survival (PFS) or differences in the ORR (Table 1.2) [61].

The difference between the Phase II and Phase III results was suggested to be due to the Phase II trial recruiting a more fit population [61]. Because such disparities are common in trials of PDAC, it was also suggested that the use of a single-arm Phase II trial is not ideal [61]. The majority of Phase II trials with other regimens were single-arm trials, and thus, most of them also concluded that the addition of bevacizumab produced questionable benefit.

Table 1.1: Phase II clinical trials using anti-angiogenic agents in pancreatic ductal adenocarcinoma (PDAC)

Ref	Phase	Group	Drug	Experimental Arm	Active Comparator Arm	Hazard Ratio
[52] Kindler et al. 2005	II	advanced	Bevacizumab (anti-VEGF-A monoclonal antibody)	• bevacizumab + gemcitabine – ORR: 21% (11–35%) – 6 m survival: 77% (63–86%) – OS: 8.8 m (7.4–9.7 m) – PFS: 5.4 m (3.7–6.2 m)	NA	NA
[54] Ko et al. 2008	II	metastatic	Bevacizumab (anti-VEGF-A monoclonal antibody)	• bevacizumab + cisplatin + gemcitabine – ORR: 19.2% – OS: 8.2 m (6.9–11.1 m) – TTP: 6.6 m (4.6–8.8 m)	NA	NA
[55] Javle et al. 2009	II	advanced	Bevacizumab (anti-VEGF-A monoclonal antibody)	• bevacizumab + capecitabine + gemcitabine – ORR: 22% – OS: 9.8 m (8.3–11.9 m) – PFS: 5.8 m (4.2–7.8 m)	NA	NA
[56] Crane et al. 2009	II	locally advanced (unresectable)	Bevacizumab (anti-VEGF-A monoclonal antibody)	• bevacizumab + capecitabine + radiation followed by gemcitabine + bevacizumab – ORR: 26% – OS: 11.9 m (9.9–14 m) – PFS: 8.6 m (6.9–10.5 m)	NA	NA
[57] Fogelman et al. 2011	II	advanced	Bevacizumab (anti-VEGF-A monoclonal antibody)	• bevacizumab + oxaliplatin + gemcitabine – ORR: 36% – 6 m survival: 74% – OS: 11.9 m – PFS: 4.9 m	NA	NA

Ref, Reference; SMI, small molecule inhibitor; ORR, objective response rate; OS, overall survival; PFS, progression free survival; TTP, time to progression; HR, Hazard Ratio; m, month(s); d, days(s); (95% confidence interval); *, statistically significant; VEGF-A, vascular endothelial growth factor A (gene: VEGFA); VEGFR, vascular endothelial growth factor receptor; PDGFR, platelet-derived growth factor receptor; SCFR, mast/stem cell growth factor receptor Kit (gene: KIT); BRAF, serine/threonine-protein kinase B-raf; VEGFR-2, vascular endothelial growth factor receptor 2 (gene: KDR); PDGFRB, platelet-derived growth factor receptor beta; CSF1R, macrophage colony-stimulating factor 1 receptor

Phase II clinical trials using anti-angiogenic agents in PDAC continued

Ref	Phase	Group	Drug	Experimental Arm	Active Comparator Arm	Hazard Ratio
[58] Small et al. 2011	II	localized	Bevacizumab (anti-VEGF-A monoclonal antibody)	• bevacizumab + radiation + gemcitabine, then surgery or bevacizumab + gemcitabine – ORR: 11% (4–24%) – 6 m survival: 86% – OS: 11.8 m – PFS: 9.9 m	NA	NA
[60] Astsaturov et al. 2011	II	metastatic	Bevacizumab (anti-VEGF-A monoclonal antibody)	• bevacizumab – ORR: 0% – OS: 165 d – PFS: 43 d	• bevacizumab + docetaxel – ORR: 0% – OS: 125 d – PFS: 48 d	NA
[59] Van Buren II et al. 2013	II	localized (potentially resectable)	Bevacizumab (anti-VEGF-A monoclonal antibody)	• neoadjuvant bevacizumab + gemcitabine, then radiation – OS: 16.8 m (14.9–21.3 m) – PFS: 6.6 m (4.9–12.4 m)	NA	NA
[68] Spano et al. 2008	II	advanced	Axitinib (SMI of VEGFRs)	• axitinib + gemcitabine – ORR: 7% (2.4–16.1%) – OS: 6.9 m (5.3–10.1 m) – PFS: 4.2 m (3.6–10.2 m)	• gemcitabine – ORR: 3% (0.1–15.3%) – OS: 5.6 (3.9–8.8) m – PFS: 3.7 (2.2–6.7) m	• OS HR 0.71 (0.44–1.13) • PFS HR 0.79 (0.43-1.45)
[69] O'Reilly et al. 2010	II	metastatic (second-line therapy)	Sunitinib (SMI of VEGFRs, PDGFRs, SCFR)	• sunitinib – ORR: 1.4% – OS: 3.68 m (3.06–4.24 m) – PFS: 1.31 m (1.25–1.38 m)	NA	NA

Ref, Reference; SMI, small molecule inhibitor; ORR, objective response rate; OS, overall survival; PFS, progression free survival; TTP, time to progression; HR, Hazard Ratio; m, month(s); d, days(s); (95% confidence interval); *, statistically significant; VEGF-A, vascular endothelial growth factor A (gene: VEGFA); VEGFR, vascular endothelial growth factor receptor; PDGFR, platelet-derived growth factor receptor; SCFR, mast/stem cell growth factor receptor Kit (gene: KIT); BRAF, serine/threonine-protein kinase B-raf; VEGFR-2, vascular endothelial growth factor receptor 2 (gene: KDR); PDGFRB, platelet-derived growth factor receptor beta; CSF1R, macrophage colony-stimulating factor 1 receptor

Phase II clinical trials using anti-angiogenic agents in PDAC continued

Ref	Phase	Group	Drug	Experimental Arm	Active Comparator Arm	Hazard Ratio
[70] Reni et al. 2013	II	metastatic (maintenance therapy)	Sunitinib (SMI of VEGFRs, PDGFRs, SCFR)	• sunitinib – ORR: 0% – OS: 10.6 m (6.2–18.9 m) – PFS: 3.2 m	• observation – ORR: 0% – OS: 9.2 m (5.9–16.3 m) – PFS: 2 m	• OS HR 0.11 (0.4–1.26) • PFS HR 0.51* (0.29–0.89)
[71] El-Khoueiry et al. 2012	II	metastatic	Sorafenib (SMI of BRAF, VEGFR-2, PDGFRB)	• sorafenib – 6 m survival: 43% – OS: 4.3 m (3.3–8.3 m) – PFS: 2.3 m (1.2–5.7 m)	• sorafenib + gemcitabine – 6 m survival: 53% – OS: 6.5 m (5.5–8 m) – PFS: 2.9 m (2.1–4.3 m)	NA
[72] Kindler et al. 2012	II	advanced	Sorafenib (SMI of BRAF, VEGFR-2, PDGFRB)	• sorafenib + gemcitabine – ORR: 0% – 6 m survival: 23% (6–47%) – OS: 4 m (3.4–5.9 m) – PFS: 3.2 m (1.6–3.6 m)	NA	NA
[73] Cascinu et al. 2014	II	advanced	Sorafenib (SMI of BRAF, VEGFR-2, PDGFRB)	• sorafenib + cisplatin + gemcitabine – ORR: 3.4% – OS: 7.5 m (5.6–9.7 m) – PFS: 4.3 m (2.7–6.5 m)	• cisplatin + gemcitabine – ORR: 3.6% – OS: 8.3 m (6.2–8.7 m) – PFS: 4.5 m (2.5–5.2 m)	• OS HR 0.95 (0.62–1.48) • PFS HR 0.92 (0.62–1.35)
[74] Dragovich et al. 2014	II	advanced (second-line therapy)	Vatalanib (SMI of VEGFRs, PDGFRs, SCFR, CSF1R)	• vatalanib – ORR: 3.1% – 6 m survival: 29% (18–41%) – PFS: 2 m	NA	NA

Ref, Reference; SMI, small molecule inhibitor; ORR, objective response rate; OS, overall survival; PFS, progression free survival; TTP, time to progression; HR, Hazard Ratio; m, month(s); d, days(s); (95% confidence interval); *, statistically significant; VEGF-A, vascular endothelial growth factor A (gene: VEGFA); VEGFR, vascular endothelial growth factor receptor; PDGFR, platelet-derived growth factor receptor; SCFR, mast/stem cell growth factor receptor Kit (gene: KIT); BRAF, serine/threonine-protein kinase B-raf; VEGFR-2, vascular endothelial growth factor receptor 2 (gene: KDR); PDGFRB, platelet-derived growth factor receptor beta; CSF1R, macrophage colony-stimulating factor 1 receptor

Table 1.2: Phase III clinical trials using anti-angiogenic agents in PDAC

Ref	Phase	Group	Drug	Experimental Arm	Active Comparator Arm	Hazard Ratio
[75] Van Cutsem et al. 2009	III	metastatic	Bevacizumab (anti-VEGF-A monoclonal antibody)	• bevacizumab + erlotinib + gemcitabine – ORR: 13.5% (9.8–17.9%) – OS: 7.1 m (0–19.8 m) – PFS: 4.6 m (0–18.3 m)	• placebo + erlotinib + gemcitabine – ORR: 8.6% (5.6–12.4%) – OS: 6 m (0.1–19.5 m) – PFS: 3.6 m (0–13.6 m)	• OS HR 0.89 (0.74–1.07) • PFS HR 0.73* (0.61–0.86)
[61] Kindler et al. 2010	III	advanced	Bevacizumab (anti-VEGF-A monoclonal antibody)	• bevacizumab + gemcitabine – ORR: 13% – OS: 5.8 m (4.9–6.6 m) – PFS: 3.8 m (3.4–4 m)	• placebo + gemcitabine – ORR: 10% – OS: 5.9 m (5.1–6.9 m) – PFS: 2.9 m (2.4–3.7 m)	• OS HR 1.044 (0.88–1.24)
[76] Kindler et al. 2011	III	advanced	Axitinib (SMI of VEGFRs)	• axitinib + gemcitabine – ORR: 5% (2.5-8.3%) – OS: 8.5 m (6.9–9.5 m) – PFS: 4.4 m (4–5.6)	• placebo + gemcitabine – ORR: 2% (0.4–4%) – OS: 8.3 m (6.9–10.3) m – PFS: 4.4 m (3.7–5.2) m	• OS HR 1.014 (0.786–1.309) • PFS HR 1.006 (0.779–1.298)
[77] Gonçalves et al. 2012	III	advanced	Sorafenib (SMI of BRAF, VEGFR-2, PDGFRB)	• sorafenib + gemcitabine – ORR: 23% – OS: 8 m (6–10.8 m) – PFS: 3.8 m (3.1–6 m)	• placebo + gemcitabine – ORR: 19% – OS: 9.2 m (7.7–11.6 m) – PFS: 5.7 m (3.7–7.5 m)	• OS HR 1.27 (0.837–1.932) • PFS HR 1.04 (0.697–1.545)
[78] Rougier et al. 2013	III	advanced	Ziv-Aflibercept (recombinant fusion protein that traps VEGF-A, VEGF-B, PlGF)	• ziv-aflibercept + gemcitabine – 6 m survival: 54% (47–61%) – OS: 6.5 m (5.6–7.9 m) – PFS: 3.7 m (3.5–4.5 m)	• placebo + gemcitabine – 6 m survival: 63% (56–69%) – OS: 7.8 m (6.8–8.6 m) – PFS: 3.7 m (3.5–4.6 m)	• OS HR 1.165 (0.921–1.473) • PFS HR 1.018 (0.828–1.253)
[79] Yamaue et al. 2015	III	advanced or metastatic	Elpamotide (epitope peptide of VEGFR-2)	• elpamotide + gemcitabine – OS: 8.36 m (7.46–10.18 m) – PFS: 3.71 m (2.10–3.98 m)	• placebo + gemcitabine – OS: 8.54 m (7.33–10.84 m) – PFS: 3.75 m (2.27–5.59 m)	• OS HR 0.87 (0.486–1.557)

Ref, Reference; SMI, small molecule inhibitor; ORR, objective response rate; OS, overall survival; PFS, progression free survival; HR, Hazard Ratio; m, month(s), (95% confidence interval); *, statistically significant; VEGF-A, vascular endothelial growth factor A (gene: VEGFA); VEGFR, vascular endothelial growth factor receptor; BRAF, serine/threonine-protein kinase B-raf; VEGFR-2, vascular endothelial growth factor receptor 2 (gene: KDR); PDGFRB, platelet-derived growth factor receptor beta; VEGF-B, vascular endothelial growth factor B (gene: VEGFB); PlGF, placenta growth factor (gene: PGF)

In addition to VEGF-A, EGFR and its ligands are commonly overexpressed in hPDAC, and high expression levels are also associated with worse outcomes [62–65]. The addition of cetuximab, a monocloncal antibody targeting EGFR, to gemcitabine has not led to improvements in ORRs, PFS, or OS [66], but the addition of erlotinib, a small molecule inhibitor of EGFR, to gemcitabine has been shown to provide a statistically significant improvement in survival [67]. However, the clinical relevance of this result is often questioned since the median gain in survival is only 10 days [67].

There is also evidence for EGFR's role in angiogenesis and simultaneous inhibition of EGFR and VEGFR-2 has been shown to be synergistic [62, 64, 80–82]. Therefore, several regimens combining cetuximab or erlotinib with bevacizumab have been tried with limited success (Table 1.3) [83–85]. A Phase III trial comparing bevacizumab plus erlotinib plus gemcitabine to placebo plus erlotinib plus gemcitabine in metastatic PDAC patients did not show benefit in OS, but it did show a statistically significant one month improvement in the median PFS (Table 1.2) [75]. Therefore, there is some rationale for using this drug combination in metastatic PDAC patients.

Additional anti-angiogenic agents that have been tried in hPDAC include axitinib, sunitinib, sorafenib, vatalanib, ziv-aflibercept, and elpamotide. The Phase II or III trial comparing axitinib, a VEGFR tyrosine kinase inhibitor, plus gemcitabine to gemcitabine alone did not provide a significant improvement in overall or PFS (Table 1.1, 1.2) [68, 76].

Sunitinib is a small molecule tyrosine kinase inhibitor of VEGFRs, PDGFRs, and SCFR. Though a Phase III study has not been done, this molecule has been tested in the metastatic setting as either a second-line therapy [69] or as a maintenance therapy in patients who did not progress after first-line chemotherapy [70]. Interestingly, in these patient groups, the drug did not do well as a second-line therapy (Table 1.1), but produced a statistically significant improvement in PFS compared to observation alone in the maintenance setting (Hazard Ratio (HR) 0.51 [95% confidence interval (CI): 0.29–0.89], p-value < 0.01) [70]. Because the duration of first-line chemotherapy is often debated due to its cumulative toxicity and unproven efficacy, sunitinib may offer an advantage in the maintenance setting.

Similarly, sorafenib is a small molecule tyrosine kinase inhibitor of BRAF, VEGFRs, and PDGFRB that has been tested in many different settings without benefit (Table 1.1, 1.3) [71–73, 86]. These observations were confirmed in a Phase III trial that observed no improvement in overall or PFS upon the addition of sorafenib to gemcitabine in the treatment of advanced PDAC patients (Table 1.2) [77].

Table 1.3: Phase II clinical trials using an anti-angiogenic agent + EGFR inhibitor in PDAC

Ref	Phase	Group	Drug	Experimental Arm	Active Comparator Arm	Hazard Ratio
[83] Ko et al. 2010	II	metastatic	Bevacizumab (anti-VEGF-A monoclonal antibody)	• bevacizumab + erlotinib – ORR: 3% – 6 m survival: 22% – OS: 102 d (74–117 d) – TTP: 40 d (35–41 d)	NA	NA
[84] Ko et al. 2012	II	advanced	Bevacizumab (anti-VEGF-A monoclonal antibody)	• bevacizumab + cetuximab – ORR: 3.4% (0.1–17.8%) – 6 m survival: 41.4% (23.7–58.3%) – OS: 4.17 m (2.69–8.74) – PFS: 1.91 m (1.81–2.76 m)	• bevacizumab + cetuximab + gemcitabine – ORR: 13.8% (3.9-31.7%) – 6 m survival: 39.3% (21.7–56.5%) – OS: 5.41 m (3.84–6.74 m) – PFS: 3.55 m (2–5.59 m)	NA
[85] Watkins et al. 2014	II	advanced	Bevacizumab (anti-VEGF-A monoclonal antibody)	• bevacizumab + erlotinib + capecitabine + gemcitabine – ORR: 23% (11-38%) – OS: 12.6 m – PFS: 8.4 m	NA	NA
[86] Cardin et al. 2014	II	advanced	Sorafenib (SMI of BRAF, VEGFR-2, PDGFRB)	• sorafenib + erlotinib – OS: 3.3 m or 99.5 d (71–188 d)	NA	NA

Ref, Reference; SMI, small molecule inhibitor; ORR, objective response rate; OS, overall survival; PFS, progression free survival; TTP, time to progression; HR, Hazard Ratio; m, month(s); d, days(s); (95% confidence interval); EGFR, epidermal growth factor receptor; VEGF-A, vascular endothelial growth factor A (gene: VEGFA); BRAF, serine/threonine-protein kinase B-raf; VEGFR-2, vascular endothelial growth factor receptor 2 (gene: KDR); PDGFRB, platelet-derived growth factor receptor beta

Vatalanib is also a multi-kinase inhibitor targeting VEGFRs, PDGFRs, SCFR, and CSF1R. In a Phase II trial, it was used as a second-line therapy in advanced PDAC patients and produced a favorable 6 month survival rate of 29% compared to historic controls (Table 1.1) [74]. However, it was only a single-arm trial, and with the failure of several other similar receptor tyrosine kinase inhibitors, it remains to be seen whether this drug will pan out.

Ziv-aflibercept, a recombinant fusion protein consisting of the extracellular portions of VEGFR-1 and VEGFR-2 and the Fc fragment of human immunoglobulin IgG1, is another drug that targets the VEGF pathway by trapping VEGF-A, VEGF-B, and PlGF (gene: PGF). This drug yielded negative results in a Phase III trial compared to gemcitabine alone (Table 1.2) [78].

Elpamotide, a VEGFR-2 peptide, is a vaccine immunotherapy that can induce a cellular immune response against VEGFR-2 expressing ECs [79, 87]. In a Phase II/III trial (Table 1.2) of locally advanced or metastatic pancreatic cancer patients, there were no improvements in overall or PFS compared to gemcitabine alone, but a subgroup with severe injection site reactions tended to do better, suggesting that this may be a sign of immune response to the vaccine [79].

Thus, targeting the VEGF pathway alone is not an efficacious route in PDAC. Even targeting multiple players in the neoplastic process, like EGFR or other receptor tyrosine kinases, produced marginal benefit, with only two trials showing an improvement in PFS, but not OS [70, 75].

1.11 Pancreatic neuroendocrine tumor (PNET)

Pancreatic neuroendocrine tumors (PNETs) are tumors that arise from the endocrine pancreas and comprise only 1–4% of pancreatic tumors [88, 89]. They are associated with a better prognosis than PDAC with a 5 year survival rate of 53% [24]. PNETs represent a spectrum of different diseases that range from indolent, well-differentiated, and low-grade to aggressive, poorly differentiated, and high-grade tumors [88]. They can also be classified as being functional or nonfunctional depending on whether they secrete a hormone that manifests in clinical symptoms [88, 89]. Usually 70–75% are nonfunctional [88, 89]. Possible hormones include gastrin, insulin, VIP, glucagon, somatostatin, growth hormone releasing hormone (gene: GHRH) (GHRH), and adrenocorticotropic hormone (gene: POMC) (ACTH) resulting in tumors called gastrinomas, insulinomas, VIPomas, glucagonomas, somatostatinomas, GRFomas, and ACTHomas, respectively [89]. Nonfunctional PNETs can also secrete peptides that

don't produce a clinical syndrome [89]. Some PNETs are caused by familial syndromes, including multiple endocrine neoplasia type-1 (MEN-1), von Hippel-Lindau disease, neurofibromatosis 1, and tuberous sclerosis [88, 89], but their clinical presentation, prognosis, and management differ from sporadic PNETs [89]. Usually 60–70% of patients have metastatic disease at presentation and except for insulinomas, malignant characteristics are present in at least 50% of cases [89]. Insulinomas are the most common type of functional PNET, and fewer than 10% are malignant [89]. Gastrinomas are the second most common type of functional PNET and though 60% demonstrate malignant behavior, the 10 year survival rate approaches 90% even with metastatic disease [89].

Therapy options for PNETs include surgery, somatostatin analogues, cytotoxic chemotherapy, and targeted agents [88]. Approximately, 80% of PNETs express somatostatin receptors (SSTRs) (usually SSTR2), and therefore, somatostatin analogues can improve hormone secretion symptoms in many patients, especially in those with VIPomas and glucagonomas [88]. Proton pump inhibitors are usually used to control the excess gastric acid production seen in gastrinomas [88]. Exome sequencing studies of sporadic PNETs have found that the most frequently mutated genes are involved in chromatin remodeling, including MEN1, DAXX, and ATRX, or the mTOR pathway [88]. Indeed, 14% of tumors have mutations in the mTOR pathway, and everolimus has been approved by the Food and Drug Administration (FDA) for patients with progressive PNETs [88].

Early studies using cytotoxic chemotherapy in PNETs have demonstrated response rates often higher than what is seen with somatostatin analogues or targeted agents. Accordingly, cytotoxic agents are often used in patients with more progressive disease [88]. Trials to date have observed response rates that range from 8% to 70% with the use of drugs like streptozocin plus doxorubicin, dacarbazine, temozolomide, or temozolomide in combination with thalidomide, bevacizumab, everolimus, or capecitabine [88].

Clinically, PNETs are vascular tumors and express VEGF proteins, including VEGF-A and VEGFR-2 [88]. Additionally, a Phase III trial using sunitinib demonstrated an improvement in PFS, 11.4 months vs. 5.5 months for placebo (HR 0.42 [0.26-0.66]), with a tumor response rate of 9% vs. 0%. Sunitinib is now FDA approved for the treatment of progressive PNETs. Additional agents tried in Phase II studies include sorafenib, pazopanib, and bevacizumab, with tumor response rates from 9%–22% [88]. There have also been Phase II trials that have combined an mTOR inhibitor with bevacizumab, and these trials have demonstrated higher levels of response compared

to single agent therapy [88]. Temsirolimus with bevacizumab has produced a 41% response rate and a 13.2 month PFS [88]. Everolimus with bevacizumab has produced a 31% response rate and a 16.7 month PFS while everolimus alone produced a 12% response rate and a 14 month PFS (response rate P-value (P)=0.005; PFS HR 0.80 [0.55–1.17], P=0.12) [88]. Overall, surgical resection is the main treatment modality for localized disease, and this along with systemic therapy options including somatostatin analogues, targeted agents, and cytotoxic chemotherapy can be used in advanced disease [88].

1.12 Need for better understanding of angiogenesis in pancreatic cancer

The overwhelming failure of anti-angiogenic agents in PDAC in the clinic leads us to speculate on the reasons for its failure and why other tumor types like PNETs respond. As is often observed in many clinical trials, patient responses are variable, with only a subset of patients benefiting from the therapy, while overall, no positive effect may be seen. Even in the PNET trials, not all patients responded. It would be useful if we could identify those patients who might benefit the most via the use of predictive biomarkers. Though some PDAC trials have attempted to look for correlations between certain known pro-angiogenic molecules circulating in the plasma and treatment response, none have been successful to date [52, 54, 60, 74]. With an increasing number of studies utilizing high throughput technologies like RNA-Seq to profile human tumors, it is possible that a gene expression signature could be used. Therefore, we utilized RNA-Seq data from TCGA to identify novel angiogenic genes and pathways important in subsets of PDAC tumors. While two studies have already utilized transcriptomics to highlight the presence of different PDAC subgroups [90, 91], both studies focused on the whole transcriptome, and only one study attempted to identify corresponding PDAC cell lines representative of that subgroup for testing responses to targeted therapies designed specifically for that subgroup [90]. For the first time, by doing a focused analysis on the expression of angiogenic genes in PDAC tumors, we have identified angiogenesis specific subgroups in hPDAC. We also identified Genetically Engineered Mouse Models (GEMMs) of PDAC that are representative of these subgroups, and we have tested responses to therapy targeting subgroup specific pathways in these models.

2 Results

2.1 Vascularity is heterogeneous among PDAC tumors

To investigate the vascularity of hPDAC tumors, we performed staining of the endothelial specific marker CD31 (gene: PECAM1) in 54 tumors and found that 28% (15/54) of tumors had strong staining (Figure S1), 37% (20/54) had moderate staining (Figure S2), and 35% (19/54) had weak staining (Figure S3) (Figure 2.1A-B). This suggests that while PDAC is hypovascular compared to the normal pancreas, significant heterogeneity still exists between PDAC tumors.

2.2 Identification of a pro-angiogenic gene signature

Because of the failure of anti-VEGF therapy in PDAC clinical trials, we sought to determine if other angiogenic genes or pathways might be important in subsets of PDAC patients. To do this, we decided to use RNA-Seq gene expression information from TCGA. In June of 2014, TCGA contained RNA-Seq gene expression information on 85 pancreatic cancer tumors: 76 PDAC, 3 colloid (mucinous non-cystic) carcinomas, and 6 of an unknown type. One approach to this problem would be to first label samples as to whether they have an angiogenic phenotype or not, and then use supervised machine learning methods on the gene expression data to identify subsets of genes that can differentiate between the two types [92, 93]. However, because all tumors require angiogenesis to grow, we can't label samples based on whether angiogenesis is occurring or not, but we could use phenotypes that score the amount of angiogenesis or the MVD of the tumor. Unfortunately, TCGA does not provide a way to score angiogenesis in the tumors, which might be obtained by quantifying the amount of proliferating ECs in the tumors. CD31 protein expression is available from a reverse phase protein array (RPPA), but as has been mentioned previously, it is not clear whether MVD is a good measure of angiogenesis [37].

Therefore, our real question is whether certain angiogenic genes or pathways might play more of a role in one tumor vs. another. To determine if subsets of TCGA samples might co-express subsets of angiogenic genes, we utilized hierarchical clustering to cluster 384 genes that were annotated to the angiogenesis Gene Ontology (GO) category (Figure 2.2A left). Hierarchical clustering is a common form of unsupervised machine learning, or a type of learning that attempts to cluster input samples into clusters without any predetermined labeling [92, 93]. Hierarchical clustering has been widely used on pre-selected gene lists to identify cancer subtypes and associated gene

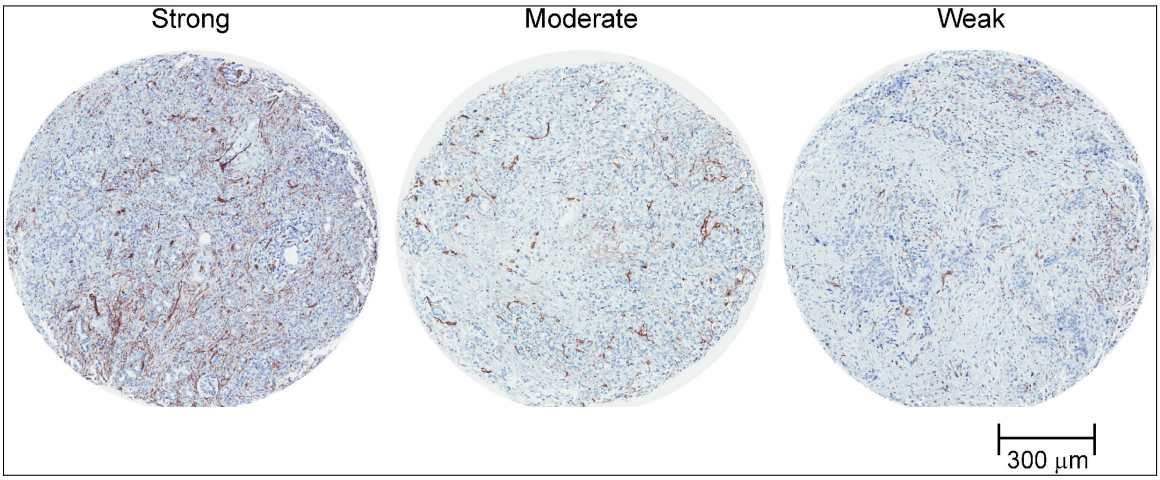

A

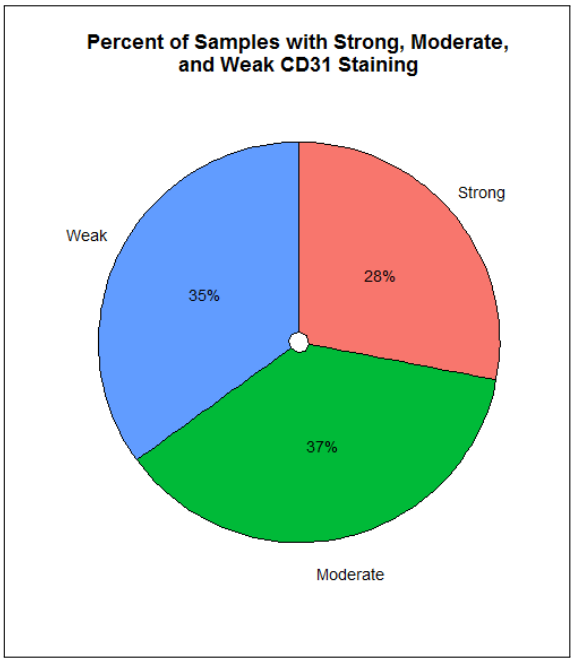

B

Figure 2.1: Vascularity is heterogeneous among PDAC tumors. (A) Representative examples of human PDAC (hPDAC) tissue with strong, moderate, and weak CD31 immunoreactivity. **(B)** CD31 immunoreactivity is strong in 28% (15/54) of PDAC tissues, moderate in 37% (20/54) of PDAC tissues, and weak in 35% (19/54) of PDAC tissues.

signatures [90, 91, 94–98]. From our initial clustering, we observed that there was a group of 129 genes that was up-regulated in a subset of tumors (Figure 2.2A left). To focus our analysis on this subset of genes, we extracted those 129 genes and re-clustered the samples using only this set of genes (Figure 2.2A middle and right). Perou et al. employed a similar analysis when they extracted an "intrinsic" gene subset from their original clustering of highly variable genes in breast cancer samples [94] and then used this "intrinsic" gene set as a starting point in subsequent clustering analyses [95, 98]. While there are other smaller clusters of angiogenic genes not part of the 129 that are up-regulated in the other pancreatic tumor samples (pointing to other angiogenic genes and pathways important in those subsets), we decided to focus our analysis on what could be driving angiogenesis in the subset of tumors that co-express this largest subset of genes. Overall, the presence of a 'strong' pro-angiogenic gene signature consisting of these 129 genes was found in ∼12% (10/85) of pancreatic tumors.

Because additional samples are being added to TCGA over time with a target goal of 500 samples, we have re-validated our previously identified pro-angiogenic gene signature on the updated TCGA sample set of 178 tumors. This updated dataset consists of 135 PDAC tumors, 14 PDAC tumors with varying subtype designations, 4 colloid (mucinous non-cystic) carcinomas, 1 undifferentiated carcinoma, 8 PNETs, and 16 of unknown histological type. Patients with PDAC tumors, colloid carcinomas, or PNETs display varying clinical courses, with PDAC having the worse prognosis [24, 25]. Because PNETs, in contrast to PDAC tumors, are inherently angiogenic and densely vascularized, we decided to focus our analysis on the 135 PDAC samples in combination with the 8 PNET samples [12]. Using our previously determined 129 gene angiogenic signature, hierarchical clustering of RNA-Seq data from these samples revealed that ∼35% (47/135) of PDAC samples now show a 'strong' pro-angiogenic gene signature while ∼47% (64/135) and ∼18% (24/135) show only a 'moderate' or 'weak' signature, respectively (Figure 2.2B). Additionally, the PNET and Strong PDAC groups have a tendency to have higher protein expression of CD31 compared to the Moderate and Weak PDAC groups, though the differences are not statistically significant (analysis of variance (ANOVA) $P = 0.464$) (Figure 2.2C).

2.3 PDACs and PNETs have distinct angiogenesis gene signatures

PDACs and PNETs exhibit an 8% or 53% 5 year survival rate, respectively [24]. Analysis of survival information from TCGA PNET and PDAC groups confirms the favorable outcome of PNET patients over PDAC patients (Kaplan-Meier log-rank

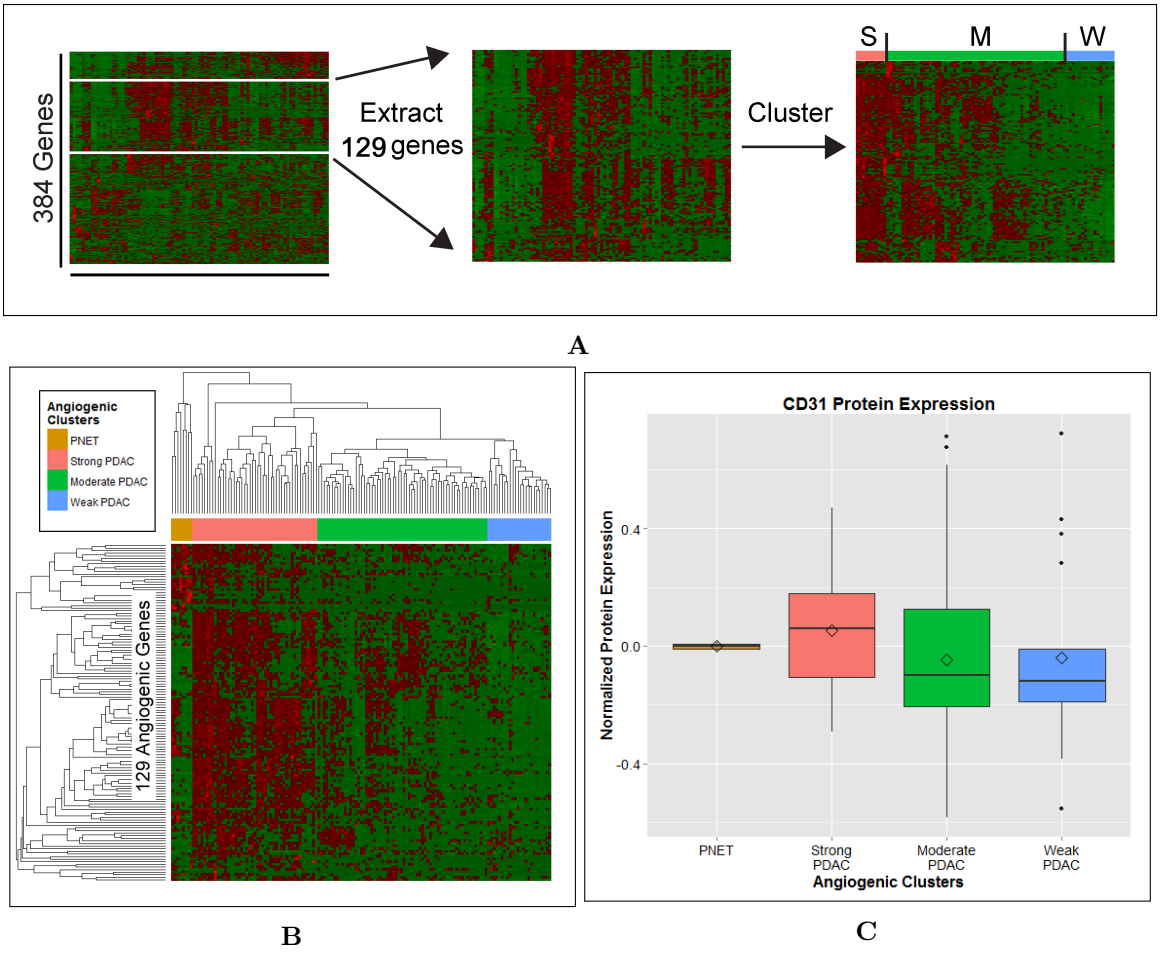

Figure 2.2: PDACs have varying degrees of an angiogenic gene signature. (A) Hierarchical clustering of RNA-Sequencing (RNA-Seq) expression values from 384 genes annotated to the angiogenesis Gene Ontology (GO) term in 85 pancreatic cancer The Cancer Genome Atlas (TCGA) samples (left). Extraction (left: white lines, and middle) and re-clustering (right) of a 129 gene signature up-regulated in a subset of samples (S = strong), whereas some (M = moderate) or few of these genes (W = weak) are increased in other samples. **(B)** Hierarchical clustering of RNA-Seq expression values from 129 angiogenic genes in 8 PNET and 135 PDAC TCGA samples confirms the presence of PDAC subgroups with Strong, Moderate, and Weak expression of these genes (red = up-regulated; green = down-regulated). **(C)** Box plots of TCGA CD31 normalized protein expression values across the different angiogenic cluster groups. The top, midline, and bottom lines of the box represent the 25th, 50th, and 75th percentiles, the diamond represents the mean, the whiskers represent values within 1.5 times the interquartile range, and the dots represent outliers outside that range.

test $P < 0.01$) (Figure 2.3A). There were no observed PNET deaths with a median follow-up of 1410 days, while the Stage IIB patients in the Strong PDAC and Weak PDAC groups had a median survival of 592 and 393 days, respectively (Figure 2.3A). While the difference between the Stage IIB Strong and Weak PDAC groups is not statistically significant (Kaplan-Meier log-rank test $P = 0.17$), there was a trend for the Strong PDAC group to do better (Figure 2.3A). Therefore, this signature is not prognostic, but it remains to be seen whether the signature could predict response to anti-angiogenic therapy as no patients received such therapy (Table 2.1).

Table 2.1: Adjuvant drug treatments

Group	**Drugs**
Strong PDAC	Gemcitabine
	Gemcitabine + Carboplatin
	5-Fluorouracil
	5-Fluorouracil + Folinic acid
	FOLFOX (Folinic acid + 5-Fluorouracil + Oxaliplatin)
	FOLFIRINOX (Folinic acid + 5-Fluorouracil + Irinotecan + Oxaliplatin)
	Capecitabine
	Cisplatin
	Radiation
Weak PDAC	Gemcitabine
	Gemcitabine + nab-paclitaxel
	Gemcitabine + Capecitabine
	5-Fluorouracil
	Capecitabine
	Radiation

To objectively assess genes up-regulated in the Strong PDAC subgroup and to look for overlap with those up-regulated in the PNET subgroup, we conducted a differential expression analysis that compared each of these groups to the Weak PDAC group. Traditionally, with microarrays, this post-clustering analysis would involve the use of algorithms like Significance Analysis of Microarrays (SAM) to identify significant genes within the identified groups [96, 99, 100]. Therefore, we opted to use one of the many available RNA-Seq based algorithms, DESeq [101], to identify significant genes. The differential expression analysis revealed that out of the 129 gene signature, 79 are up-regulated between the Strong and Weak PDAC group and 41 are up-regulated between the PNET and Weak PDAC group (Fold Change (FC) ≥ 1.5, False Discovery Rate (FDR) < 0.05) (Table 2.2). Overall, 31 genes are commonly up-regulated by both groups (FC ≥ 1.5, FDR < 0.05) while 48 or 10 genes are uniquely up-regulated

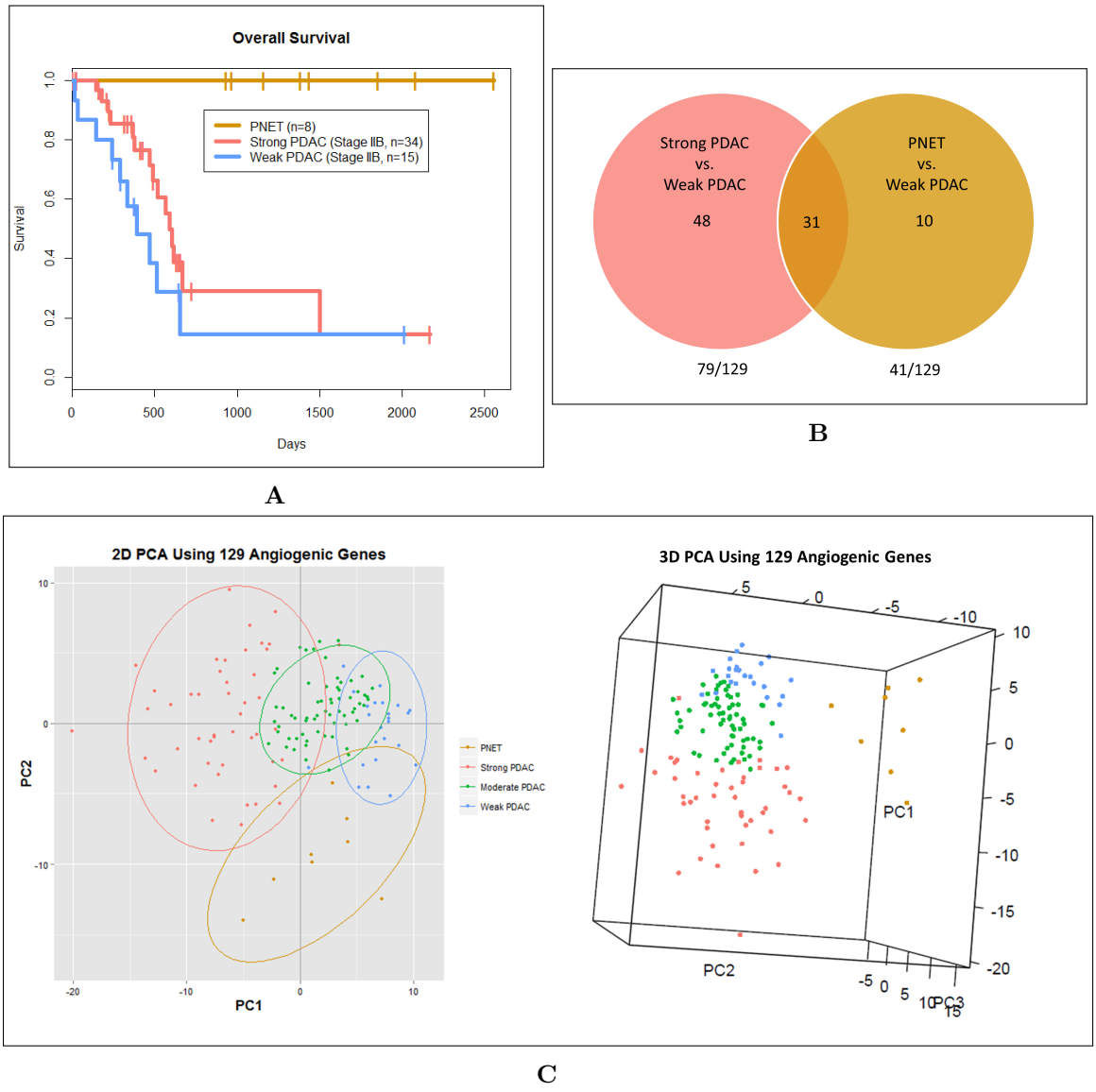

Figure 2.3: PDACs have varying degrees of an angiogenic gene signature that is distinct from pancreatic neuroendocrine tumors (PNETs). (A) Kaplan-Meier survival plot of patients presenting with Stage IIB PDAC and whose tumors express a Strong (n = 34, median: 592 days) or Weak (n = 15, median: 393 days) angiogenic profile shows no significant difference in overall survival (OS) (P-value (P) = 0.17) between the two groups, whereas PNET survival is significantly longer than both PDAC subgroups ($P < 0.01$). **(B)** Differential expression analysis of the 129 genes between the Strong PDAC group vs. the Weak PDAC group and the PNET group vs. Weak PDAC group reveals that 31 angiogenic genes are common to both tumor types, whereas 48 and 10 are unique to Strong PDACs or PNETs, respectively (Fold Change (FC) ≥ 1.5, False Discovery Rate (FDR) < 0.05). **(C)** Two or three dimensional Principal Component Analysis (PCA) of expression values from the 129 angiogenic genes in the 8 PNET and 135 PDAC The Cancer Genome Atlas (TCGA) samples indicates significant variability in the expression of the angiogenic gene signature among the different groups.

in the Strong PDAC or PNET groups, respectively (FC $\geq$ 1.5, FDR $<$ 0.05) (Figure 2.3B, Table 2.2). For example, certain VEGF pathway genes, such as FLT1 (protein: VEGFR-1), KDR (protein: VEGFR-2), or FLT4 (protein: VEGFR-3), were found to be commonly up-regulated by both the Strong PDAC and PNET groups while other genes like ISL1 or SCG2 were uniquely up-regulated in PNETs and ANGPT1, TEK (protein: TIE2), TIE1, HIF1A, EPAS1 (protein: HIF-2α), TGFBR1, TGFBR2, and ACVRL1 were uniquely up-regulated by the Strong PDAC group (Table 2.2). To visualize these results in a different way, the expression values of the 129 genes for all group samples were subjected to Principal Component Analysis (PCA) in order to simplify the variability down to either 2 or 3 principal components (PCs) which could then be visualized on a 2 dimensional or 3 dimensional plane, respectively (Figure 2.3C).

Table 2.2: Expression of 129 angiogenic genes in Strong PDAC and pancreatic neuroendocrine tumor (PNET) vs. Weak PDAC

Entrez Gene ID	Gene Symbol	Strong PDAC vs. Weak PDAC			PNET vs. Weak PDAC		
		Fold Change	P-value	FDR	Fold Change	P-value	FDR
90	ACVR1	1.28	0.134419	0.283918	-1.55	0.053462	0.134242
94	ACVRL1	1.76	0.000104	0.000761	1.06	0.697914	0.84304
118	ADD1	1.20	0.276847	0.482664	1.42	0.093408	0.208904
55109	AGGF1	1.25	0.096651	0.220962	1.47	0.089227	0.201602
183	AGT	-1.21	0.824471	0.936687	37.33	0.085506	0.195078
284	ANGPT1	3.38	4.31E-08	8.07E-07	1.05	0.742976	0.876605
27329	ANGPTL3	1.15	0.92155	1	17.34	0.006417	0.024057
347	APOD	2.07	0.002255	0.01042	-4.75	0.000466	0.002631
350	APOH	1.57	0.725697	0.874353	42.65	0.018246	0.056763
81575	APOLD1	2.87	2.04E-09	5.67E-08	2.74	2.19E-05	0.000179
358	AQP1	1.34	0.017158	0.055445	-2.24	0.050883	0.129064
83478	ARHGAP24	1.31	0.035347	0.099629	-1.22	0.778738	0.904047
577	BAI3	4.25	0.016713	0.054225	47.69	2.18E-06	2.31E-05
168667	BMPER	4.36	0.001766	0.00849	12.06	6.04E-05	0.000439
718	C3	2.10	1.30E-05	0.000124	-9.90	5.24E-12	1.98E-10
719	C3AR1	3.23	2.08E-11	1.04E-09	-1.62	0.032684	0.091125
729	C6	2.32	0.005793	0.022837	-1.03	0.789036	0.911819

PDAC: Pancreatic ductal adenocarcinoma; PNET: Pancreatic neuroendocrine tumor; FDR: False Discovery Rate; 31 genes up-regulated in both Strong PDAC and PNET vs. Weak PDAC; 79 differentially expressed genes in Strong PDAC vs. Weak PDAC (79 up-regulated, 0 down-regulated); 50 differentially expressed genes in PNET vs. Weak PDAC (41 up-regulated, 9 down-regulated); Differential expression cut off: |Fold Change| >= 1.5, FDR < 0.05

Entrez Gene ID	Gene Symbol	Strong PDAC vs. Weak PDAC			PNET vs. Weak PDAC		
		Fold Change	P-value	FDR	Fold Change	P-value	FDR
10203	CALCRL	4.15	3.29E-19	1.72E-16	1.91	0.001772	0.008227
729230	CCR2	5.70	3.24E-13	2.90E-11	-1.83	0.100532	0.220636
947	CD34	2.31	4.65E-09	1.15E-07	1.89	0.001753	0.008154
25932	CLIC4	2.75	5.92E-12	3.47E-10	-1.48	0.066506	0.159899
1215	CMA1	11.66	0.001092	0.005646	1.38	0.379612	0.586507
1306	COL15A1	3.20	2.23E-15	4.01E-13	-1.94	0.006385	0.023948
1285	COL4A3	3.72	0.001814	0.008666	1.11	0.824543	0.939269
1464	CSPG4	1.02	0.75723	0.893452	-1.31	0.447436	0.653026
1524	CX3CR1	2.85	6.95E-06	7.15E-05	2.29	0.014731	0.047777
6387	CXCL12	3.48	2.35E-11	1.16E-09	-1.29	0.983107	1
1545	CYP1B1	7.40	1.51E-29	1.50E-25	-1.37	0.095421	0.211965
57105	CYSLTR2	4.06	0.000438	0.002612	7.66	0.000206	0.001284
23405	DICER1	1.49	0.004659	0.019015	1.66	0.019014	0.058703
641700	ECSCR	1.69	0.004009	0.01686	1.42	0.179689	0.343343
54583	EGLN1	1.00	0.882916	0.976375	-1.16	0.580403	0.749433
2004	ELK3	2.62	1.16E-08	2.57E-07	-1.24	0.340933	0.54456
2028	ENPEP	2.73	2.38E-08	4.86E-07	1.66	0.04932	0.126023
2034	EPAS1	1.65	0.000206	0.001367	1.53	0.028162	0.080727
2047	EPHB1	3.18	0.043333	0.117391	2.63	0.231459	0.412084
51752	ERAP1	1.28	0.068527	0.16901	-1.11	0.624052	0.784646
356	FASLG	2.80	0.051675	0.135245	-1.52	0.642535	0.798728
2254	FGF9	1.94	0.06792	0.167857	3.84	0.006958	0.025646
2260	FGFR1	1.87	1.11E-06	1.43E-05	3.24	3.92E-10	1.02E-08
2263	FGFR2	-1.16	0.420471	0.640822	-17.60	3.68E-16	3.17E-14
2277	FIGF	3.59	0.018226	0.058344	3.28	0.06252	0.15215
2321	FLT1	2.11	1.30E-08	2.83E-07	3.36	1.04E-09	2.43E-08
2324	FLT4	2.46	1.25E-07	2.07E-06	3.77	2.77E-08	4.76E-07
51738	GHRL	1.41	0.288334	0.496086	-6.85	0.052634	0.132638
2702	GJA5	1.87	0.000107	0.000777	-1.03	0.829247	0.943158
10672	GNA13	1.73	0.000231	0.001498	-1.25	0.254681	0.441674
2822	GPLD1	3.50	0.006407	0.024772	21.29	1.37E-06	1.53E-05
25960	GPR124	2.89	1.72E-12	1.21E-10	1.69	0.01807	0.056321
26585	GREM1	3.82	0.00029	0.001829	-3.27	0.016599	0.05258
2969	GTF2I	1.37	0.039113	0.108126	2.22	9.34E-05	0.000647
9421	HAND1	42.99	0.256031	0.456074	26.50	0.196605	0.366146

PDAC: Pancreatic ductal adenocarcinoma; PNET: Pancreatic neuroendocrine tumor; FDR: False Discovery Rate; 31 genes up-regulated in both Strong PDAC and PNET vs. Weak PDAC; 79 differentially expressed genes in Strong PDAC vs. Weak PDAC (79 up-regulated, 0 down-regulated); 50 differentially expressed genes in PNET vs. Weak PDAC (41 up-regulated, 9 down-regulated); Differential expression cut off: |Fold Change| >= 1.5, FDR < 0.05

Entrez Gene ID	Gene Symbol	Strong PDAC vs. Weak PDAC			PNET vs. Weak PDAC		
		Fold Change	P-value	FDR	Fold Change	P-value	FDR
9464	HAND2	2.28	0.000147	0.001022	1.43	0.330874	0.533066
9734	HDAC9	1.82	0.009783	0.034952	1.22	0.512487	0.707316
3087	HHEX	-1.02	0.837256	0.946165	-1.56	0.184215	0.349603
3091	HIF1A	2.01	2.14E-06	2.54E-05	-1.24	0.259919	0.447496
204851	HIPK1	1.63	0.000516	0.003004	1.19	0.388465	0.594742
28996	HIPK2	1.35	0.02309	0.070767	2.66	1.52E-06	1.67E-05
9394	HS6ST1	1.30	0.064347	0.160585	1.12	0.508225	0.705822
3553	IL1B	1.82	0.037926	0.105491	-1.44	0.366107	0.571362
3670	ISL1	1.69	0.178856	0.350616	19.37	1.82E-06	1.97E-05
3685	ITGAV	2.20	1.10E-07	1.86E-06	-2.45	4.19E-05	0.000321
3688	ITGB1	1.68	0.000343	0.002112	-1.41	0.101044	0.22149
83700	JAM3	1.75	0.000241	0.001559	1.61	0.02388	0.070574
3791	KDR	3.04	4.57E-14	5.61E-12	4.37	2.56E-13	1.29E-11
11061	LECT1	1.38	0.560306	0.772961	1.65	0.554378	0.730645
6885	MAP3K7	1.57	0.004483	0.018433	1.10	0.663338	0.814751
4162	MCAM	1.96	2.13E-06	2.54E-05	1.74	0.011287	0.038288
5469	MED1	1.33	0.073878	0.178863	1.19	0.558488	0.733027
4223	MEOX2	3.63	2.35E-08	4.81E-07	-1.08	0.861664	0.966734
79812	MMRN2	2.25	2.82E-08	5.62E-07	1.79	0.003774	0.015521
92140	MTDH	1.34	0.036302	0.101787	-1.21	0.358553	0.563493
80155	NAA15	1.18	0.212152	0.398612	-1.16	0.530401	0.713916
4763	NF1	1.39	0.022444	0.069223	1.47	0.103588	0.225862
4775	NFATC3	1.22	0.140951	0.2946	-1.64	0.064087	0.155272
4881	NPR1	2.48	2.86E-08	5.69E-07	2.63	2.71E-05	0.000217
4897	NRCAM	2.39	1.15E-05	0.000112	13.16	2.44E-15	1.74E-13
8829	NRP1	2.38	8.17E-10	2.59E-08	1.32	0.111065	0.238476
9378	NRXN1	4.30	5.12E-06	5.47E-05	20.78	3.32E-12	1.31E-10
9369	NRXN3	3.83	0.000877	0.004694	12.05	7.04E-06	6.57E-05
116150	NUS1	1.29	0.043239	0.117168	1.03	0.757191	0.887489
55742	PARVA	1.36	0.025279	0.076065	-2.06	0.004041	0.016436
5140	PDE3B	2.34	0.004105	0.017186	5.72	2.92E-05	0.000232
5290	PIK3CA	2.24	1.89E-06	2.27E-05	-1.28	0.31137	0.510688
5294	PIK3CG	5.16	1.46E-12	1.06E-10	-2.09	0.010269	0.035493
5316	PKNOX1	1.13	0.400487	0.619976	1.14	0.441351	0.647094
57125	PLXDC1	1.95	3.71E-05	0.000311	1.53	0.138244	0.281608

PDAC: Pancreatic ductal adenocarcinoma; PNET: Pancreatic neuroendocrine tumor; FDR: False Discovery Rate; 31 genes up-regulated in both Strong PDAC and PNET vs. Weak PDAC; 79 differentially expressed genes in Strong PDAC vs. Weak PDAC (79 up-regulated, 0 down-regulated); 50 differentially expressed genes in PNET vs. Weak PDAC (41 up-regulated, 9 down-regulated); Differential expression cut off: |Fold Change| >= 1.5, FDR < 0.05

Entrez Gene ID	Gene Symbol	Strong PDAC vs. Weak PDAC			PNET vs. Weak PDAC		
		Fold Change	P-value	FDR	Fold Change	P-value	FDR
23129	PLXND1	1.63	0.001399	0.006985	1.27	0.36716	0.572789
23509	POFUT1	1.24	0.100837	0.228037	1.53	0.041843	0.111043
5578	PRKCA	1.03	1	1	-1.81	0.004233	0.017093
5613	PRKX	1.35	0.076365	0.183542	-3.49	1.54E-05	0.000132
84432	PROK1	4.43	0.110425	0.244269	-1.46	1	1
60675	PROK2	2.95	0.433556	0.654636	-1.97	0.831581	0.94463
5728	PTEN	1.57	0.000789	0.004287	-1.04	0.943968	1
5787	PTPRB	2.19	1.37E-07	2.22E-06	2.66	1.21E-05	0.000106
5797	PTPRM	1.76	8.35E-05	0.00063	2.64	8.02E-07	9.52E-06
10266	RAMP2	1.50	0.003989	0.016798	1.83	0.004153	0.016826
6091	ROBO1	3.82	1.68E-16	4.23E-14	-1.17	0.463909	0.668963
54538	ROBO4	1.97	6.59E-06	6.84E-05	2.79	2.22E-06	2.35E-05
6093	ROCK1	1.67	0.001488	0.007347	-1.09	0.542624	0.722145
9475	ROCK2	1.74	0.000324	0.002018	-1.49	0.081406	0.187464
6095	RORA	2.53	4.57E-09	1.13E-07	1.88	0.004834	0.019105
1901	S1PR1	3.52	2.73E-16	6.45E-14	1.65	0.013022	0.043103
23328	SASH1	2.69	1.71E-10	6.53E-09	2.27	1.61E-05	0.000137
7857	SCG2	3.51	0.057532	0.147316	65.37	7.42E-06	6.87E-05
9723	SEMA3E	3.64	0.000257	0.001651	4.75	0.001244	0.006095
29072	SETD2	1.32	0.051775	0.135422	1.22	0.301772	0.499009
6422	SFRP1	9.57	4.36E-07	6.22E-06	29.50	1.53E-09	3.46E-08
23411	SIRT1	1.67	0.001562	0.00765	1.24	0.358061	0.562989
9990	SLC12A6	1.42	0.038293	0.10623	-1.08	0.662316	0.81414
9353	SLIT2	8.61	1.44E-22	1.90E-19	2.52	0.002719	0.011783
6722	SRF	1.15	0.357784	0.575258	-1.12	0.67388	0.823416
6733	SRPK2	1.49	0.006965	0.026514	2.14	0.00067	0.00359
23166	STAB1	2.29	2.32E-08	4.76E-07	1.19	0.527104	0.712285
6886	TAL1	2.52	0.000161	0.001104	2.60	0.004552	0.018169
7010	TEK	3.74	1.13E-14	1.57E-12	1.65	0.026744	0.077372
7046	TGFBR1	1.53	0.00904	0.032787	-1.02	0.751031	0.883048
7048	TGFBR2	1.86	4.36E-05	0.000356	-1.56	0.018017	0.056204
7060	THBS4	5.55	7.95E-11	3.27E-09	1.98	0.068252	0.163316
221981	THSD7A	4.72	7.58E-11	3.14E-09	-1.08	0.708204	0.850732
7075	TIE1	2.21	1.46E-07	2.35E-06	1.58	0.026074	0.075776
55273	TMEM100	3.80	4.42E-05	0.00036	5.52	0.000318	0.001886

PDAC: Pancreatic ductal adenocarcinoma; PNET: Pancreatic neuroendocrine tumor; FDR: False Discovery Rate; 31 genes up-regulated in both Strong PDAC and PNET vs. Weak PDAC; 79 differentially expressed genes in Strong PDAC vs. Weak PDAC (79 up-regulated, 0 down-regulated); 50 differentially expressed genes in PNET vs. Weak PDAC (41 up-regulated, 9 down-regulated); Differential expression cut off: |Fold Change| >= 1.5, FDR < 0.05

Entrez Gene ID	Gene Symbol	Strong PDAC vs. Weak PDAC			PNET vs. Weak PDAC		
		Fold Change	P-value	FDR	Fold Change	P-value	FDR
164656	TMPRSS6	-1.49	0.641486	0.833109	23.17	0.02359	0.069884
23554	TSPAN12	1.00	0.885861	0.978542	3.37	0.000204	0.001275
7342	UBP1	1.19	0.231426	0.42474	-1.16	0.564326	0.736234
22846	VASH1	2.06	1.72E-06	2.10E-05	3.61	2.33E-09	5.06E-08
10451	VAV3	1.56	0.068866	0.169688	2.21	0.035368	0.09703
7716	VEZF1	1.33	0.033594	0.095708	1.73	0.007181	0.026347
10163	WASF2	1.58	0.001278	0.006463	-1.17	0.490966	0.692833

PDAC: Pancreatic ductal adenocarcinoma; PNET: Pancreatic neuroendocrine tumor; FDR: False Discovery Rate; 31 genes up-regulated in both Strong PDAC and PNET vs. Weak PDAC; 79 differentially expressed genes in Strong PDAC vs. Weak PDAC (79 up-regulated, 0 down-regulated); 50 differentially expressed genes in PNET vs. Weak PDAC (41 up-regulated, 9 down-regulated); Differential expression cut off: |Fold Change| >= 1.5, FDR < 0.05

To further delineate the differences between these two groups, the 10 unique PNET genes, 48 unique Strong PDAC genes, and the 31 common genes were analyzed using GeneMANIA to identify which of these gene products participate in the same pathway (Figure 2.4, black: common genes, pink: unique to Strong PDAC, mustard: unique to PNET) [102]. After removal of any unconnected genes from the network, it was found that in addition to up-regulation of VEGF pathway genes, PDACs and PNETs also commonly up-regulate FGFR1, S1PR1, and PTPRB (Figure 2.4). S1P is a pro-angiogenic sphinogolipid that is known to act through S1PR1 [103] while PTPRB has been shown to regulate the spreading and migration of ECs during angiogenesis [104].

However, these commonly up-regulated gene products are only highly connected to one another via angiogenic molecules that are uniquely up-regulated in PDAC (Figure 2.4). Very few connections are found between the gene products that are uniquely up-regulated in PNETs, suggesting that such connections are still unknown. PDACs also up-regulate many other highly connected pro-angiogenic genes, including TGFBR1, TGFBR2, HIF1A, ANGPT1, and several integrins/collagens (ITGAV, ITGB1, COL4A3, COL15A1).

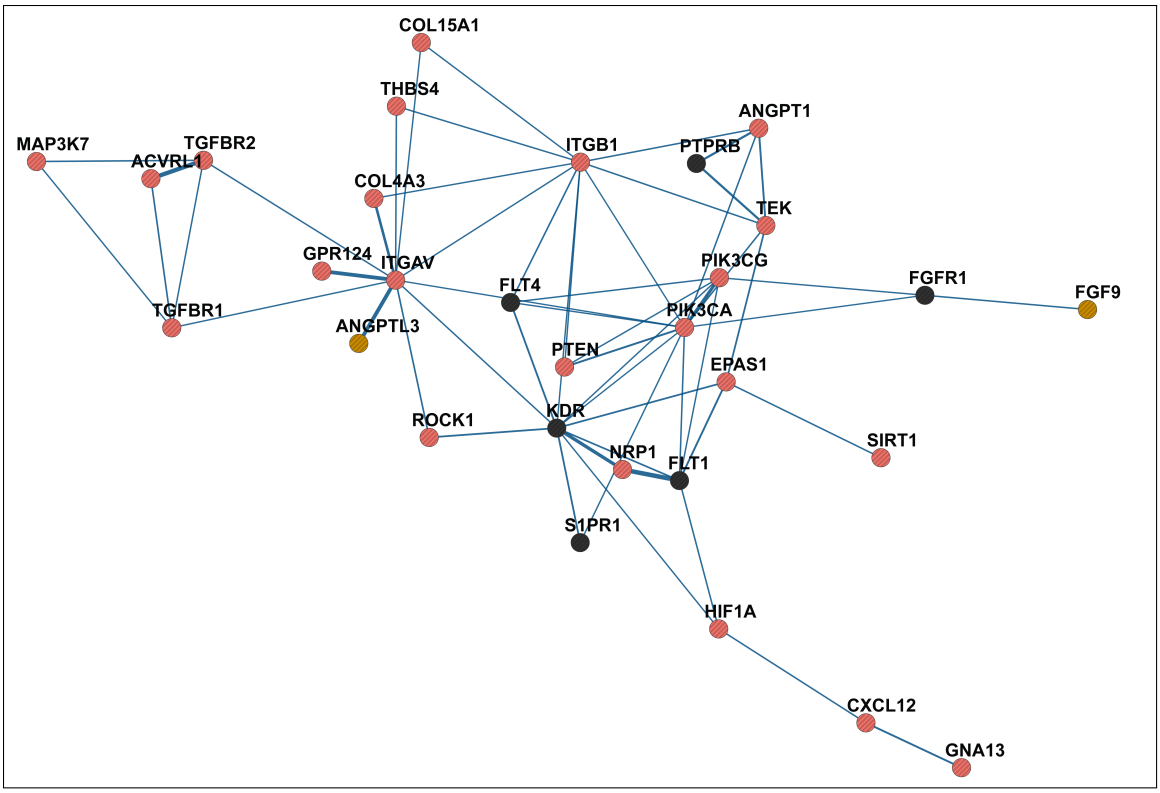

Figure 2.4: Interconnectivity of angiogenesis genes unique to the Strong PDAC group, unique to PNETs, or common to both. After GeneMANIA pathway analysis of 48, 10, and 31 genes uniquely up-regulated in the Strong PDAC group, the PNET group, or common between them, respectively, 22, 2, and 6 interconnected angiogenesis related genes remain. Common genes (black) are dominated by vascular endothelial growth factor (VEGF) pathway members, while genes unique to the Strong PDAC group (pink) also involve integrins, collagens, HIF1A, and TGF-β related pathway members. Genes unique to PNET (mustard) do not have known pathway connections except for ANGPTL3 and FGF9.

2.4 Isolated PDAC mutations do not explain the presence of an angiogenic gene signature

To determine if the different angiogenic groups are associated with a specific mutational burden, we gleaned curated mutation data from TCGA dataset which includes information on 98 PDAC and 3 PNET cases. Overall, PDACs exhibit more non-silently mutated genes (median = 47) than PNETs (median = 19) (P = 0.0232, Wilcoxon rank sum test) (Figure 2.5A). Additionally, the PNET (median = 19), Strong PDAC (median = 40), Moderate PDAC (median = 48), and Weak PDAC (median = 64) groups differ significantly (P = 0.0003, Kruskal-Wallis rank sum test) (Figure 2.5A). Specifically, the Strong and Weak PDAC group are significantly different (P =

0.0038, post-hoc Wilcoxon rank sum test with Bonferroni correction) as well as the PNET and Moderate PDAC group (P = 0.0442, post-hoc Wilcoxon rank sum test with Bonferroni correction).

KRAS (86%, 84/98), TP53 (55%, 54/98), SMAD4 (19%, 19/98), and CDKN2A (19%, 19/98) were four of the five most frequently mutated genes across the PDAC samples (Figure 2.5A, Table 2.3), and except for KRAS, their mutation frequencies are consistent with recent PDAC genome sequencing studies (KRAS 92-100%, TP53 33-84%, SMAD4 16-33%, CDKN2A 2-24%) [27, 28, 105, 106]. Because SMAD4 [107–109] and CDKN2A [110] are often altered via deletion in addition to mutation, analysis of TCGA copy number data indicated that SMAD4 and CDKN2A are also deleted in 14% (19/134) and 26% (35/134) of PDAC samples, respectively (Figure 2.5B). TTN, which codes for a giant muscle protein consisting of ∼27,000 to ∼33,000 amino acids depending on the isoform, was also found to be one of the top five most frequently mutated genes (20.4%, 20/98) in PDAC (Figure 2.5A, Table 2.3). However, due to its massive size, lack of potential cancer causing role, and frequent mutation in other cancer genome studies, it is often considered to be a false positive [111, 112]. To determine if a mutation in any single gene could explain the expression of the angiogenic gene signature, the mutation frequencies of all genes were compared between the Strong and Weak PDAC groups. This showed that only one gene, KBTBD6, differed significantly between the two groups, with 0/41 mutations in the Strong PDAC group and 5/19 (26%) mutations in the Weak PDAC group ($P < 0.05$) (Table 2.3). KBTBD6 is a substrate adaptor in an E3 CUL3 RING ubiquitin ligase complex that so far has only been shown to mediate ubiquitination and proteasomal degradation of TIAM1, a RAC1 specific guanine exchange factor (GEF) [113]. KBTBD6 currently has no known angiogenic role, but it is likely to be involved in the proteasomal degradation of other proteins which theoretically could have such a role.

2.5 TGF-β is an upstream regulator of genes from the angiogenic gene signature

To determine other potential drivers of the angiogenic gene signature, we subjected the 79 differentially expressed angiogenesis genes from the signature to Ingenuity Pathway Upstream Regulator Analysis and identified TGF-β as a major upstream regulator of 17 of the 79 genes (P = 1.17E-11) (Table 2.4). Because this suggests that the Strong PDAC group might exhibit a TGF-β signaling signature, we identified a set of 188 TGF-β responsive genes from the TGFB_UP.V1_UP gene set from the

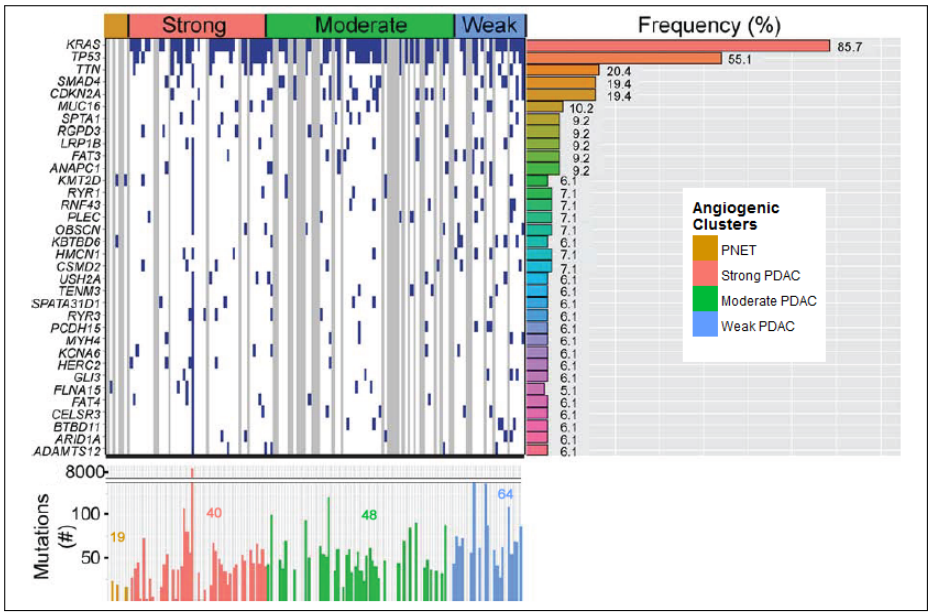

A

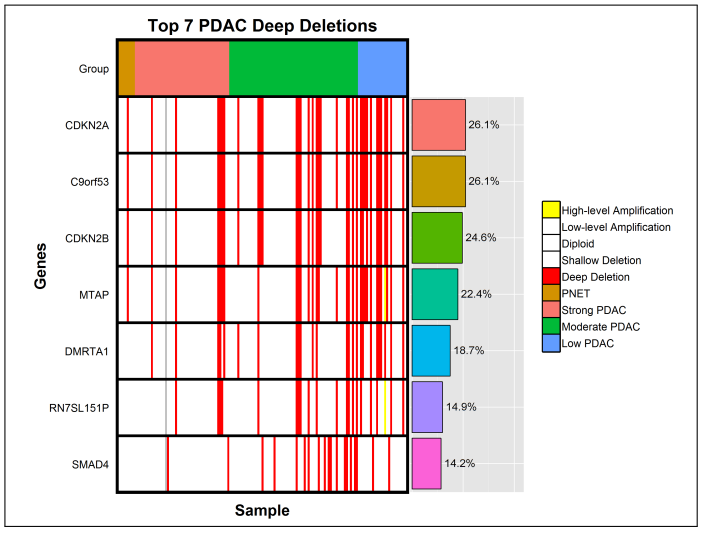

B

Figure 2.5: Median mutation counts and frequently mutated or deleted genes in PDAC. **(A)** The top 34 non-silently mutated genes that appear with a frequency of 6% or more in the 3 PNET + 98 PDAC cases combined are listed on the left while their mutation frequencies in PDAC alone are graphed to the right. Samples (left) appear in the same order as the angiogenic cluster analysis with (top) blue indicating a non-silently mutated gene, white a silently mutated or wild type (WT) gene, and gray a sample lacking mutation data. Total counts (below) of non-silently mutated genes in 3 PNET and 98 PDAC samples were graphed with median counts as follows: PNET: 19, PDAC: 47, Strong PDAC: 40, Moderate PDAC: 48, Weak PDAC: 64. **(B)** (Left) Distribution of the top 7 PDAC deep deletions across the different PNET and PDAC angiogenic groups (8 PNET and 134 of 135 PDAC samples had copy number data. The missing PDAC sample is shown in gray). Several samples show deletion of many of these genes due to the top 6 genes appearing within the same cytoband. (Right) Frequency of the top 7 PDAC genes with deep deletions. Frequency is shown as overall percent of deletion in the 134 samples with copy number data.

Table 2.3: Mutation frequency in PNET and PDAC angiogenic groups

Gene Symbol	Total # Mutated	Total # Sequenced	Total % Mutated	PNET # Mutated	PNET # Sequenced	PNET % Mutated	PDAC # Mutated	PDAC # Sequenced	PDAC % Mutated	Strong PDAC # Mutated	Strong PDAC # Sequenced	Strong PDAC % Mutated	Moderate PDAC # Mutated	Moderate PDAC # Sequenced	Moderate PDAC % Mutated	Low PDAC # Mutated	Low PDAC # Sequenced	Low PDAC % Mutated
KRAS	84	101	83.17	0	3	0	84	98	85.71	33	41	80.49	36	38	94.74	15	19	78.95
TP53	54	101	53.47	0	3	0	54	98	55.1	19	41	46.34	26	38	68.42	9	19	47.37
TTN	20	101	19.8	0	3	0	20	98	20.41	8	41	19.51	6	38	15.79	6	19	31.58
SMAD4	19	101	18.81	0	3	0	19	98	19.39	4	41	9.76	9	38	23.68	6	19	31.58
CDKN2A	19	101	18.81	0	3	0	19	98	19.39	2	41	4.88	14	38	36.84	3	19	15.79
MUC16	10	101	9.9	0	3	0	10	98	10.2	4	41	9.76	3	38	7.89	3	19	15.79
SPTA1	9	101	8.91	0	3	0	9	98	9.18	3	41	7.32	4	38	10.53	2	19	10.53
RGPD3	9	101	8.91	0	3	0	9	98	9.18	4	41	9.76	4	38	10.53	1	19	5.26
LRP1B	9	101	8.91	0	3	0	9	98	9.18	3	41	7.32	3	38	7.89	3	19	15.79
FAT3	9	101	8.91	0	3	0	9	98	9.18	2	41	4.88	4	38	10.53	3	19	15.79
ANAPC1	9	101	8.91	0	3	0	9	98	9.18	2	41	4.88	4	38	10.53	3	19	15.79
KMT2D	8	101	7.92	2	3	66.67	6	98	6.12	2	41	4.88	2	38	5.26	2	19	10.53
RYR1	7	101	6.93	0	3	0	7	98	7.14	2	41	4.88	3	38	7.89	2	19	10.53
RNF43	7	101	6.93	0	3	0	7	98	7.14	1	41	2.44	3	38	7.89	3	19	15.79
PLEC	7	101	6.93	0	3	0	7	98	7.14	2	41	4.88	3	38	7.89	2	19	10.53
OBSCN	7	101	6.93	0	3	0	7	98	7.14	3	41	7.32	2	38	5.26	2	19	10.53
KBTBD6	7	101	6.93	1	3	33.33	6	98	6.12	0	41	0	1	38	2.63	5	19	26.32
HMCN1	7	101	6.93	0	3	0	7	98	7.14	3	41	7.32	1	38	2.63	3	19	15.79
CSMD2	7	101	6.93	0	3	0	7	98	7.14	3	41	7.32	2	38	5.26	2	19	10.53
USH2A	6	101	5.94	0	3	0	6	98	6.12	3	41	7.32	2	38	5.26	1	19	5.26
TENM3	6	101	5.94	0	3	0	6	98	6.12	1	41	2.44	4	38	10.53	1	19	5.26
SPATA31D1	6	101	5.94	0	3	0	6	98	6.12	3	41	7.32	2	38	5.26	1	19	5.26
RYR3	6	101	5.94	0	3	0	6	98	6.12	4	41	9.76	2	38	5.26	0	19	0
PCDH15	6	101	5.94	0	3	0	6	98	6.12	1	41	2.44	2	38	5.26	3	19	15.79
MYH4	6	101	5.94	0	3	0	6	98	6.12	2	41	4.88	2	38	5.26	2	19	10.53
KCNA6	6	101	5.94	0	3	0	6	98	6.12	3	41	7.32	2	38	5.26	1	19	5.26
HERC2	6	101	5.94	0	3	0	6	98	6.12	5	41	12.2	1	38	2.63	0	19	0
GLI3	6	101	5.94	0	3	0	6	98	6.12	2	41	4.88	1	38	2.63	3	19	15.79
FLNA	6	101	5.94	1	3	33.33	5	98	5.1	3	41	7.32	2	38	5.26	0	19	0
FAT4	6	101	5.94	0	3	0	6	98	6.12	4	41	9.76	2	38	5.26	0	19	0
CELSR3	6	101	5.94	0	3	0	6	98	6.12	2	41	4.88	2	38	5.26	2	19	10.53
BTBD11	6	101	5.94	0	3	0	6	98	6.12	1	41	2.44	2	38	5.26	3	19	15.79
ARID1A	6	101	5.94	0	3	0	6	98	6.12	3	41	7.32	1	38	2.63	2	19	10.53
ADAMTS12	6	101	5.94	0	3	0	6	98	6.12	3	41	7.32	2	38	5.26	1	19	5.26

PNET: Pancreatic neuroendocrine tumor, PDAC: Pancreatic ductal adenocarcinoma, #: Number, %: Percent

Gene Set Enrichment Analysis (GSEA) Molecular Signatures Database (MSigDB) in order to query their expression values across the different PDAC samples. This gene set represents genes up-regulated in a panel of epithelial cell lines by TGF-β. From this gene set, two genes, FLT4 and ELK3, were already a part of the angiogenic gene signature, and were thus removed from the gene set to avoid any overlap with the existing angiogenesis analysis. To visualize the expression of the remaining 186 TGF-β responsive genes across the different PDAC samples, we performed hierarchical clustering of the genes while preserving the order of the patient samples according to how they clustered in the angiogenesis analysis (Figure 2.6A).

Table 2.4: Angiogenic TGF-β responsive genes

Gene Symbol	Gene Name
TGFBR2	transforming growth factor beta receptor II
TGFBR1	transforming growth factor beta receptor I
RORA	RAR related orphan receptor A
RAMP2	receptor (G protein-coupled) activity modifying protein 2
NRP1	neuropilin 1
ITGB1	integrin subunit beta 1
ITGAV	integrin subunit alpha V
HIF1A	hypoxia inducible factor 1 alpha subunit
GREM1	gremlin 1, DAN family BMP antagonist
GNA13	guanine nucleotide binding protein (G protein), alpha 13
FLT1	fms related tyrosine kinase 1 (protein: VEGFR-1)
FGFR1	fibroblast growth factor receptor 1
ELK3	ELK3, ETS transcription factor
CLIC4	chloride intracellular channel 4
CCR2	chemokine (C-C motif) receptor 2
C3AR1	complement component 3a receptor 1
ACVRL1	activin A receptor type IL

From this analysis, it is clear that the Strong PDAC group up-regulates a subset of TGF-β target genes compared to the Moderate or Weak PDAC groups (Figure 2.6A). To determine which of these genes meets statistical significance, differential expression analysis between the Strong and Weak PDAC groups confirms that 50

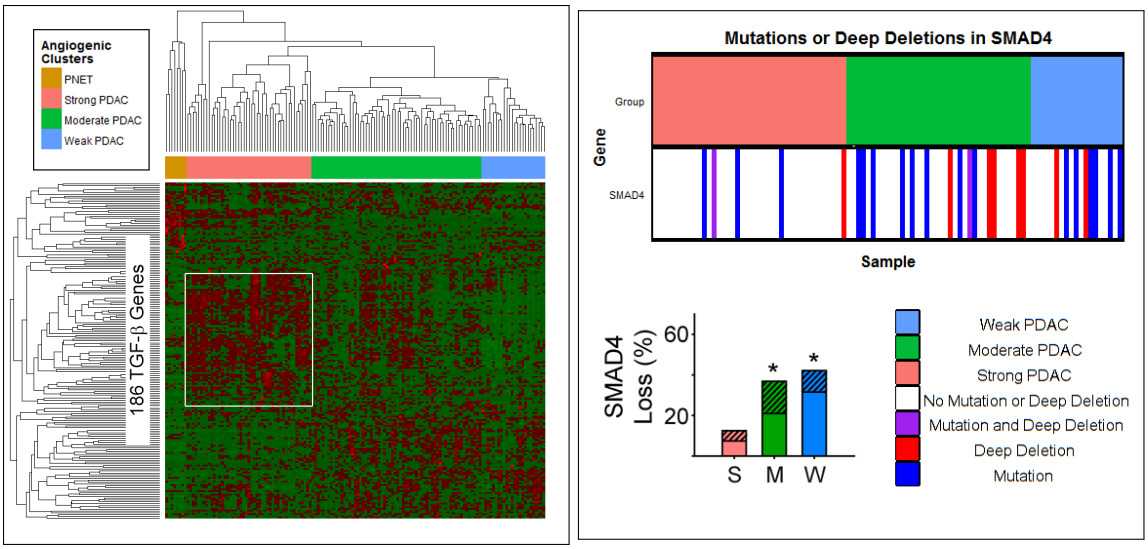

A **B**

Figure 2.6: Angiogenic gene signature correlates with increased expression of TGF-β target genes and wild type (WT) SMAD4. (A) While preserving the order of the 8 PNET and 135 PDAC The Cancer Genome Atlas (TCGA) patient samples according to the angiogenesis cluster analysis, hierarchical clustering of TCGA RNA-Sequencing (RNA-Seq) expression values from 186 TGF-β responsive genes indicates that a subset of TGF-β target genes (white box) is up-regulated in the Strong PDAC group (red = up-regulated; green = down-regulated). **(B)** (Top) Distribution of SMAD4 mutations or deletions across the clustered TCGA samples. (Bottom) Overall SMAD4 loss by mutation or deletion was significantly higher in the Moderate (M) (37%) and Weak (W) (42%) PDAC subgroups compared with the Strong (S) (13%) PDAC subgroup. Stacked bars show the total percent of patients in each subgroup with SMAD4 mutations (solid bars) or deletions (hatched bars) (*P-value (P) < 0.05).

TGF-β target genes are up-regulated, including pro-angiogenic CTGF (FC 3.33, FDR 1.86E-06) and ITGA5 (FC 1.88, FDR 0.007113) (Table S1). Additionally, TGFB3, but not TGFB1 or TGFB2, is up-regulated in the Strong PDAC group (FC 3.40, FDR 1.31E-10). Analysis of PDAC tissues has also shown that there is an abundance of phosphorylated SMAD2 (p-SMAD2) in pancreatic cancer cell (PCC) and stromal cell nuclei [114].

Since SMAD4 is a critical mediator of TGF-β signaling that is often inactivated by mutation or deletion in PDAC, we investigated its mutation or copy number status across the different PDAC groups and found that it was only altered in 13% of cases in the Strong PDAC group, but in 37% and 42% of cases in the Moderate and Weak PDAC groups, respectively (Figure 2.6B). This inactivation rate in the Strong PDAC group is significantly different from the rate in the Moderate (P = 0.017261) and Weak (P = 0.017587) PDAC groups and supports the finding of active TGF-β signaling in the Strong PDAC group.

Because immunohistochemical staining or immunoblotting of SMAD4 protein has been shown to correlate with its wild type (WT) status [109] and TCGA has protein array information on SMAD4 and CD31, we did a correlation analysis between SMAD4 and CD31 protein expression in TCGA samples (Figure 2.7A). We found that SMAD4 and CD31 protein expression is significantly correlated with a correlation coefficient of +0.70 (P = 2.60e-14) for all samples, and a correlation coefficient of +0.72 (P = 1.20e-14) for just the PDAC samples.

To confirm these findings, we assessed SMAD4 and CD31 protein expression in a tissue microarray (TMA) of 54 hPDAC tissues using CD31 and WT SMAD4 detecting antibodies (Figure 2.7B) [109]. Nuclear SMAD4 was present in the cancer cell nuclei of 23 PDACs in which CD31-positive ECs and vessels were abundant (Figure 2.7B). By contrast, wild-type SMAD4 immunoreactivity was not detectable in the cancer cells in 31 PDACs, and in these tissues CD31 immunoreactivity was sparse (Figure 2.7B). These data therefore suggest that the presence of wild-type SMAD4 in PCCs correlates with EC abundance.

2.6 PDACs with an angiogenesis gene signature are enriched in inflammation related genes

To identify additional pathways active in the Strong PDAC group vs. the Weak PDAC group, we subjected a ranked list of genes sorted by their FC differences between the two groups to GSEA. GSEA indicated that the Strong PDAC group is dominated by expression of inflammatory genes as evidenced by major overlap with hallmark genes involved in transplant rejection (Figure 2.8A) or the inflammatory response (Figure 2.8B). Moreover, leading edge analysis of these GSEAs indicated that genes up-regulated in the Strong PDAC group include both pro-inflammatory members, such as CD28, IL6, JAK2, CCR7, LTA, OSMR, and TLR2, and anti-inflammatory members, such as SOCS3, IL2RA, and MEFV.

To further explore this balance between pro- and anti-inflammatory molecules, gene expression values for 85 positive regulators and 81 negative regulators of the inflammatory response were visualized using hierarchical clustering of the genes while preserving the order of the patient samples according to how they clustered in the angiogenesis analysis (Figure 2.9A). This analysis indicates that many more positive regulators are up-regulated than negative regulators in the Strong PDAC group (Figure 2.9A). Differential expression analysis confirms that 28 positive regulators are up-regulated compared to only 16 negative regulators in the Strong PDAC group vs. the

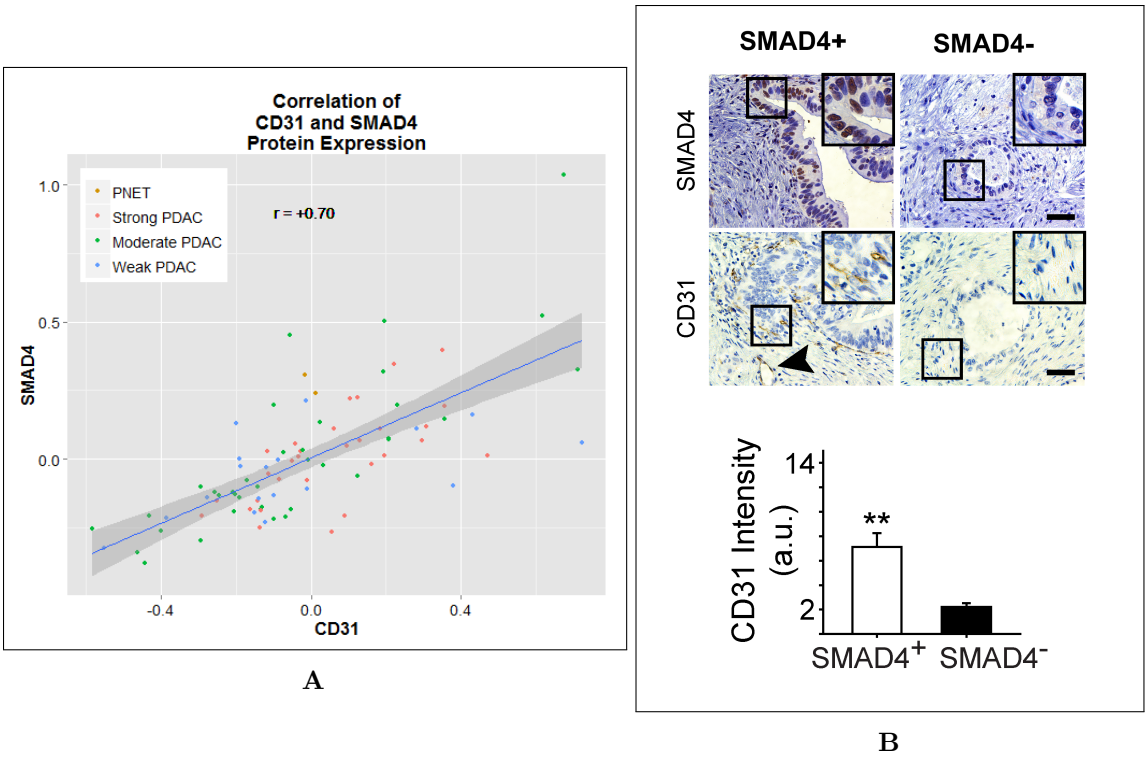

Figure 2.7: Correlation of CD31 and SMAD4 protein expression. (A) Analysis of protein expression data from The Cancer Genome Atlas (TCGA) shows that SMAD4 and CD31 levels correlate in pancreatic cancer (PNET+PDAC: r = +0.70, PDAC: r = +0.72, P-value (P) < 0.01). **(B)** (Top) Representative images of the SMAD4 and CD31 immunostaining on the tissue microarray (TMA) shows that CD31 positive endothelial cells (ECs) and vessels (arrowhead) are present in PDACs with SMAD4 immunoreactivity in the pancreatic cancer cells (PCCs) (left panels), whereas in SMAD4 negative tumors, CD31 immunoreactivity is rarely present (right panels). Insets show magnified images of boxed areas. Scale bars 50 μm. (Bottom) Quantification of CD31 and SMAD4 immunostaining of a human PDAC (hPDAC) TMA shows that in SMAD4 positive tumors (open bar), CD31 immunoreactivity is significantly higher than in SMAD4 negative tumors (closed bar) (**P < 0.01).

Weak PDAC group (FC >= 1.5, FDR < 0.05) (Table S2 and S3). Additionally, only 7 positive regulators are down-regulated while 17 negative regulators are down-regulated (FC <= −1.5, FDR < 0.05) (Table S2 and S3).

Additional investigation of these inflammatory gene lists revealed up-regulation of several genes related to the IL6–JAK–STAT3 signaling pathway, including IL6, both components of the IL6 signaling complex, IL6R and IL6ST, as well as JAK2 and another IL6 family member, OSMR, that can transduce signals through STAT3. Moreover, analysis of additional known JAK–STAT pathway genes revealed that 40 additional genes in this pathway are up-regulated including JAK1, JAK3, STAT1, STAT4, PIAS2, and 4 different SOCS genes (Figure 2.9B, Table S4).

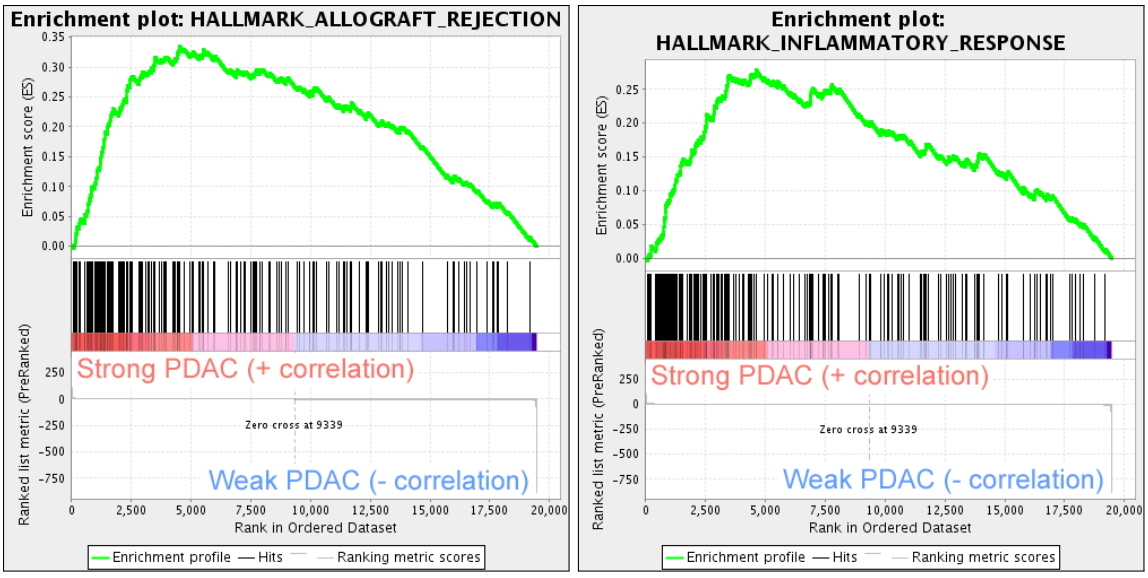

A **B**

Figure 2.8: Angiogenic PDACs also demonstrate an inflammatory profile. (A) Gene Set Enrichment Analysis (GSEA) indicates that genes up-regulated during transplant rejection correlate with genes up-regulated in the Strong PDAC subgroup when compared to the Weak PDAC subgroup (family-wise error rate (FWER) < 0.001). **(B)** GSEA indicates that genes up-regulated during the inflammatory response correlate with genes up-regulated in the Strong PDAC subgroup when compared to the Weak PDAC subgroup (FWER < 0.001).

2.7 TGF-β receptor type-1 and JAK inhibition blocks angiocrine effects

Our findings indicate that PDACs in the Strong PDAC subgroup are associated with increased expression of TGF-β target genes and an inflammation signature in which several pro-inflammatory genes, including JAK1 and JAK2 were increased. Moreover, the Strong PDAC group expresses wild-type SMAD4 protein that correlates with CD31 levels. Therefore, we next sought to determine whether inhibition of the TGF-β receptor type-1 (gene: TGFBR1) and/or JAK signaling pathways can block angiogenic effects. We used the well-known PANC-1 human PCCs, as well as our recently established IUSCC-PC1 cell line in 3-dimensional (3D) co-cultures with non-immortalized human vascular endothelial cells (HUVECs). Both PANC-1 cells and IUSCC-PC1 cells harbor mutated KRAS ($KRAS^{G12D/+}$) and express wild-type SMAD4 as determined by DNA sequencing. Importantly, establishing new PCCs diminishes the potential for additional mutations and clonal selections that may arise from serial *in vivo* and *in vitro* passaging. Thus, IUSCC-PC1 cells were used to confirm findings with PANC-1 cells which were established in 1975 [115].

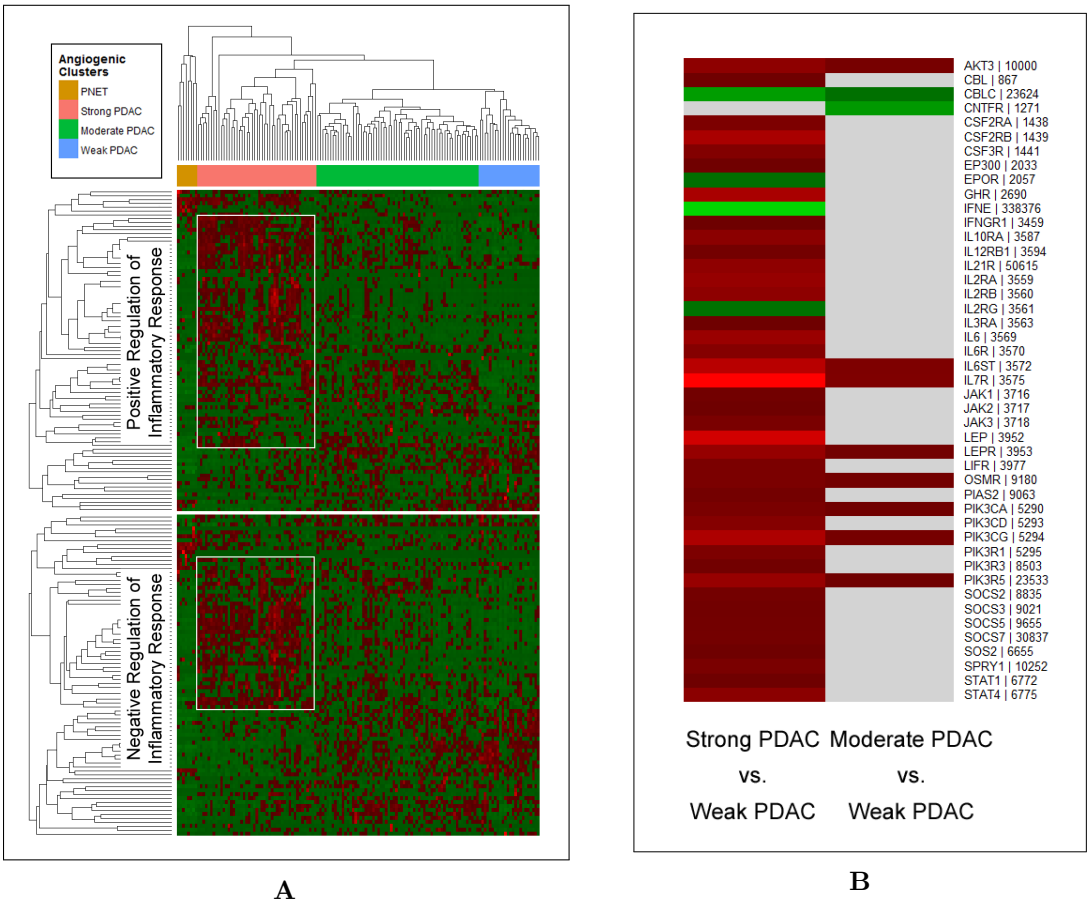

Figure 2.9: Angiogenic PDACs exhibit up-regulation of both pro-inflammatory and anti-inflammatory molecules and are enriched in JAK/STAT signaling genes. (A) While preserving the order of the 8 PNET and 135 PDAC The Cancer Genome Atlas (TCGA) patient samples according to the angiogenesis cluster analysis, hierarchical clustering of RNA-Sequencing (RNA-Seq) expression values from 85 positive (top) or 81 negative (bottom) regulators of inflammation indicates that the Strong PDAC subgroup up-regulates subsets (white boxes) of both positive and negative regulators of inflammation (red = up-regulated; green = down-regulated). Differential expression analysis reveals up-regulation of 28 positive and 16 negative regulators of inflammation and down-regulation of 7 positive and 17 negative regulators of inflammation, suggesting a tipping of the scale to a pro-inflammatory environment (|Fold Change (FC)| >= 1.5, False Discovery Rate (FDR) < 0.05). **(B)** Compared with the Weak PDAC group, 40 or 8 JAK/STAT signaling pathway genes are up-regulated in the Strong or Moderate PDAC groups, respectively (FC >= 1.5, FDR < 0.05) (red = up-regulated; green = down-regulated; gray = not differentially expressed).

To monitor changes in the growth for each cell type in the co-culture studies, PCCs and HUVECs were labeled with green and red fluorescence, respectively. By comparison to 3D cultures in which PCCs and HUVECs were cultured separately (Figure 2.10A (DMSO rows, PCC and EC columns) and 2.10B), IUSCC-PC1 and PANC-1 cell proliferation was significantly enhanced by co-culture with HUVECs (Figure 2.10A (DMSO rows, merged column) and 2.10B). Moreover, HUVEC proliferation was enhanced in co-cultures with either PCC line (Figure 2.10A (DMSO rows, merged column) and 2.10B). These mitogenic effects were completely blocked by the combination of the JAK1/JAK2 inhibitor, ruxolitinib [100 nM], and the TGF-β receptor type-1 inhibitor, SB505124 [2 μM] (Figure 2.10A (DMSO vs. SB+Rux rows, merged column) and 2.10B), but not by either inhibitor alone [100 nM ruxolitinib or 2 μM SB505124] (Figure 2.10B). These results therefore suggest that human PCCs exert growth-promoting angiogenic effects on ECs, that ECs exert mitogenic effects on PCCs, and that these events are suppressible by combinatorial targeting of JAK and TGF-β signaling pathways.

2.8 SB505124+Ruxolitinib block pancreatic cancer cell (PCC) mediated activation of JAK1 in endothelial cells (ECs)

Because ruxolitinib selectively targets JAK1 and JAK2 [116], we next assessed whether one or both of these kinases are involved in the mitogenic crosstalk between human PCCs and HUVECs. Phosphorylated JAK1 (p-JAK1) was only detectable in co-cultures of PCCs and HUVECs, and its levels were suppressed by the combination of SB505124 and ruxolitinib (Figure 2.11A). By contrast, JAK2 phosphorylation was not affected by co-culture, or by SB505124 and ruxolitinib (Figure 2.11A). Moreover, this combination failed to induce cleaved PARP (gene: PARP1) in PCCs or HUVECs, or in co-cultures of these cells (Figure 2.11A). To determine whether increased p-JAK1 occurred in HUVECs, PCCs or both cell types, we added conditioned media (CM) from IUSCC-PC1 or PANC-1 cells to HUVECs, and, conversely, CM from HUVECs to PCCs. CM from the PCCs markedly enhanced p-JAK1 levels and induced SMAD phosphorylation in HUVECs (Figure 2.11B). By contrast, CM from HUVECs failed to induce JAK1 phosphorylation in the PCCs, but stimulated SMAD phosphorylation (Figure 2.11C). Thus, JAK1 activation is EC specific whereas canonical TGF-β signaling pathways are activated in both cell types.

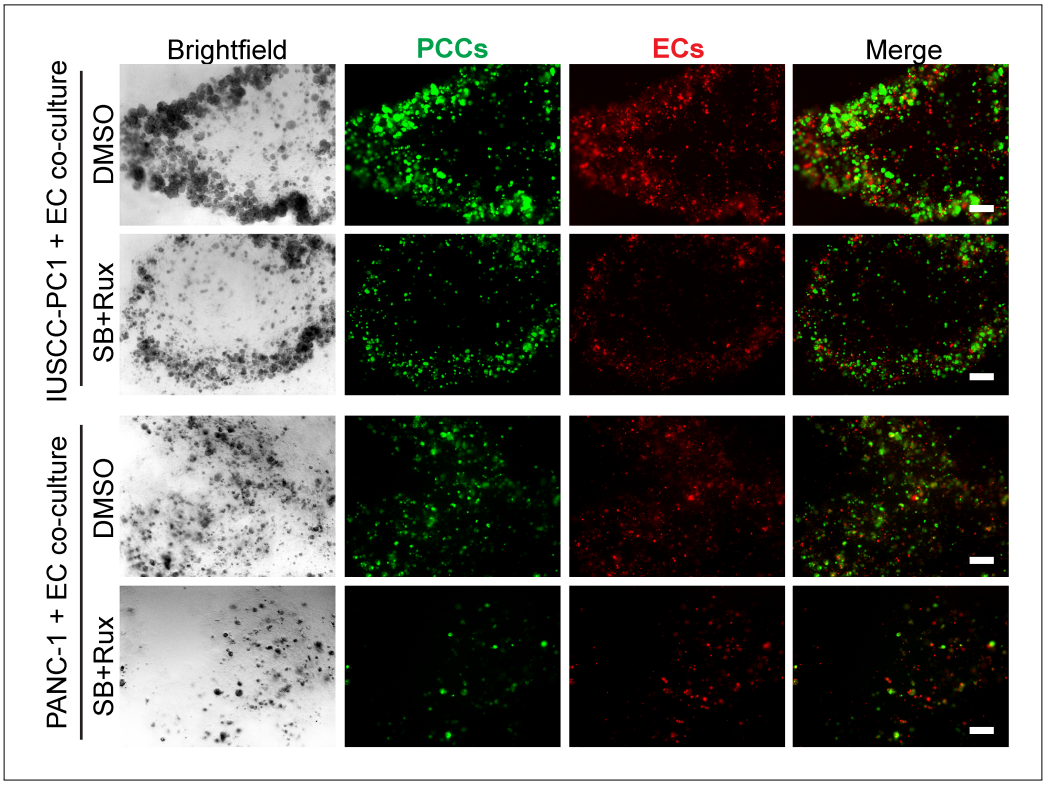

A

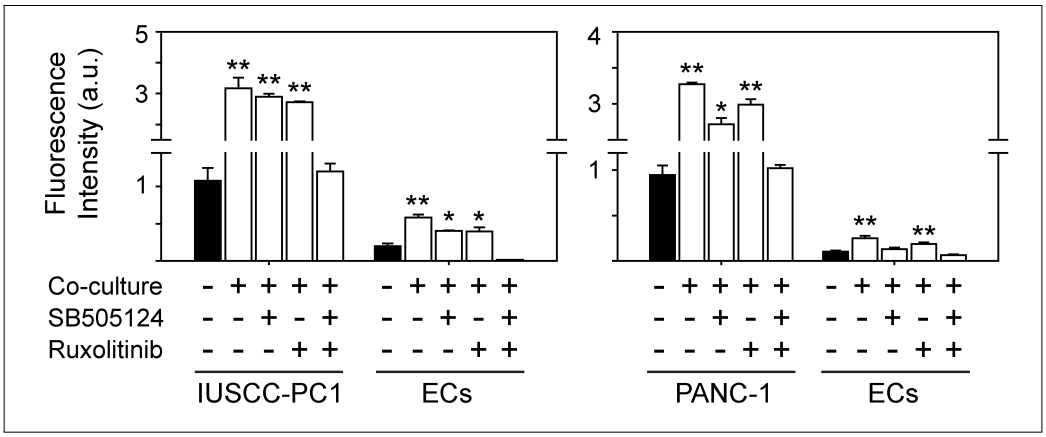

B

Figure 2.10: TGF-β receptor type-1 and JAK1/JAK2 inhibition suppress human pancreatic cancer cell (PCC) and endothelial cell (EC) growth. (A) 3-dimensional (3D) co-cultures of IUSCC-PC1 or PANC-1 human pancreatic cancer cells (PCCs) (green) and human endothelial cells (ECs) (human vascular endothelial cells (HUVECs), red) shows that compared with vehicle (DMSO [0.05%]), ruxolitinib [100 nM] together with SB505124 [2 μM] suppress PCC and EC growth. Shown are representative brightfield and fluorescent images from three independent experiments. Scale bars, 200 μm. **(B)** Fluorescence intensity quantification shows that compared with 3D cultures in which IUSCC-PC1 or PANC-1 PCCs and HUVECs are cultured independently (closed bars), culturing ECs and PCCs together in 3D (open bars) significantly enhances PCC and EC growth, which is completely blocked when ruxolitinib and SB505124 are combined, but not by either inhibitor alone. Data are mean $\pm$ standard error of the mean (SEM) from three independent experiments. *P-value (P) < 0.05, and **P < 0.01.

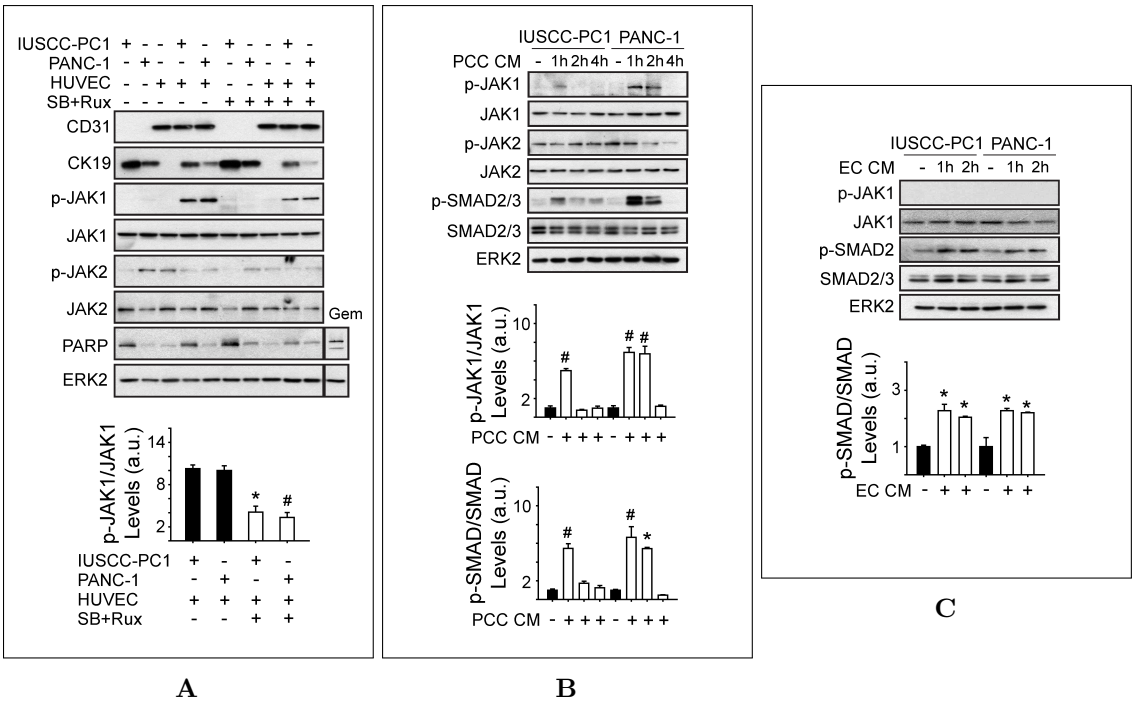

Figure 2.11: SB505124+Ruxolitinib block PCC mediated activation of JAK1 in ECs. **(A)** Immunoblots with 3-dimensional (3D) culture lysates from IUSCC-PC1 or PANC-1 human pancreatic cancer cells (PCCs) with or without human vascular endothelial cells (HUVECs) (endothelial cells (ECs)) show that endothelial (CD31) and epithelial (CK19 (gene: KRT19)) markers are present in PCC:EC co-cultures, in which phosphorylated JAK1 (p-JAK1) but not phosphorylated JAK2 (p-JAK2) levels are markedly increased. SB505124 [2 μM] together with ruxolitinib [100 nM] suppresses p-JAK1, but does not induce PARP (gene: PARP1) cleavage. By contrast, gemcitabine (Gem, [10 μM]) enhances cleaved PARP levels in co-cultured cells. (bottom) Quantification confirms that SB505124 and ruxolitinib (open bars) significantly decreases p-JAK1 levels in co-cultured cells. **(B-C)** Immunoblots with EC (B) or PCC (C) lysates show that conditioned media (CM) from PCCs increases p-JAK1 and phosphorylated SMAD (p-SMAD) levels in ECs (B, top), whereas CM from ECs increases p-SMAD levels in PCCs (C, top). Quantification confirms that PCC CM (B, bottom, open bars) significantly increases p-JAK1 and p-SMAD in ECs, and that EC CM (C, bottom, open bars) significantly increases p-SMAD in PCCs. ERK2 in A, B, and C confirms equivalent lane loading. Data in A, B, and C are presented as mean ± standard error of the mean (SEM) from three independent experiments. *P-value (P) < 0.05, #P < 0.01.

To assess the role of JAK1 in EC growth, and in mediating angiocrine effects on PCCs we used small hairpin RNAs (shRNAs) to suppress JAK1 expression in HUVECs. Both shRNAs markedly attenuated JAK1 expression levels in HUVECs (Figure 2.12A), and suppressed their proliferation (Figure 2.12B) and ability to stimulate PCC growth (Figure 2.12C). Therefore, endothelial JAK1 is required for the angiocrine effects of ECs on PCCs.

The JAK1/JAK2 inhibitor, ruxolitinib [100 nM], and the TGF-β receptor type-1 inhibitor, SB505124 [2 μM], have no effect on IUSCC-PC1 proliferation in single cell type 3D cultures (Figure 2.13). Therefore, we did not deem it necessary to perform additional single culture experiments assessing proliferation with the inhibitors. Instead, we focused on what happens in the co-culture setting due to our findings from the mechanistic studies. We know that JAK1 is not phosphorylated in single 3D cultures of IUSCC-PCC1, PANC-1, or HUVECs with or without SB505124+Ruxolitinib treatment (Figure 2.11A), and that there is a lack of p-SMAD2/3 when HUVECs are cultured alone (Figure 2.11B, no CM timepoint). CM from each cell type placed on the other cell type also leads to an increase in p-SMAD2/3 beyond what is observed in single culture for both cell types (Figure 2.11B-C). Increases in p-JAK1 only occur when the two cell types are co-cultured (Figure 2.11A), and CM experiments indicate that this phosphorylation is exclusive to the ECs (Figure 2.11B). Treatment of the co-cultures with SB505124+Ruxolitinib leads to a decrease in this p-JAK1 (Figure 2.11A). While knocking down JAK1 in ECs does lead to a decrease in their proliferation alone (Figure 2.12B), it also suppresses PCC growth in co-culture experiments (Figure 2.12C), suggesting the importance of this EC pathway in stimulating the PCC growth (Figure 2.12C).

2.9 KRC mice exhibit abundant tumor angiogenesis

Kras$^{\text{LSL-G12D/+}}$; **R**b1$^{\text{-/-}}$; Pdx-1-**C**re (KRC) mice, which express oncogenic Kras in the pancreas, but lack Rb1 function, exhibit rapid pancreatic intraepithelial neoplasia (PanIN) formation and progression to murine PDAC (mPDAC) with a median survival of 10 weeks [117]. While RB1 mutations are rare (0-1%) in hPDAC [27–29, 105, 106], loss of RB1 function is common [91, 106, 114]. KRC mPDACs express high levels of pro-angiogenic cytokines [117], and so we sought to determine whether KRC mPDACs exhibit angiogenesis. CD31 (gene: Pecam1) immunoreactivity in KRC mPDAC was present in sinusoidal-like blood vessels within the collagen-rich stroma adjacent to CK19 (gene: Krt19) positive cancer cells (Figure 2.14A), and in relatively larger

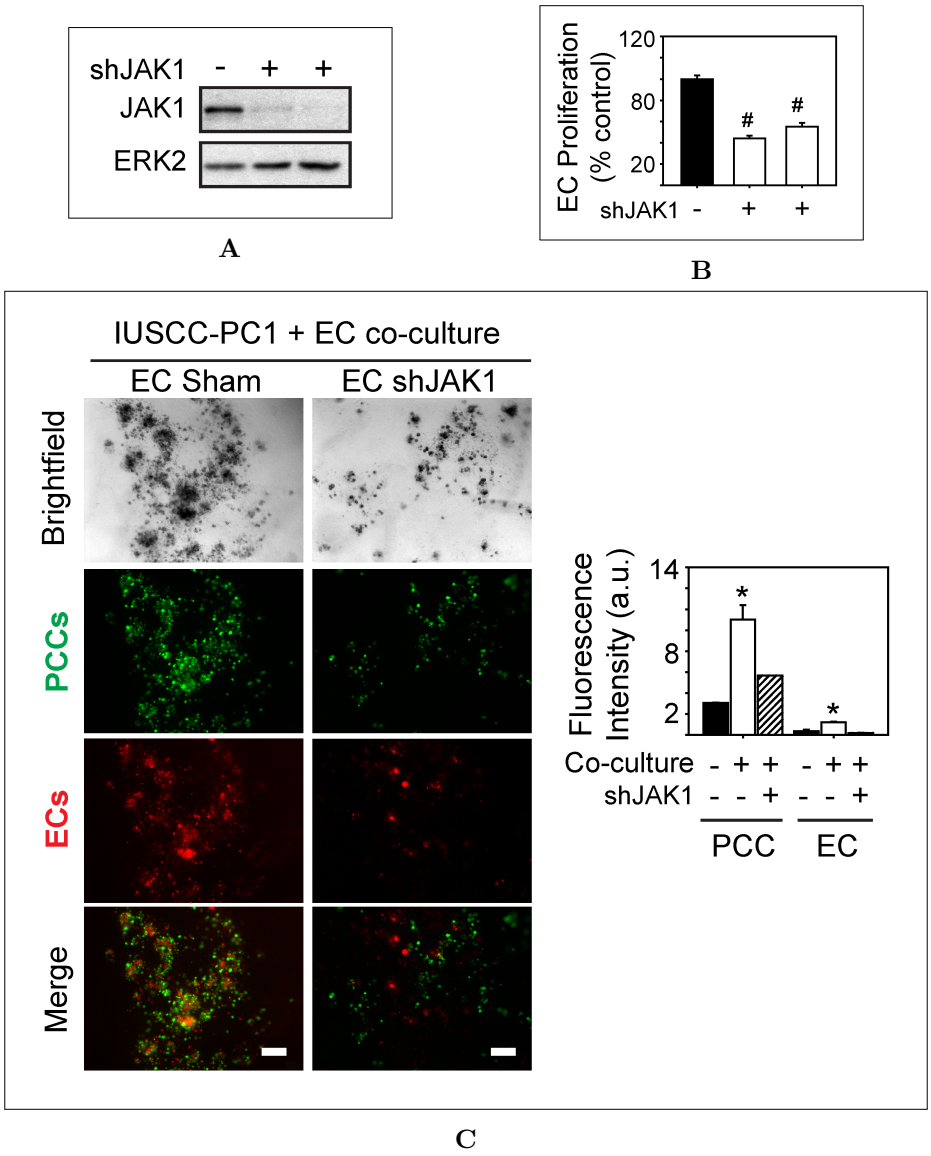

Figure 2.12: JAK1 is required for EC growth and angiocrine effects on PCCs. (A-B) Two different JAK1 targeting shRNAs decrease JAK1 expression in human vascular endothelial cells (HUVECs) (A), and significantly decrease HUVEC proliferation (B, open bars) compared with Sham transduced control cells. Cell proliferation was assessed using MTT assay, and data are presented as mean ± standard error of the mean (SEM) from three independent experiments. ERK2 in (A) confirms equivalent lane loading. **(C)** 3-dimensional (3D) co-cultures with IUSCC-PC1 pancreatic cancer cells (PCCs) (green) and HUVECs (red) transduced with a non-targeting control (endothelial cell (EC) Sham) or JAK1 shRNA (EC shJAK1) shows that JAK1 knockdown in ECs suppresses PCC and EC growth. Shown are representative brightfield and fluorescent images from three independent experiments. Scale bars, 200 μm. (right) Fluorescence intensity quantification confirms that JAK1 knockdown in ECs suppresses PCC and EC growth in 3D co-cultures (hatched bars). Data are mean ± SEM from three independent experiments. *P-value (P) < 0.05, #P < 0.01.

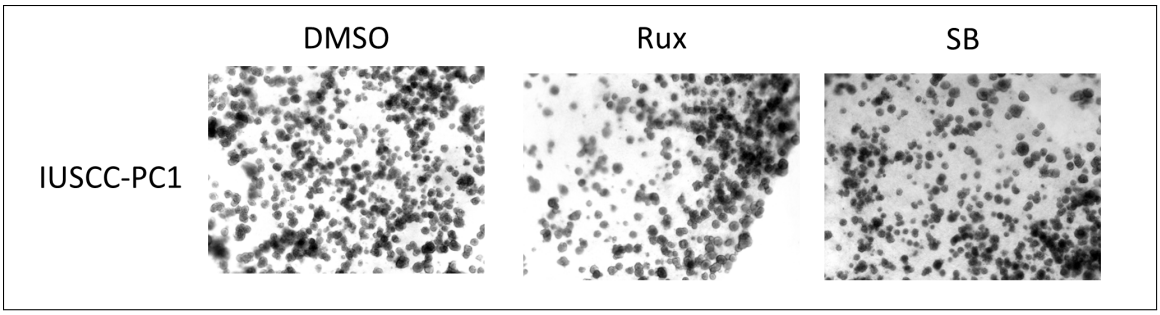

Figure 2.13: SB505124 and ruxolitinib alone do not inhibit PCC growth in single 3-dimensional (3D) cultures. Treatment of single 3D cultures of IUSCC-PC1 cells with DMSO, 100 nM ruxolitinib (Rux), or 2 μM SB505124 (SB) results in no differences in proliferation.

blood vessels within the stromal compartment (Figure 2.14B). Moreover, intravenous injection of tetramethylrhodamine (TRITC) conjugated dextran followed by intravital imaging using two-photon confocal microscopy, demonstrated many dextran-positive vessels (Figure 2.14C), confirming the presence of blood flow.

We next conducted an array analysis using KRC tumor-derived RNA to determine if they exhibit a pro-angiogenic gene expression profile compared to RNA derived from age matched WT murine pancreata. GO analysis revealed that KRC tumors exhibited significant enrichment of pro-angiogenic processes compared to age matched WT murine pancreata (Figure 2.15A and 2.15B). Increased expression of pro-angiogenic genes in KRC tumors could arise as a consequence of their up-regulation in the cancer cells. Therefore, we next evaluated KRC-derived PCCs for a pro-angiogenic gene expression profile. Accordingly, we conducted a GO analysis of microarray data comparing KRC PCCs with PCCs derived from KC tumors, which also express oncogenic Kras, but retain Rb1 function and express low levels of pro-angiogenic cytokines [114]. These KRC PCCs derived from KRC tumors also exhibited significant enrichment of pro-angiogenic processes (Figure 2.16).

qPCR validated the arrays and confirmed that KRC tumors and PCCs expressed relatively high levels of Ctgf, Cyr61, Egfr, Nrp2, Serpine1, Tgfbr1 and Vegfc mRNA (Figure 2.17A and 2.17B). By contrast, Vegfa mRNA levels were similar in KRC and KC cells, in agreement with the observation that oncogenic Kras, per se, can up-regulate Vegfa mRNA expression [118].

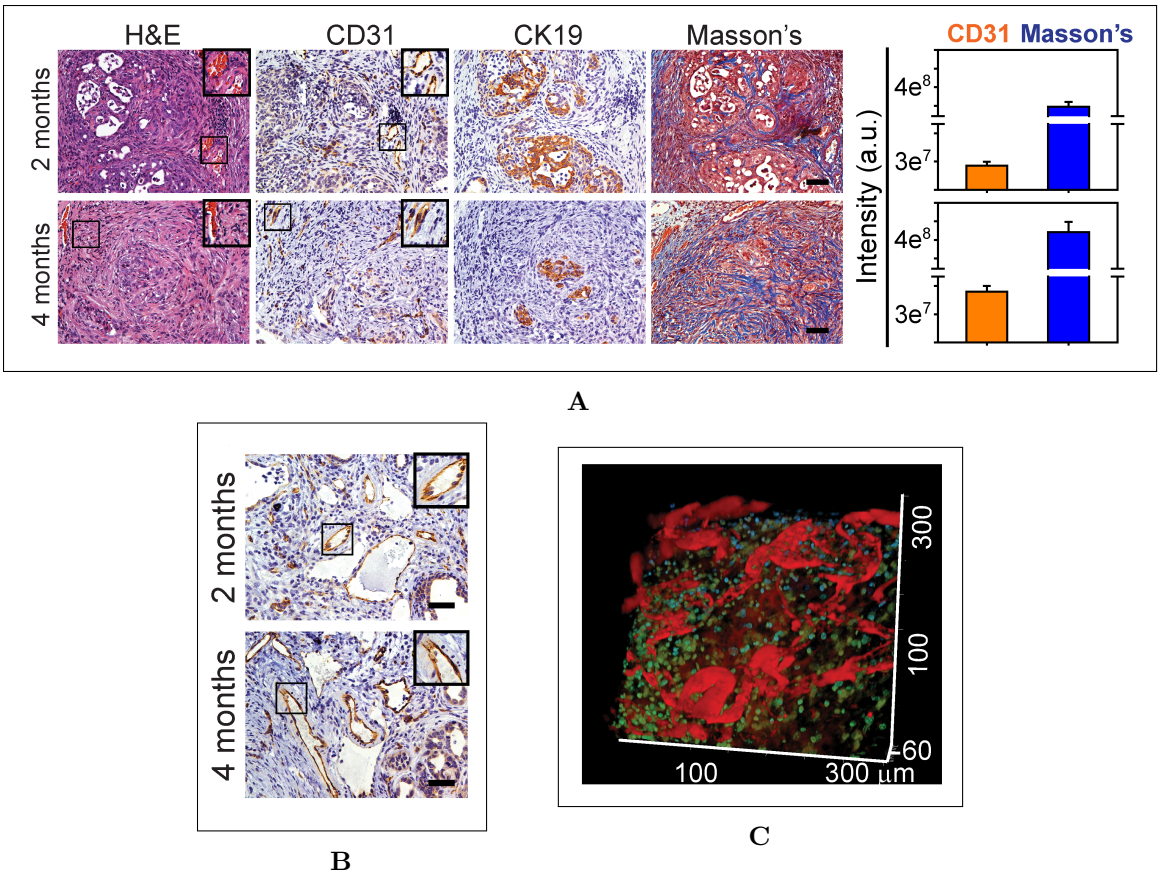

Figure 2.14: KRC murine PDACs (mPDACs) exhibit angiogenesis. (A) **K**ras$^{LSL\text{-}G12D/+}$; **R**b1$^{-/-}$; Pdx-1-**C**re (KRC) mPDACs harbor endothelial cells (ECs) adjacent to CK19 positive cancer cells in the collagen-rich stroma as evidenced by Masson's Trichrome staining of serial sections. Quantitation (right) of CD31 and Masson's Trichrome staining shows that EC abundance and stromal content increases from postnatal months 2 to 4. **(B)** CD31 positive vessels are also present throughout KRC mPDACs. Shown in (A–B) are representative images from 5 KRC mice at each age. Insets in (A–B) are magnified images of boxed areas. Scale bars, 50 μm. **(C)** Intravital microscopy shows that KRC tumors have blood flow as evidenced by the abundance of dextran-positive (red) vessels. Shown is a representative image from 1 of 2 KRC mice.

2.10 KRC tumors show superior enrichment and differential expression of The Cancer Genome Atlas (TCGA) angiogenic gene signature compared to KPC tumors

While we have shown that KRC mPDACs exhibit abundant angiogenesis, KPC mice are classically hypovascular [35, 36]. KPC mice express oncogenic Kras and mutant Trp53 in the pancreas, and they progress from preinvasive disease to invasive and widely metastatic mPDAC with a median survival of 19 weeks [119, 120]. To determine if tumors from either of these models is enriched in the human pro-angiogenic gene signature identified from TCGA, GSEA was executed on array data from both of

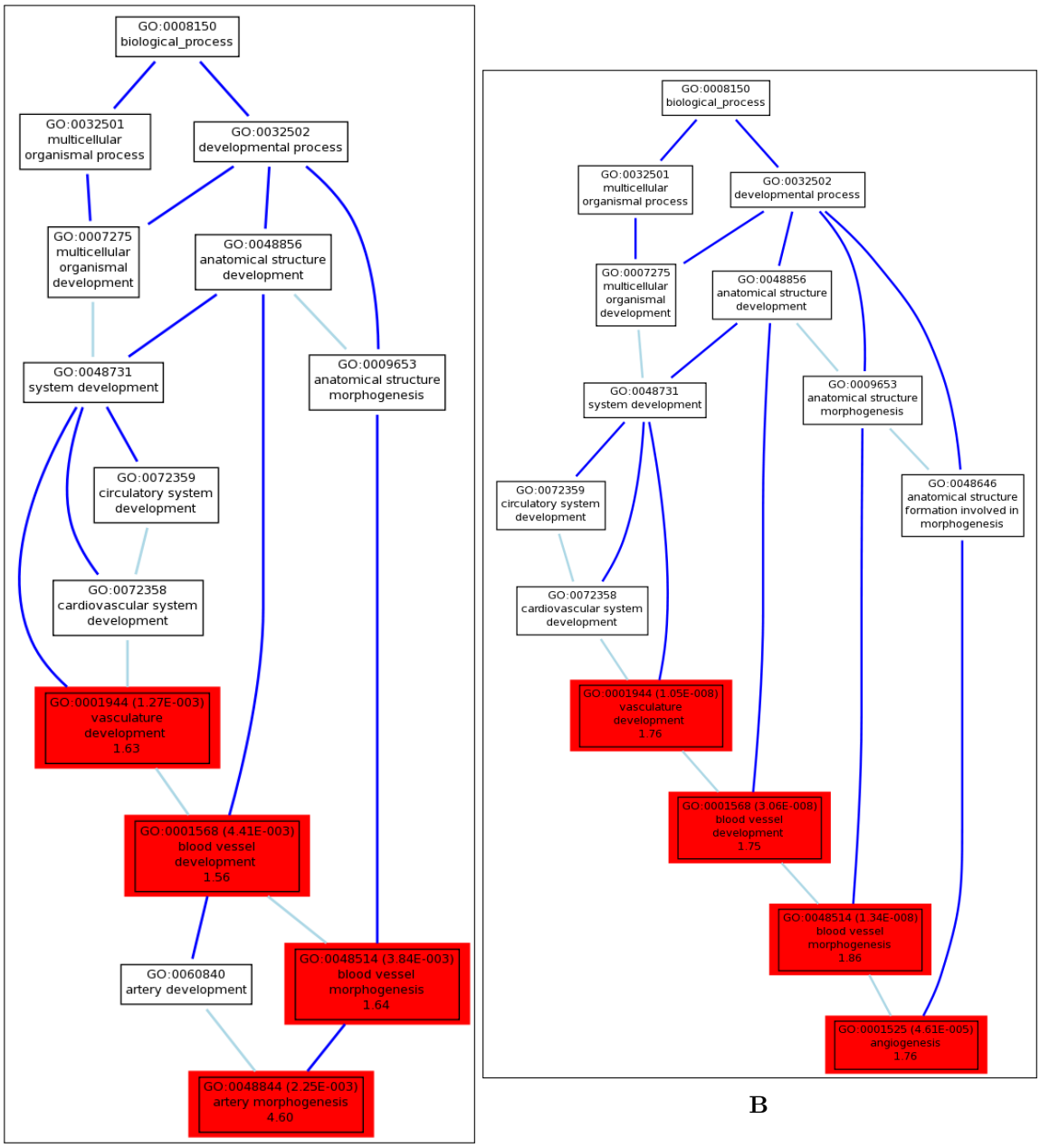

Figure 2.15: KRC tumors are enriched in angiogenesis related Gene Ontology (GO) terms. (A-B) Gene Ontology (GO) analysis of differentially expressed genes (|Fold Change (FC)| >= 2, P-value (P) < 0.01) in tumors from 2 month old **K**ras$^{LSL\text{-}G12D/+}$; **R**b1$^{-/-}$; Pdx-1-**C**re (KRC) mice (A) or 4 month old KRC mice (B) compared to age matched wild type (WT) murine pancreas shows that genes annotated to vasculature development, blood vessel development, blood vessel morphogenesis, artery morphogenesis, and angiogenesis are significantly enriched (P < 0.01).

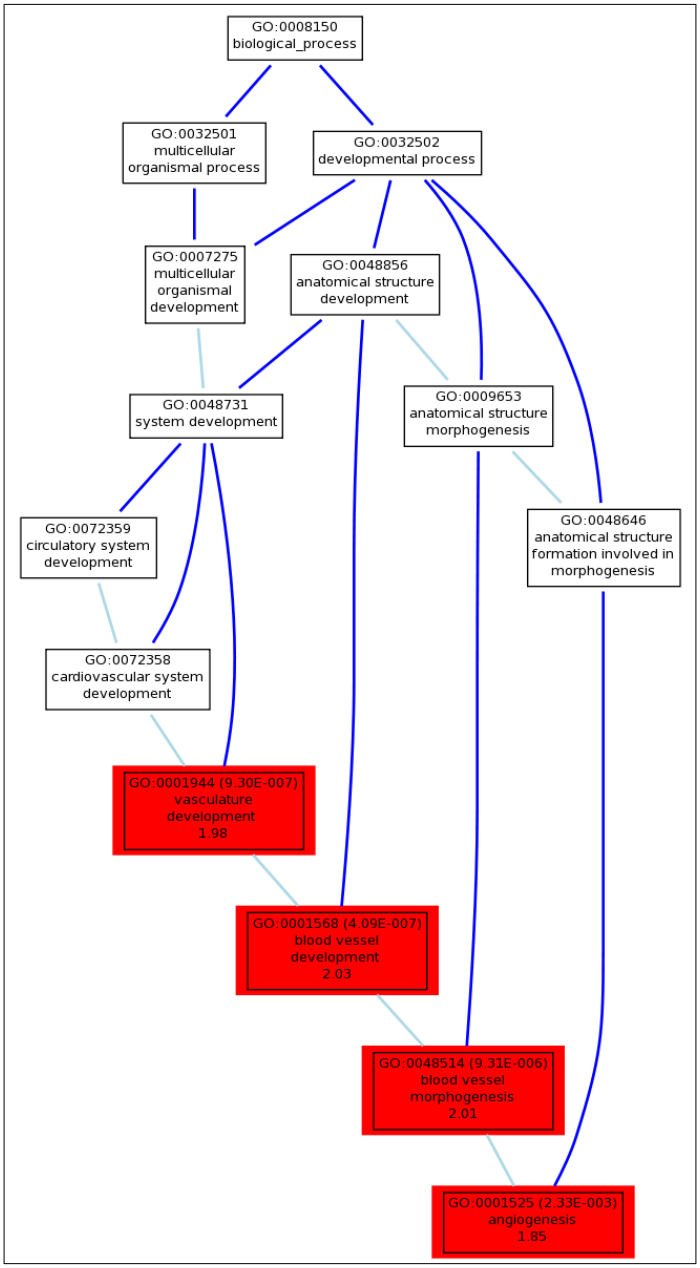

Figure 2.16: KRC cells are enriched in angiogenesis related GO terms. Gene Ontology (GO) analysis of differentially expressed genes (|Fold Change (FC)| >= 2, P-value (P) < 0.01) in **K**ras$^{LSL\text{-}G12D/+}$; **R**b1$^{-/-}$; Pdx-1-**C**re (KRC) cells compared to **K**ras$^{LSL\text{-}G12D/+}$; Pdx-1-**C**re (KC) cells shows that genes annotated to vasculature development, blood vessel development, blood vessel morphogenesis, and angiogenesis are significantly enriched (P < 0.01).

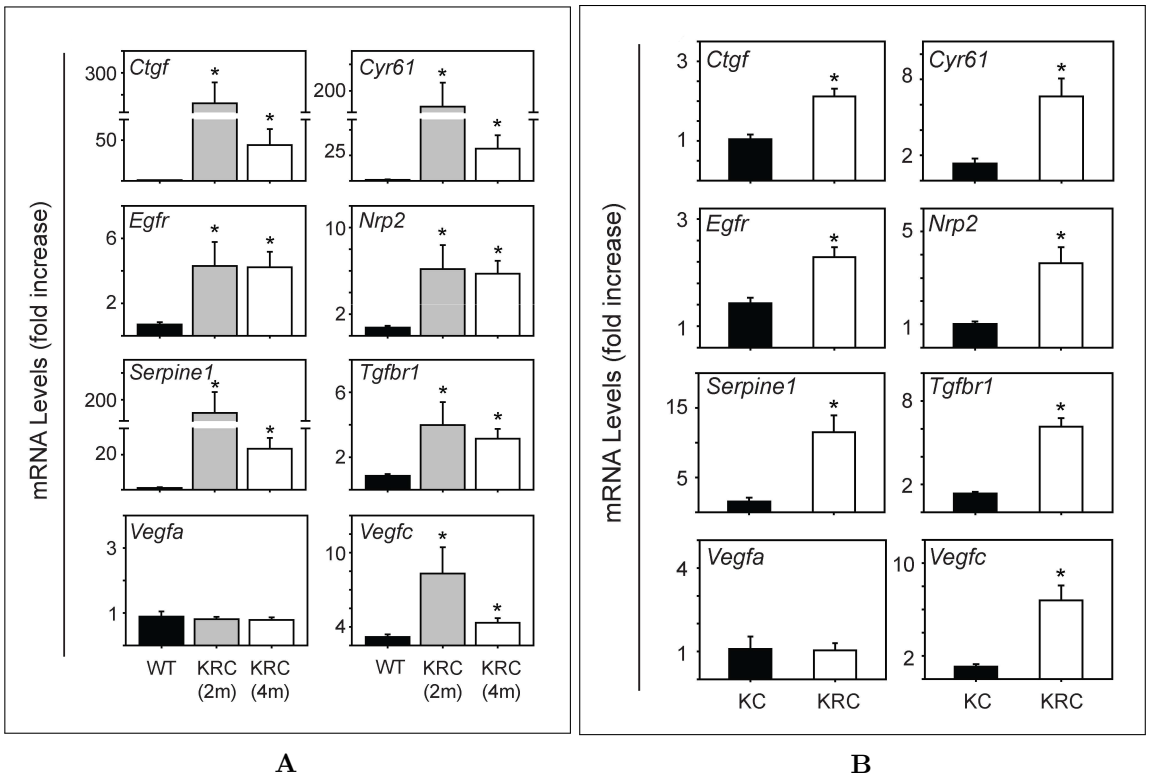

Figure 2.17: Quantitative Polymerase Chain Reaction (qPCR) validation of angiogenic genes up-regulted in KRC tumors and cells. (A-B) Quantitative Polymerase Chain Reaction (qPCR) for the indicated mRNAs validates the array data, and confirms that Ctgf, Cyr61, Egfr, Nrp2, Serpine1, Tgfbr1, and Vegfc are significantly increased in 2 month (A, gray bars) and 4 month old (A, open bars) **K**ras$^{LSL\text{-}G12D/+}$; **R**b1$^{-/-}$; Pdx-1-**C**re (KRC) tumors compared with their respective littermate controls (A, wild type (WT), closed bars), and in KRC cells (B, open bars) compared with **K**ras$^{LSL\text{-}G12D/+}$; Pdx-1-**C**re (KC) cells (B, closed bars). Data in (A-B) are mean ± standard error of the mean (SEM). *P-value (P) < 0.05.

these models. Overall, 2 month KRC tumors from 2 month and 4 month old mice and KPC tumors from 3 month old mice all show enrichment of the signature (family-wise error rate (FWER) < 0.001) with normalized enrichment scores (NESs) of 2.08, 2.11, and 1.87, respectively (Figure 2.18A-2.18C top).

Visual representation of the expression differences in heatmaps confirms this trend, with 4 month KRC tumors showing the largest difference in expression of this signature (Figure 2.18A-2.18C bottom). However, it is important to note that the 4 month group would consist of tumors obtained only from the ∼10% of KRC mice that survived longer than the median of 10 weeks. While GSEA uses a rank based method, application of stringent cut offs for differential expression (FC >= 1.5, FDR < 0.05) indicates that 2 month KRC tumors, 4 month KRC tumors, and 3 month KPC tumors differentially express 13, 43 and 0 genes from the 77 gene signature (77 mouse homologs to the 79

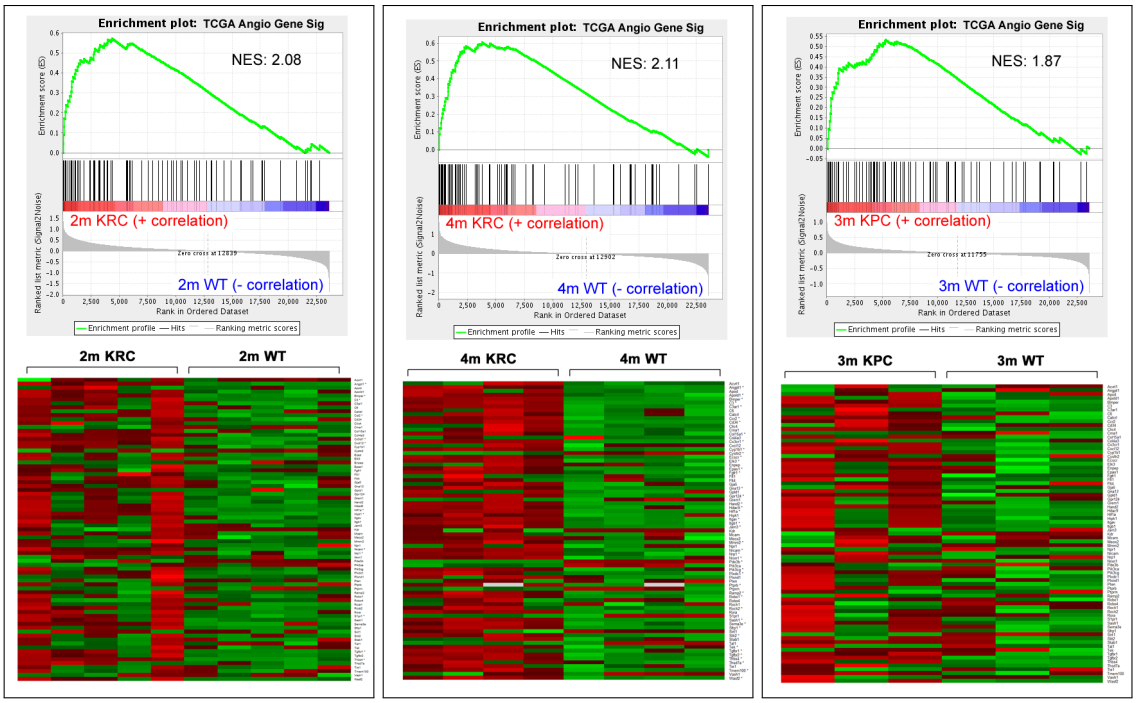

Figure 2.18: KRC tumors show superior enrichment and differential expression of The Cancer Genome Atlas (TCGA) angiogenic gene signature. (A) (top) Gene Set Enrichment Analysis (GSEA) of 2 month **K**ras$^{\text{LSL-G12D/+}}$; **R**b1$^{-/-}$; Pdx-1-**C**re (KRC) tumor array data shows enrichment of The Cancer Genome Atlas (TCGA) angiogenic gene signature (normalized enrichment score (NES): 2.08, family-wise error rate (FWER) < 0.001). (bottom) Heatmap of expression values from the 2 month KRC tumor array data for TCGA angiogenic genes. **(B)** (top) GSEA of 4 month KRC tumor array data shows enrichment of TCGA angiogenic gene signature (NES: 2.11, FWER < 0.001). (bottom) Heatmap of expression values from the 4 month KRC tumor array data for TCGA angiogenic genes. **(C)** (top) GSEA of 3 month **K**ras$^{\text{LSL-G12D/+}}$; Tr**p**53$^{\text{LSL-R172H/+}}$; Pdx-1-**C**re (KPC) tumor array data shows enrichment of TCGA angiogenic gene signature (NES: 1.87, FWER $<$ 0.001). (bottom) Heatmap of expression values from the 3 month KPC tumor array data for TCGA angiogenic genes. **(A-C)** (bottom) (red = up-regulated; green = down-regulated).

differentially expressed angiogenesis genes between the Strong PDAC and Weak PDAC groups). Therefore, while KPC tumors may display enrichment of the signature, none of the angiogenic genes meet stringent criteria for differential expression.

2.11 TGF-β promotes angiogenesis indirectly

We next assessed the ability of CM from KRC cells to enhance the proliferation and migration of murine SVEC4–10 ECs that are commonly used to study angiogenesis pathways *in vitro* [121]. CM from three KRC derived PCCs markedly enhanced EC proliferation and migration (Figure 2.19A), suggesting that KRC cells may secrete factors that promote EC proliferation *in vivo*. Because TGF-β signaling activity was

present in the Strong PDAC group, we conducted GSEA on KRC tumor and cell array data and found enrichment of a TGF-β gene set in 2 month (Figure 2.19B) and 4 month KRC (Figure 2.19C) tumors as well as in KRC cells (Figure 2.19D) derived from the tumors (Figure 3B). Additionally, enrichment of the TGF-β gene set was found in 3 month KPC tumors (Figure 2.19E).

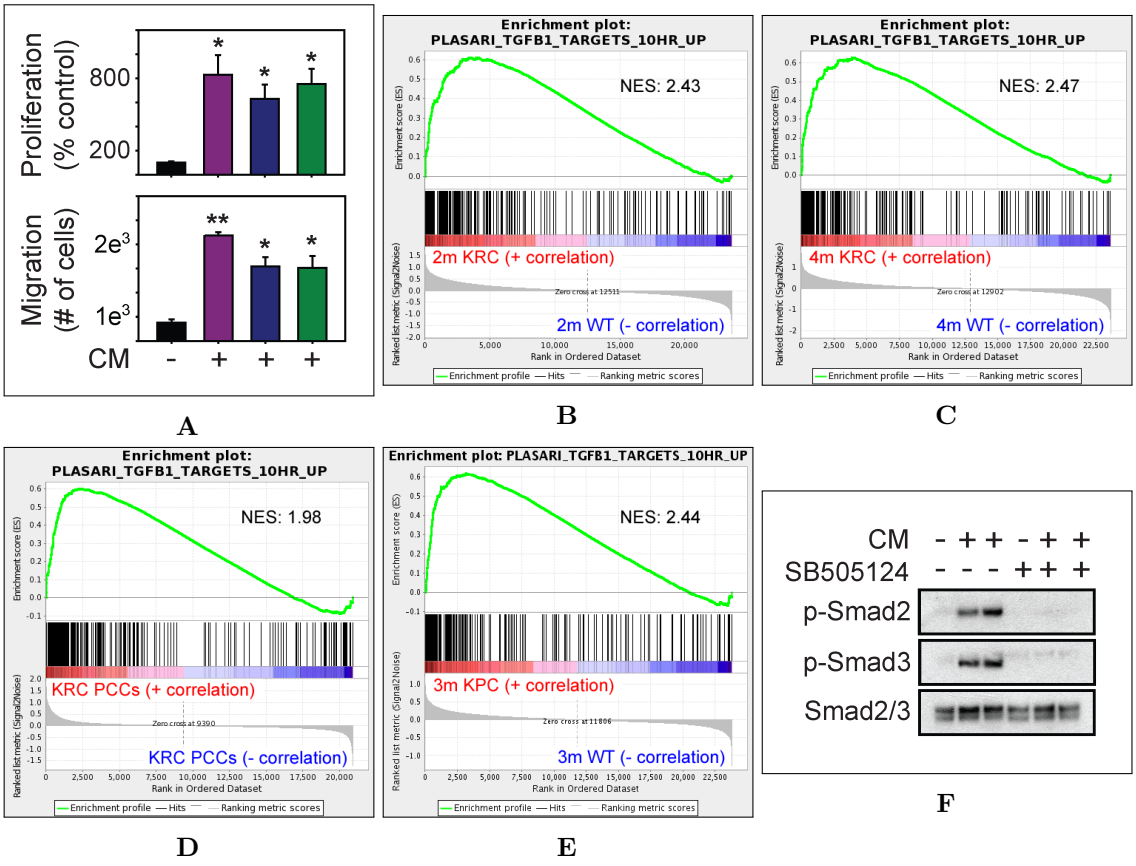

Figure 2.19: KRC conditioned media (CM) enhances angiogenesis and TGF-β signaling in ECs. (A) Compared with control media (black bars), conditioned media (CM) from three **K**ras$^{\text{LSL-G12D/+}}$; **R**b1$^{-/-}$; Pdx-1-**C**re (KRC) cell lines (purple, blue, or green bars) significantly enhances endothelial cell (EC) proliferation (top) and migration (bottom). Data are mean $\pm$ standard error of the mean (SEM). **P-value (P) < 0.01; *P < 0.05. **(B-E)** Gene Set Enrichment Analysis (GSEA) shows that 2 month KRC tumors (B, normalized enrichment score (NES): 2.43, family-wise error rate (FWER) < 0.001), 4 month KRC tumors (C, NES: 2.47, FWER < 0.001), KRC pancreatic cancer cells (PCCs) (D, NES: 1.98, FWER < 0.001), and 3 month **K**ras$^{\text{LSL-G12D/+}}$; Tr**p**53$^{\text{LSL-R172H/+}}$; Pdx-1-**C**re (KPC) tumors (E, NES: 2.44, FWER < 0.001) are enriched in genes up-regulated by TGF-β. **(F)** CM from KRC cells markedly increases murine phosphorylated SMAD2 (p-SMAD2) and murine phosphorylated SMAD3 (p-SMAD3) levels in ECs, which is blocked by SB505124 [2 μM]. Shown are representative immunoblots from three independent experiments.

The presence of TGF-β signaling does not seem to be unique to a specific GEMM as nuclear and stromal murine phosphorylated SMAD2 (p-SMAD2) immunoreactivity has been observed in KC, KRC, **K**ras$^{\text{LSL-G12D/+}}$; Cdkn2a$^{\text{LoxP/LoxP}}$; Pdx-1-**C**re (KIC),

and KPC mPDACs [114, 122]. Murine phosphorylated SMAD3 (p-SMAD3) immunoreactivity has also been demonstrated in KRC mPDACs [114, 122]. While only TGFB3 was up-regulated in the Strong PDAC group (FC 3.40, FDR 1.31E-10), both Tgfb2 (FC 3.50, FDR 0.046) and Tgfb3 (FC 4.15, FDR 0.006) were up-regulated in 4 month KRC tumors, and all three ligands were up-regulated in KRC cells compared to KC cells (Tgfb1: FC 1.52, FDR 0.001; Tgfb2: FC 3.05, FDR 0.0001; Tgfb3: FC 2.23, FDR 0.0001). However, none of these were up-regulated in 3 month KPC tumors.

While TGF-β has been shown to induce SMAD2 phosphorylation, the nuclear translocation of SMAD2/3/4, and SMAD transcriptional activity in KRC cells, KRC cells are not growth inhibited by TGF-β in contrast to KC cells [114]. In 3D cultures, TGF-β induces the proliferation of KRC cells, but both control and treated cells show co-expression of p-SMAD2 and Ki67 (gene: Mki67) [114].

The pro-angiogenic actions of KRC CM could be due to direct effects of TGF-β on ECs, or through the up-regulation of pro-angiogenic genes in the PCCs and cells within the tumor microenvironment (TME). To explore whether TGF-β acts directly on ECs, we next assessed the ability of CM derived from KRC PCCs to activate canonical TGF-β signaling in SVEC4–10 ECs. Indeed, KRC derived CM increased SMAD2 and SMAD3 phosphorylation in ECs, which was blocked by the TGF-β receptor type-1 (gene: Tgfbr1) inhibitor, SB505124 (Figure 2.19F), pointing to TGF-β pathway activation in ECs. However, SB505124 failed to block the ability of KRC derived CM to stimulate EC proliferation or migration (Figure 2.20A), indicating that TGF-β does not directly enhance angiogenesis. To determine if TGF-βs promote pro-angiogenic gene expression in KRC cells, we suppressed TGF-β receptor type-1 signaling with SB505124, and assayed Ctgf, Wisp1, Cyr61, Pdgfa, and Vegfc, all of which were elevated in the Strong PDAC group except PDGFA. SB505124 blocked SMAD2 phosphorylation [114] and markedly suppressed the levels of all five mRNAs (Figure 2.20B). This suggests that TGF-β can promote angiogenesis indirectly by up-regulating pro-angiogenic genes in the PCCs.

2.12 STAT3 is required for EC activation by PCCs

Out of 25 cytokines assayed by multiplex enzyme-linked immunosorbent assay (ELISA) in KRC CM, only CXCL1, CXCL5, MCP-1 (gene: Ccl2), GM-CSF (gene: Csf2), VEGF-A (gene: Vegfa), and VEGF-C (gene: Vegfc) were readily detected in KRC CM, and TGF-β increased the levels of the latter three (Figure 2.21A). Importantly, TGF-β increased GM-CSF by 14.7-fold and VEGF-A by 42-fold, whereas

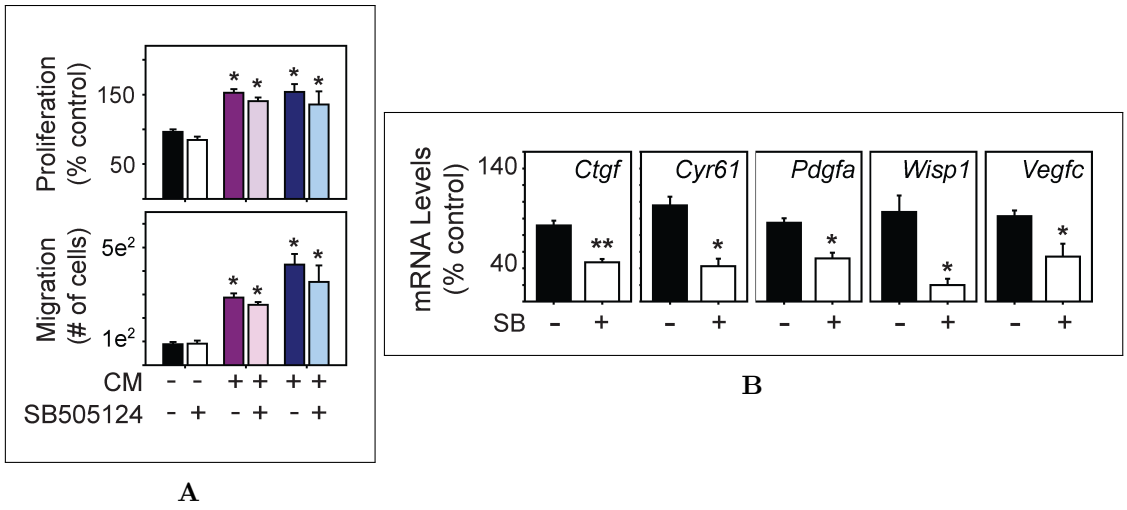

Figure 2.20: TGF-β receptor type-1 inhibition does not block endothelial activation but suppresses angiogenic gene expression in PCCs. (A) SB505124 [2 μM] does not prevent **K**ras$^{LSL\text{-}G12D/+}$; **R**b1$^{-/-}$; Pdx-1-**C**re (KRC) conditioned media (CM) from enhancing endothelial cell (EC) proliferation (top) or migration (bottom). **(B)** SB505124 [2 μM] significantly attenuates the levels of the indicated mRNAs in KRC pancreatic cancer cells (PCCs). Data in (A-B) are mean $\pm$ standard error of the mean (SEM). **P-value (P) < 0.01; *P < 0.05.

IL6 (gene: Il6), a potent inducer of STAT3, was below the level of detection. All six of the detectable factors are pro-angiogenic and activate STAT3, an oncogene and survival factor that can be activated by many additional cytokines and growth factors [123, 124], that has been implicated in promoting tumor angiogenesis [125] and modulating the TME [126]. Additionally, STAT3 has been shown to be active in the endothelium of KRC mPDACs and 59% of hPDAC tumors [114].

We next determined if PCC derived factors activate endothelial STAT3 by using CM from KRC PCCs. CM robustly increased STAT3 phosphorylation (Figure 2.21B) and STAT3 dependent transcription in ECs (Figure 2.21C), which was completely blocked by the JAK1/2 inhibitor, ruxolitinib, or by silencing Stat3 in ECs with a shRNA that suppressed STAT3 to undetectable levels (Figure 2.21C). Ruxolitinib and Stat3 silencing also blocked the ability of CM to stimulate EC proliferation (Figure 2.21D). Together, these results suggest that KRC derived factors promote EC growth through STAT3 dependent pathways.

2.13 Ruxolitinib suppresses mitogenic crosstalk between ECs and PCCs

We next co-cultured fluorescently-labeled SVEC4–10 ECs and KRC PCCs in a 3D culture system [114]. Remarkably, PCC growth was enhanced in the co-culture model compared with 3D cultures in which PCCs were cultured separately from ECs, and

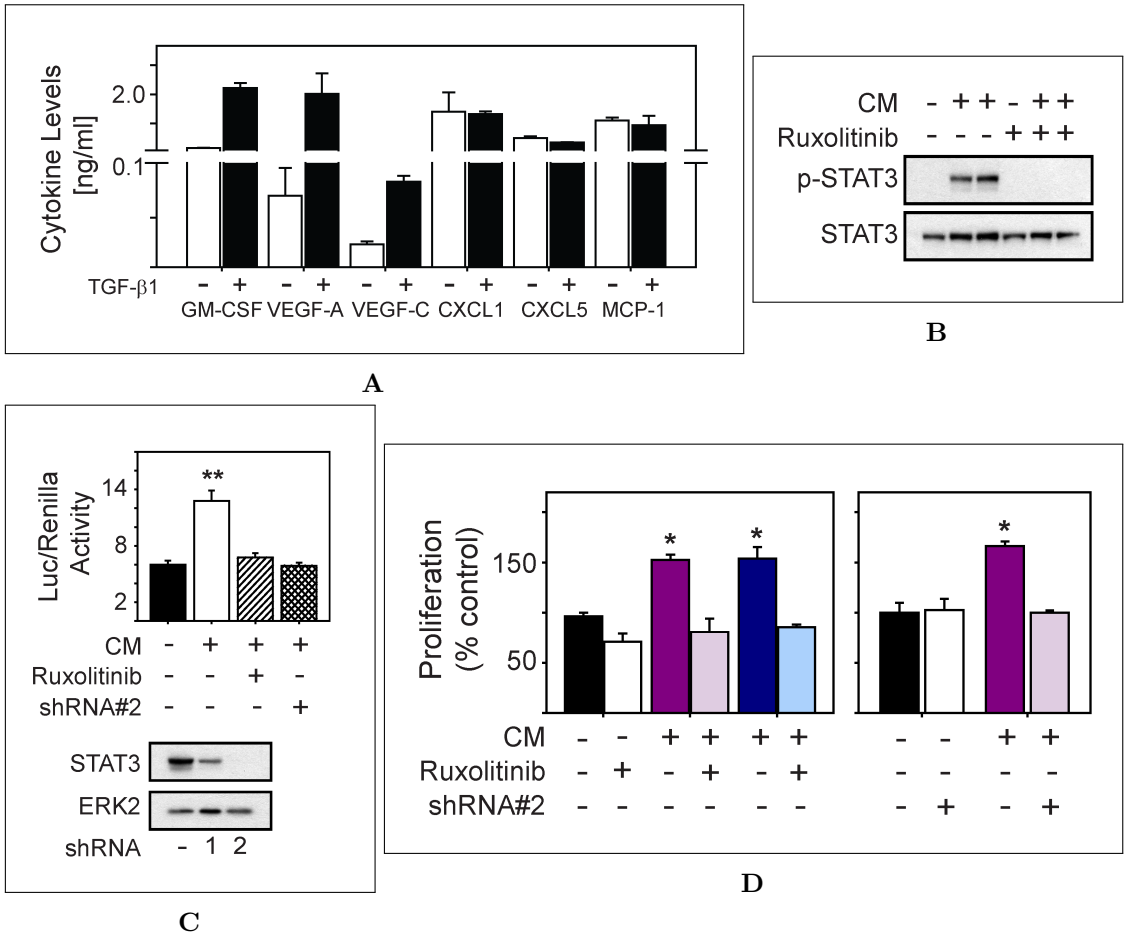

Figure 2.21: KRC CM stimulates EC proliferation through STAT3. (A) Enzyme-linked immunosorbent assay (ELISA) shows the levels of the indicated cytokines in **K**ras$^{\text{LSL-G12D/+}}$; **R**b1$^{-/-}$; Pdx-1-**C**re (KRC) conditioned media (CM) in the absence (open bars) or presence (closed bars) of TGF-β. Data are mean ± standard deviation (SD) from two different cell lines. **(B)** KRC CM markedly increases murine phosphorylated STAT3 (p-STAT3) levels in endothelial cells (ECs), which is blocked by ruxolitinib [100 nM]. **(C)** KRC CM significantly enhances STAT3 luciferase reporter activity in ECs (top), which is blocked by ruxolitinib [100 nM] or a Stat3 targeting shRNA. Immunoblotting (bottom) shows the knockdown efficiency of Stat3 targeting shRNAs. ERK2 confirms equivalent lane loading. Shown in (B-C) are representative immunoblots from three independent experiments. **(D)** CM from KRC cells significantly enhances EC proliferation, but in the presence of ruxolitinib ([100 nM], left) or in ECs transduced with a Stat3 targeting shRNA (right), CM fails to enhance EC proliferation. Data in (C-D) are mean ± standard error of the mean (SEM). *P-value (P) < 0.05, and **P < 0.01.

this enhanced growth in co-culture was completely suppressed by ruxolitinib (Figure 2.22A, 2.22B). By contrast, ruxolitinib failed to inhibit the growth of either PCCs or ECs when cultured separately (Figure 2.22B). Thus, ECs can enhance PCC growth through an angiocrine mechanism, which is suppressible by targeting JAK1/2 with ruxolitinib. Unlike ruxolitinib, inhibiting TGF-β receptor type-1 with SB505124 was able to inhibit the growth of KRC cells when cultured alone [114].

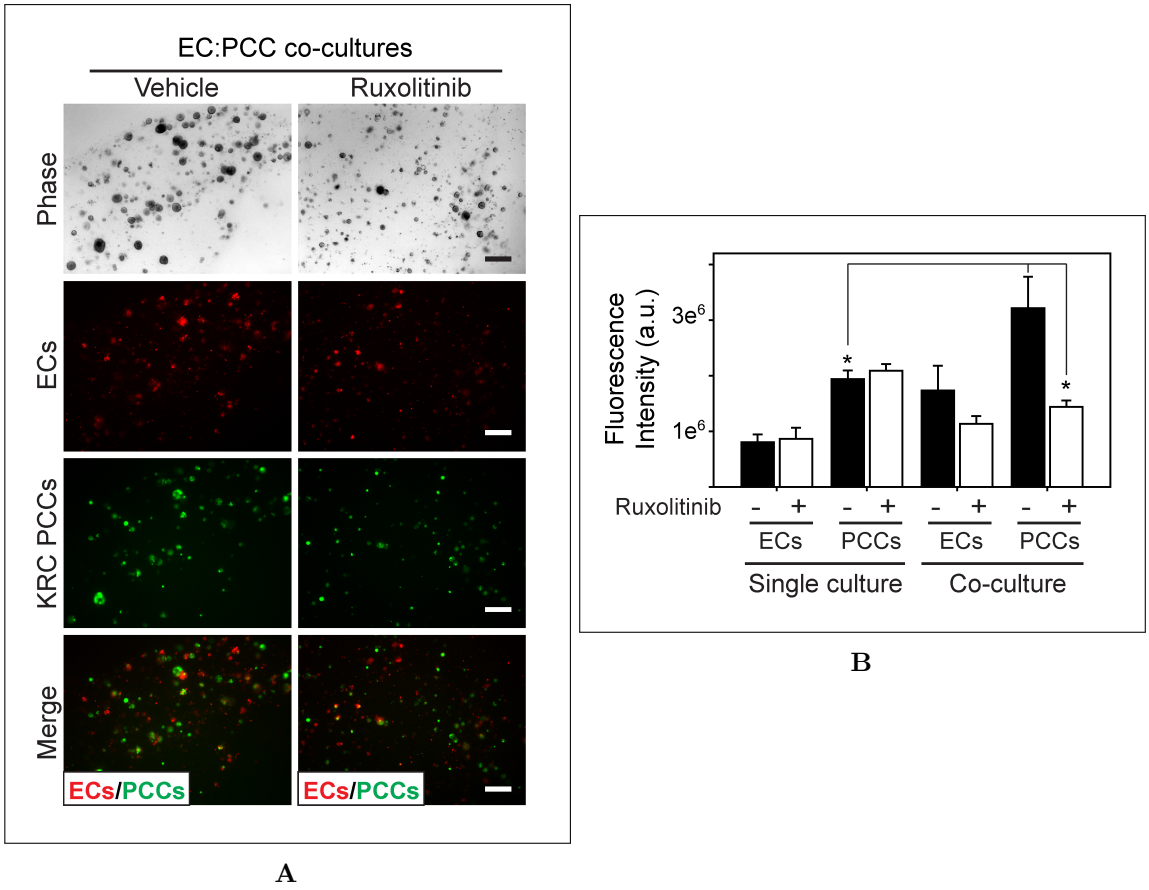

Figure 2.22: Ruxolitinib suppresses mitogenic crosstalk between ECs and PCCs. (A) 3-dimensional (3D) co-cultures of endothelial cells (ECs) (red) and **K**ras$^{LSL\text{-}G12D/+}$; **R**b1$^{-/-}$; Pdx-1-**C**re (KRC) pancreatic cancer cells (PCCs) (green) shows that compared with vehicle (DMSO, left), ruxolitinib ([100 nM], right) suppresses PCC growth. Shown are representative phase contrast and fluorescent images taken on day 8. Scale bars, 200 μm. **(A)** Fluorescence intensity quantitation shows that compared with 3D cultures in which ECs and PCCs are cultured independently (single culture), culturing ECs and PCCs together (co-culture) in 3D significantly enhances PCC growth, which is blocked by ruxolitinib (open bars). Data are mean $\pm$ standard error of the mean (SEM) from three independent experiments. *P-value (P) < 0.05, and **P < 0.01.

2.14 SB505124 attenuates PDAC growth and prolongs survival in KRC mice

We next evaluated the impact of TGF-β receptor type-1 signaling blockade on tumor growth and survival in the context of an intact immune system using KRC cells in a syngeneic orthotopic model. Treatments began on day 10 after intra-pancreatic PCC injection. By day 17, tumors in vehicle-treated mice had grown by 810%, whereas in SB505124-treated mice, tumors had grown by 195% (Figure 2.23A). Overall, 100% of vehicle-treated mice succumbed to disease by day 26 (Figure 2.23B). By contrast, SB505124-treated mice survived as long as 50 days (Figure 2.23B). Additionally, SB505124 treated tumors showed attenuated CD31 immunoreactivity (Figure 2.23C).

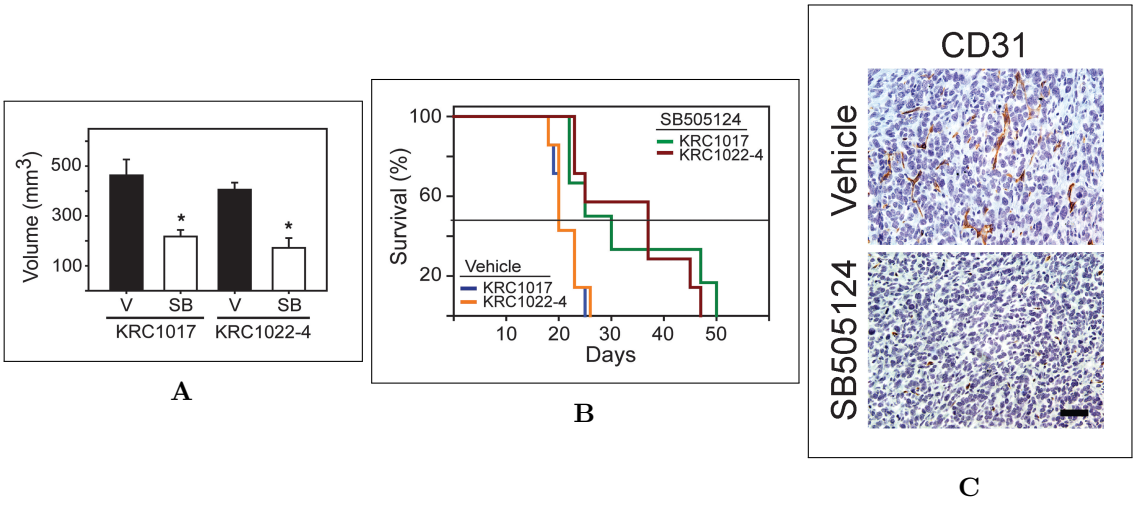

Figure 2.23: SB505124 attenuates PDAC growth and prolongs survival in KRC mice. **(A)** Quantitation shows that SB505124 (SB, white bars) significantly attenuated tumor volumes compared to Vehicle (V, black bars). *P-value (P) < 0.031. **(B)** Kaplan-Meier survival curves reveal that SB505124 significantly prolonged the survival of mice bearing KRC1017-derived (green versus blue line, P = 0.026) and KRC1022-4–derived (red versus orange line, P = 0.007) tumors. Horizontal line indicates 50% survival. **(C)** Vehicle-treated tumors (top) display abundant CD31 immunoreactivity, which is markedly attenuated in (bottom) SB505124-treated tumors. Shown are representative images from 3 mice per group. Scale bars, 50 μm.

2.15 Ruxolitinib attenuates PDAC growth and prolongs survival in KRC mice

Endothelial recruitment and growth is an important aspect of tumor biology, including the progression of pre-malignant lesions to cancer [12]. KRC mice develop acinar-to-ductal metaplasia (ADM) and PanIN lesions that rapidly and frequently progress to mPDAC [117]. Moreover, lesion initiation and progression occurs in

conjunction with the appearance of inflammatory infiltrates and increased cytokine expression [117]. Therefore, we next used this GEMM to determine if inhibiting JAK1/2 with ruxolitinib could act to impede angiogenesis and suppress PanIN progression and mPDAC growth. Accordingly, we administered ruxolitinib to KRC mice at postnatal month 1, an age at which ADM, PanIN, and mPDAC are commonly observed in the pancreas. After 3 weeks of therapy, we evaluated their pancreata for extent and severity of disease. All vehicle-treated mice exhibited multiple foci of ADM, PanIN, and mPDAC (Figure 2.24A) that occurred in conjunction with strong, nuclear murine phosphorylated STAT3 (p-STAT3) immunoreactivity (Figure 2.24B). The cancer cells and ADM were proliferative as evidenced by the presence of nuclear phosphorylated Histone H3 (p-Histone H3), and were surrounded by an abundance of CD31 positive ECs (Figure 2.24B). Moreover, ECs in vehicle-treated mice frequently harbored nuclear p-STAT3 (Figure 2.24C). Remarkably, the pancreata of KRC mice receiving ruxolitinib were mostly normal, and only displayed small foci of ADM (Figure 2.24A) that exhibited weak p-STAT3 immunoreactivity and markedly attenuated proliferation, and were associated with few ECs (Figure 2.24B) in which nuclear p-STAT3 immunoreactivity was markedly attenuated (Figure 2.24C).

Moreover, in a survival study, 100% of ruxolitinib-treated mice were alive and healthy at postnatal week 14, with only one mouse succumbing at postnatal week 15 (Figure 2.24D). By contrast, all vehicle-treated mice succumbed by postnatal week 8.5 (Figure 2.24D). Therefore, ruxolitinib attenuates ADM progression to PanIN and mPDAC, while suppressing angiogenesis and markedly prolonging survival in this autochthonous model.

We next used the KPC GEMM to determine whether targeting JAK1/2 with ruxolitinib suppresses PanIN progression and mPDAC growth in this model. We administered ruxolitinib to KPC mice at postnatal month 3 when they often exhibited ADM, PanIN, and mPDAC. After 3 weeks of therapy, pancreatic histology from vehicle and ruxolitinib treated mice were similar (Figure 2.25A), and frequently exhibited abundant ADM, PanIN and mPDACs, with many p-Histone H3 positive nuclei but few CD31 positive ECs (Figure 2.25B). Therefore, ruxolitinib failed to suppress cancer cell proliferation or mPDAC progression in KPC mice.

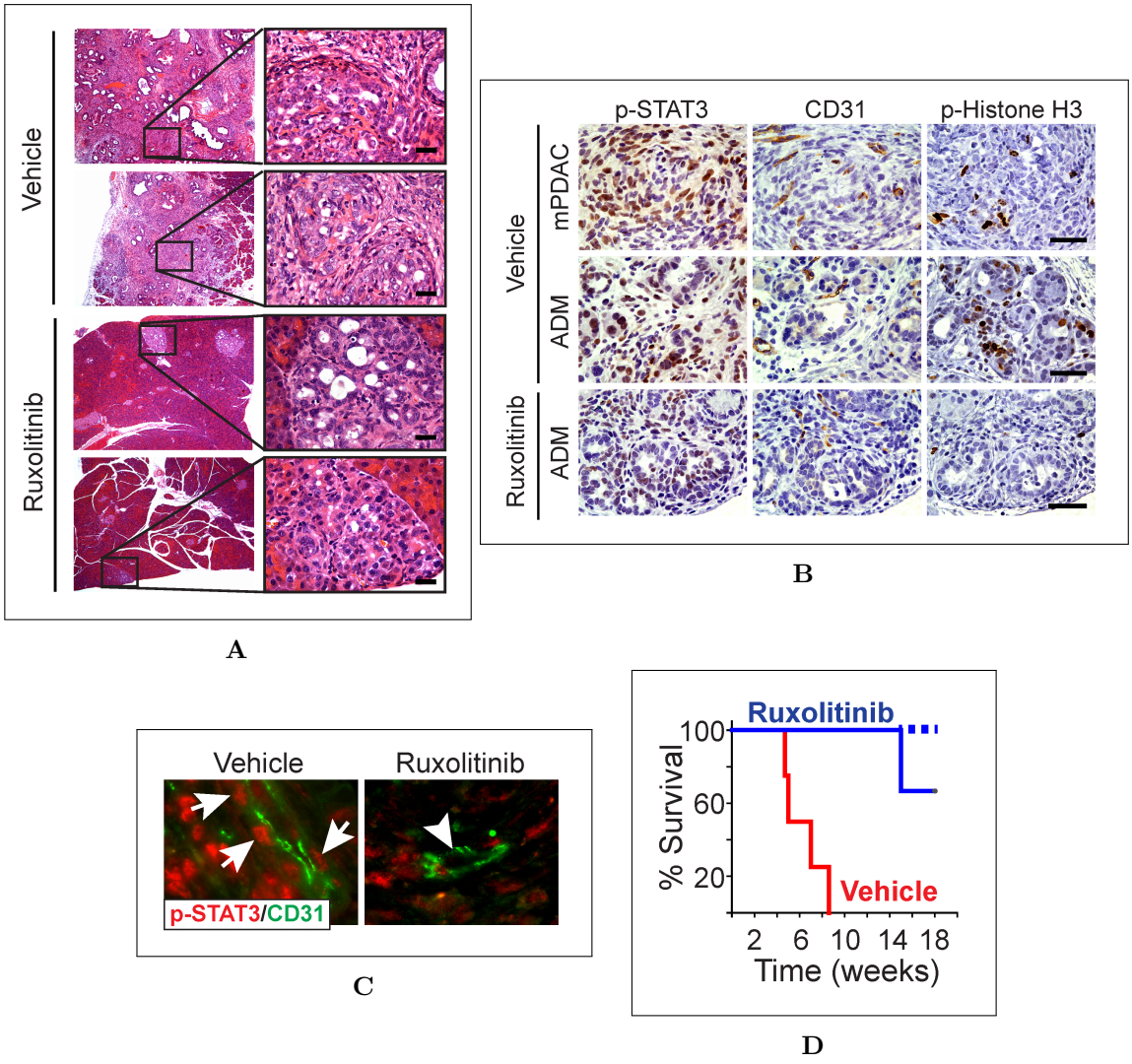

Figure 2.24: Ruxolitinib attenuates PDAC growth and prolongs survival in KRC mice. **(A)** Vehicle-treated mice display abundant lesions and murine PDAC (mPDAC), whereas ruxolitinib treated pancreata are mostly normal and only display small foci of acinar-to-ductal metaplasia (ADM). Shown are representative images from two mice per group. Right panels are high magnification images of boxed areas. **(B)** Nuclear murine phosphorylated STAT3 (p-STAT3) (left) is abundant in **K**ras$^{LSL\text{-}G12D/+}$; **R**b1$^{-/-}$; Pdx-1-**C**re (KRC) mPDACs (top) and ADM (middle) in vehicle treated mice, whereas ADM in ruxolitinib treated mice (bottom) have weak p-STAT3 immunoreactivity. mPDACs and ADM in vehicle treated mice also have abundant endothelial cells (ECs) and are highly proliferative as evidenced by the presence CD31 and phosphorylated Histone H3 (p-Histone H3) immunoreactivity, respectively. ADM in ruxolitinib treated mice have few CD31 positive ECs, and p-Histone H3 is mostly absent. **(C)** VE-cadherin (gene: Cdh5) positive ECs (green) in vehicle-treated KRC mice harbor nuclear p-STAT3 (left, red, arrows), whereas ECs in ruxolitinib treated mice lack nuclear p-STAT3 (right, arrowhead). All images were acquired using the same exposure time. Scale bars in (A-C), 50 μm. **(D)** Kaplan-Meier analysis shows that compared to vehicle (red line), ruxolitinib (blue line) significantly (P-value (P) = 0.018) prolongs survival of KRC mice. Dashed line indicates that two ruxolitinib treated mice were alive beyond postnatal week 18.

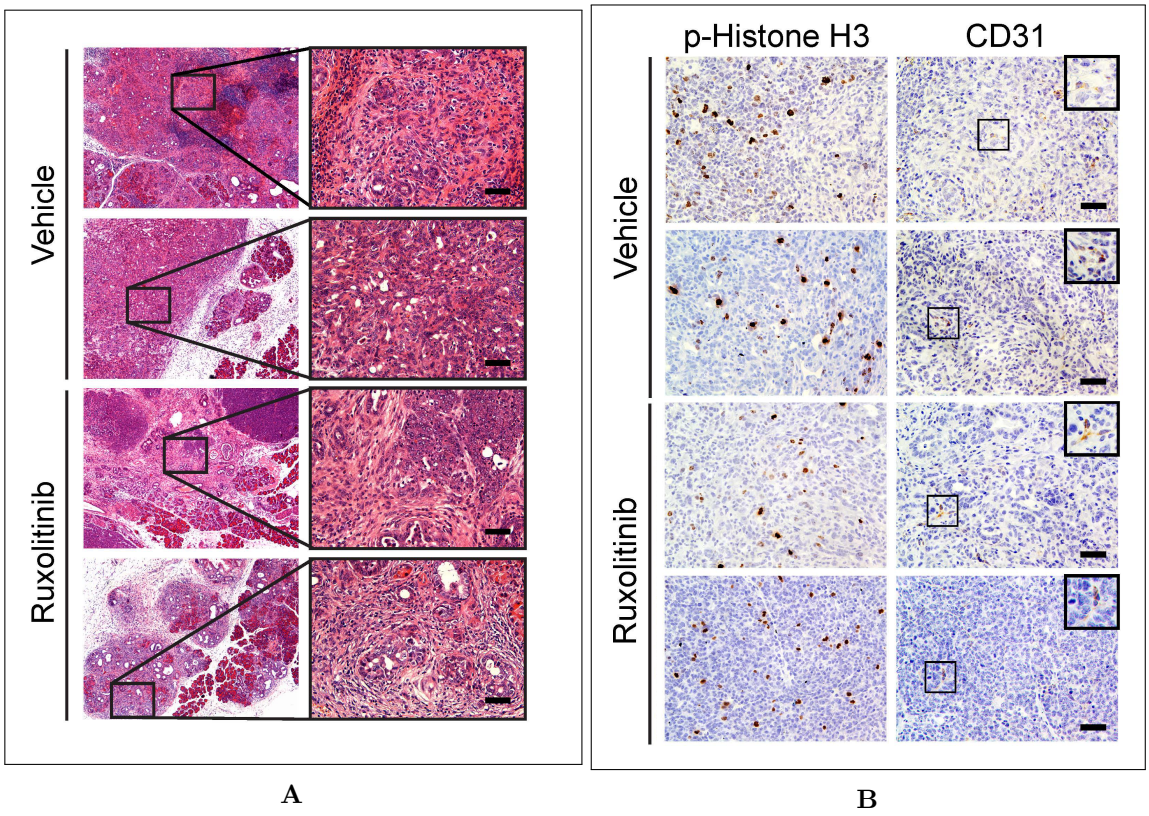

Figure 2.25: KPC mice do not benefit from Ruxolitinib. (A) Pancreata from vehicle and ruxolitinib treated **K**ras$^{\text{LSL-G12D/+}}$; Tr**p**53$^{\text{LSL-R172H/+}}$; Pdx-1-**C**re (KPC) mice are similar, and exhibit an abundance of lesions and murine PDAC (mPDAC). Right panels are high magnification images of boxed areas. **(B)** mPDACs in vehicle and ruxolitinib treated KPC mice harbor highly proliferative cancer cells, as evidenced by the presence of strong, nuclear phosphorylated Histone H3 (p-Histone H3) immunoreactivity, but few endothelial cells (ECs), as evidenced by the paucity of CD31 immunoreactivity. Shown in (A-B) are representative images from two mice per group. Scale bars, 50 μm.

3 Discussion

While the adult vasculature is primarily quiescent, notable examples of physiologic angiogenesis include wound healing or female reproductive processes [7, 8, 10–15]. Tumors, on the other hand, demonstrate pathologic angiogenesis, which often results in abnormal and leaky vessels [8, 10–13, 15–17, 19, 21]. Angiogenesis is required for tumor growth, as tumor fragments or cells placed in an avascular environment like a rabbit cornea are growth inhibited unless they can attract new capillaries [7]. Because both angiogenesis inducers and inhibitors can be active at the same time, tumors often undergo what is called an 'angiogenic switch' when the number of inducers begin to dominate [7, 8, 20]. Much effort has been spent on identifying the critical inducers or inhibitors in order to synthesize the endogenous inhibitors for use as anti-angiogenic drugs or to develop drugs that can block the inducers [127]. Known inducers include VEGFs, fibroblast growth factors (FGFs), platelet derived growth factors (PDGFs), angiopoietins (ANGPTs), TGF-β, and cytokines like IL-8 (gene: CXCL8) [81, 128], while inhibitors include interferons (IFNs), thrombospondins (TSPs), endostatin (gene: COL18A1) (endostatin), and angiostatin (gene: PLG) (angiostatin) [7, 127].

PDACs are often not considered to be angiogenic tumors or to be good candidates for anti-angiogenic therapy because of their lack of vasculature compared to a normal human pancreas [35, 36]. However, many tumor types display reduced MVDs compared to their normal tissue counterparts, including lung, mammary, renal cell, and colon carcinomas [37, 129]. Additionally, we have shown that MVD can be quite heterogeneous among PDAC tumors with 28%, 37%, and 35% of samples showing strong, moderate, and weak staining of the EC marker CD31. It is well established that MVD is useful as a prognostic marker for many cancers, including malignant melanoma, non-small-cell lung, genitourinary, esophageal, and gastrointestinal cancers [37], and one [40] of two [43] PDAC studies have shown that increased MVD is associated with decreased patient survival.

However, while MVD can account for the presence of blood vessels in tumors, it does not measure the rate of ongoing angiogenesis in the tumor. To measure that, other methods must be utilized such as dual staining for both endothelial and proliferative markers. Such methods have identified tumor types that are more angiogenic, such as glioblastoma and renal cell cancer, but there is still great variability in the angiogenic rate among different samples from these tumor types and all tumor types tested

(glioblastoma, renal cell, colon, breast, lung, prostate) have shown angiogenic rates above that of normal tissue, which usually is undetectable [129]. This confirms the importance of angiogenesis for all tumor growth.

To help identify important angiogenic pathways in PDAC, we analyzed RNA-Seq data from known angiogenic genes in TCGA and found that 35%, 47%, and 18% of PDAC samples demonstrate a Strong, Moderate, and Weak pro-angiogenic gene signature. While immunohistochemical analysis of TCGA samples is not possible, the mean and median levels of CD31 protein expression were higher in the PNET and Strong PDAC groups as compared to the Moderate and Weak PDAC groups, though there was significant variability within the samples of each group. While this classification was made using RNA-Seq technology, it would be interesting to see if this gene expression signature would correlate with protein expression as mRNA levels do not always correlate with protein expression levels [130]. Importantly, there are a number of pancreatic cancer studies that have utilized mass spectrometry to identify overexpressed proteins [131–133]. Additionally, the proteomic equivalent of TCGA, Clinical Proteomic Tumor Analysis Consortium (CPTAC) has released Funding Opportunity Announcements (FOAs) at the end of 2015 to support efforts that would explore the connections between cancer proteomes and cancer genomes, and it includes protocols for collecting PDAC samples. While there are many examples of the use of individual proteins as cancer biomarkers in clinical practice, the clinical use of a panel of molecular markers is currently limited to genomic based assays like Oncotype DX, MammaPrint, Prosigna, and Endopredict for breast cancer [134, 135].

TCGA dataset consisted of 8 PNET samples, which afforded a great opportunity to compare and contrast these two pancreatic tumor types in regards to angiogenic gene expression. In contrast to PDAC tumors, PNETs confer a better prognosis [24], exhibit abundant vasculature [88, 136], and respond to anti-VEGF directed therapy, including bevacizumab and multi-kinase inhibitors like sunitinib, sorafenib, and pazopanib, albeit with response rates of only 9-22% [88]. PNETs displayed a median of 19 non-silent somatic gene mutations while PDACs had a median of 47 non-silent somatic mutations. As expected, PDACs displayed frequent mutations or deletions in the KRAS, TP53, CDKN2A, or SMAD4 genes. While only 3 of the 8 PNET samples had DNA-Sequencing (DNA-Seq) data, none displayed mutations in genes commonly altered in PNETs, such as the chromatin modifiers MEN1, DAXX and ATRX, or mTOR pathway members [25, 137]. Two, however, displayed mutations in a different chromatin modifier, KMT2D. While the Weak PDAC group had a higher median number of mutations (64) than the Strong PDAC group (40), there was no

difference in the mutation rate of any individual known angiogenic gene between the two groups. While PDAC groups with differing amounts of structural chromosomal variation have been described before [28], this is the first time such a difference has been associated with the expression of an angiogenic gene signature.

Differential expression analysis comparing the PNET or Strong PDAC group to the Weak PDAC group revealed that the Strong PDAC group up-regulated 79 of 129 angiogenic genes while the PNET group up-regulated 41 of 129 angiogenic genes. Of these, 48 were unique to the Strong PDAC group, 10 were unique to the Weak PDAC group, and 31 were common between them.

While comparing PNETs to a PDAC subgroup may not be ideal, such comparisons have been done previously even when gene expression information on multiple pancreatic tissue types was available [100]. For example, Lowe et al. obtained gene expression information from PNETs, PDACs, normal pancreatic tissue, PCC lines, primary human cultures of pancreatic duct cells, and purified normal human islets [100]. Instead of comparing PNETs to normal human islets and PDAC tumors or PCC lines to normal pancreatic tissue (representing acinar cells) or pancreatic duct cells, Lowe et al. utilized the SAM algorithm to identify genes differentially expressed in one group as compared to all these other groups [100]. This analysis identified up-regulation of PNET genes like SCG2 (FC: 27.44), TTR (FC: 5.07), INSM1 (FC: 6.65), PCSK2 (FC: 20.44), QPCT (FC: 13.61), and PTPRN2 (FC: 6.81). For these same genes, our TCGA PNET vs. Weak PDAC comparison showed the following fold changes: SCG2 (FC: 65.37, FDR: 6.87E-05), TTR (FC: 51.23, FDR: 0.0014), INSM1 (FC: 43.76, FDR: 05.35E-08), PCSK2 (FC: 73.22, FDR: 5.86E-05), QPCT (FC: 15.03, FDR: 2.86E-05), and PTPRN2 (FC: 10.53, FDR: 5.35E-14), suggesting that such a comparison can correctly identify genes commonly up-regulated in PNETs [100, 138]. Because PNETs often arise from different cells within the islet to produce insulinomas vs. glucagonomas vs. somatostatinomas, one might also argue that normal human islets are not specific enough of a comparator for PNETs. Similarly, the cell of origin for PDAC tumors is still debated, and though PDACs appear ductal like, there is a large body of evidence that they originate from acinar cells instead of ductal cells [139]. Therefore, our choice to compare PNETs and one PDAC subgroup to another PDAC subgroup is befitting considering the uncertainty around what is the appropriate comparator and given the data available to us in TCGA.

Both SCG2 and ISL1 are also angiogenic genes that were uniquely up-regulated in PNETs. SCG2 can produce a peptide, secretoneurin, that can stimulate EC migration, induce capillary tube formation in a matrigel assay, and induce neovascularization in a mouse cornea model [140, 141]. ISL1 overexpression has also been shown to enhance the survival, migration, and the tube forming ability of HUVECs [142].

Interestingly, commonly up-regulated genes included all three of the VEGF receptor genes: FLT1, KDR, and FLT4. Additionally, both groups up-regulate other less well known angiogenic genes such as APOLD1, which encodes for vascular early response gene (VERGE) [143]; GPLD1, which is an enzyme that can cleave glycosylphosphatidylinositol (GPI) anchored proteins like Cripto-1 (gene: TDGF1), which then functions as a chemoattractant for ECs [144]; BMPER, an activator of FGF signaling [145]; and SFRP1, a pro-angiogenic molecule only expressed during the formation of neovessels and no longer present after vascular maturation [146]. PNETs and the Strong PDAC group also up-regulate many genes which traditionally have played a role in the nervous system, but now have been shown to also operate in the vascular system such as neurexin genes NRXN1 and NRXN3, ROBO4, SLIT2, and SEMA3E [147–151]. In regards to FGF signaling, both also up-regulate FGFR1, but only PNETs up-regulate FGF9 while also significantly down-regulating FGFR2 (FC: -17.60 , FDR: 3.17e-14). While the significance of the FGFR2 down-regulation in PNETs is unknown, such down-regulation has also been reported in prostate cancer [152] and use of a dominant negative FGFR2 in a prostate cancer mouse model has resulted in a neuroendocrine-like phenotype [153]. Neuroendocrine differentiation is a common phenotypic change observed in prostate cancer [154] and thus, low FGFR2 may be a characteristic of neuroendocrine differentiation.

The Strong PDAC group, on the other hand, expresses even more unique angiogenic genes, including pro-angiogenic collagens and integrins like COL15A1, COL4A3, ITGAV, ITGB1 and integrin interacting proteins like GPR124 (gene: ADGRA2) [155–157]. This group also overexpresses genes from the angiopoietin–Tie system, including ANGPT1, TEK, and TIE1; hypoxia related genes HIF1A and EPAS1, and TGF-β family members, including TGFBR1, TGFBR2, and ACVRL1. Overall, PNETs and PDACs have distinct angiogenesis gene signatures, which might explain their differential response to existing anti-angiogenic treatments.

Further investigation of the TGF-β signaling pathway identified 12 of the 79 angiogenic signature genes as known downstream targets, and an additional 50 TGF-β responsive genes were up-regulated in the Strong PDAC group. In line with this, the Strong PDAC group was less likely to have a mutation or deletion in SMAD4 (13%) as

compared to the Moderate (37%) or Weak (42%) PDAC groups, and SMAD4 protein expression correlated with CD31 protein expression ($r = +0.72$, $P < 0.01$) both in TCGA and a TMA. While TGF-β can inhibit cell proliferation, it also plays many other roles in embryogenesis, differentiation, apoptosis, motility, invasion, extracellular matrix production, angiogenesis, and the immune response [158, 159]. In tumor progression, TGF-β's tumor suppressor roles become inactivated, thus turning it into a tumor promoting molecule [158, 159]. While this inactivation might occur via mutations or deletions of genes in the canonical TGF-β pathway like SMAD4, we have also shown that deletion of Rb1 can produce this effect in the context of intact canonical TGF-β signaling [114]. Therefore, when we highlight that the Strong PDAC subgroup has active TGF-β signaling with an intact SMAD4 axis, we do so to emphasize that TGF-β's angiogenic role likely occurs through the canonical pathway and that inhibition of this angiogenic axis through TGF-β inhibition could be useful in this subgroup. Therefore, it is still possible that TGF-β inhibition could be useful in the other subgroups due to other active TGF-β tumor promoting properties in those samples.

Additional comparisons of differentially expressed genes between the Strong and Weak PDAC groups also identified enrichment of inflammatory gene sets, including up-regulation of 40 JAK/STAT signaling genes. In line with this, 3D co-culturing of human PCCs and human ECs showed activation of p-JAK1 (Figure 3.1A) and use of CM from human PCCs on human ECs or from human ECs on human PCCs revealed that this increase in p-JAK1 occurred in ECs alone (Figure 3.1B). Additionally, CM from both human cell types could increase p-SMAD levels in the other cell type (Figure 3.1B). Subsequently, targeting both TGF-β signaling with a TGF-β receptor type-1 inhibitor, SB505124, and JAK/STAT signaling with a JAK1/2 inhibitor, ruxolitinib, blocked human PCCs and human ECs from stimulating the proliferation of one another in a 3D co-culture system (Figure 3.1A). Similarly, ruxolitinib alone was able to prevent murine ECs from stimulating the proliferation of KRC PCCs in a 3D co-culture system (Figure 3.1C). However, in the mouse system, even though KRC CM was shown to stimulate the proliferation of murine ECs through p-STAT3, this proliferation of ECs was not seen in the 3D culture system. Therefore, in both human and murine cells, the more dramatic proliferation occurred in PCCs through a mechanism involving angiocrine signaling from ECs to PCCs. It is possible, however, that PCCs could induce this signaling by first stimulating the ECs to release proliferative growth factors.

To translate these findings to an *in vivo* system, KRC and KPC mice were given a course of ruxolitinib at a point when ADM, PanIN, and mPDAC lesions were

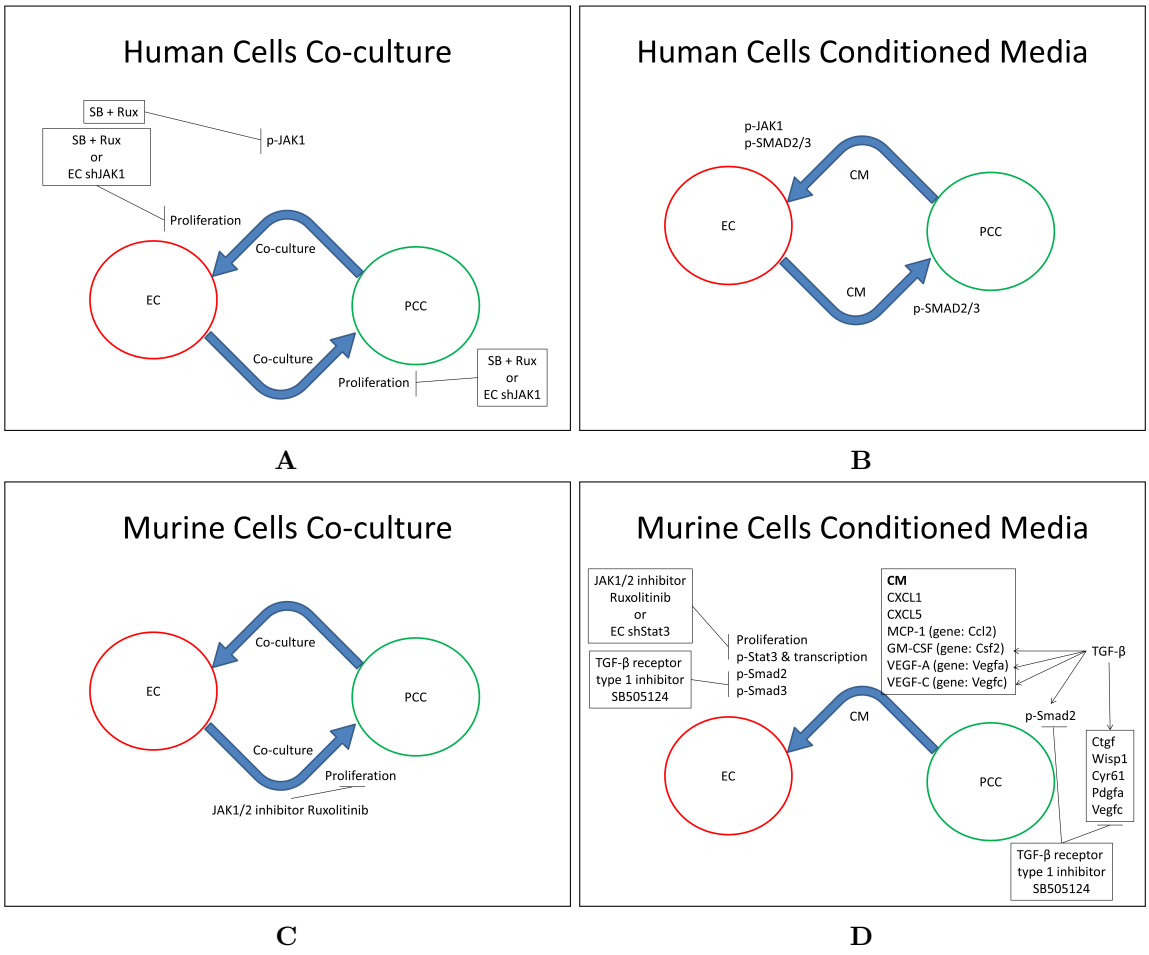

Figure 3.1: Ruxolitinib alone blocks murine SVEC4-10 EC + murine PCC proliferation while Ruxolitinib and SB505124 together block human vascular endothelial cell (HUVEC) + human PCC proliferation. (A) 3-dimensional (3D) co-culturing of human pancreatic cancer cells (PCCs) with human endothelial cells (ECs) leads to proliferation of both cell types, and this proliferation is blocked by treatment with SB505124 (SB) [2 μM]+Ruxolitinib (Rux) [100 nM] or shRNA knockdown of JAK1 in ECs. 3D co-culturing of human PCCs with ECs leads to phosphorylation of JAK1 and this is also blocked by SB505124 (SB) [2 μM]+Ruxolitinib (Rux) [100 nM] treatment. **(B)** Applying conditioned media (CM) from human PCCs to human ECs leads to activation of phosphorylated JAK1 (p-JAK1) and phosphorylated SMAD2/3 (p-SMAD2/3) whereas applying CM from human ECs to human PCCs only leads to activation of p-SMAD2/3. **(C)** 3D co-culturing of murine **K**ras$^{LSL\text{-}G12D/+}$; **R**b1$^{-/-}$; Pdx-1-**C**re (KRC) PCCs with murine ECs leads to the proliferation of KRC PCCs, and this is blocked by Ruxolitinib [100 nM] treatment. **(D)** Applying CM from murine KRC PCCs to ECs leads to the proliferation of ECs, and this is blocked by treatment with Ruxolitinib [100 nM] or shRNA knockdown of Stat3 in ECs. CM from KRC PCCs also leads to murine phosphorylated STAT3 (p-STAT3), murine phosphorylated SMAD2 (p-SMAD2), and murine phosphorylated SMAD3 (p-SMAD3) activation in ECs. Application of CM from KRC PCCs to ECs along with treatment of SB505124 [2 μM] blocks p-SMAD2 and p-SMAD3 activation in these cells, but it does not prevent the CM from stimulating proliferation of the ECs. CM from KRC PCCs contains CXCL1, CXCL5, MCP-1 (gene: Ccl2), GM-CSF (gene: Csf2), VEGF-A (gene: Vegfa), and VEGF-C (gene: Vegfc); TGF-β treatment [0.5 nM] of KRC PCCs increases the levels of the latter three. TGF-β treatment [0.5 nM] of KRC PCCs leads to increased SMAD2 phosphorylation and transcription of the pro-angiogenic Ctgf, Cyr61, Egfr, Nrp2, Serpine1, Tgfbr1 and Vegfc genes in these cells, and this is blocked by treatment with SB505124 [2 μM].

present. KRC mice demonstrated an improvement in survival and delayed mPDAC progression while KPC mice were refractory to treatment. Gene expression analysis of KRC and KPC tumors revealed significant expression of the previously identified TCGA angiogenic signature in the KRC model but not in the KPC model, giving a possible explanation for the refractoriness of KPC mice. However, some patient samples from the Strong PDAC group have mutations in both the KRAS and TP53 genes, suggesting it is not that simple of an explanation. While Kras and Trp53 are initiating mutations in the KPC model, different mice acquire distinct mutations during mPDAC progression and this results in more heterogeneous gene expression in KPC tumors than what we have observed in KRC tumors. Because PANC-1 cells also have a TP53 mutation, perhaps KPC mice and 'KP' patients in the Strong PDAC group would only benefit from the dual therapy treatment regimen. Overall, we have uncovered an important angiocrine mechanism in PDAC that could be targeted using dual TGF-β receptor type-1 and JAK1/2 inhibitors in the 35% of patients with a Strong pro-angiogenic gene signature.

4 Conclusion

Over the last 20 years, efforts in targeting angiogenesis in cancer have focused almost entirely on the pro-angiogenic molecule VEGF-A, and there are now several FDA approved drugs for various cancers [10, 13, 16, 17, 21, 160]. In reality, despite very convincing pre-clinical data, some cancers are completely resistant to such therapy, such as PDAC, or develop resistance over time [10, 13, 16, 17, 20, 21, 160]. This suggests that other angiogenic pathways that we have yet to address are involved.

Our analysis of TCGA RNA-Seq data from both PNET and PDAC tumors identified angiogenic pathways and genes unique to each tumor type. While we have successfully targeted the common TGF-β and JAK/STAT signaling pathways in pre-clinical PDAC models in this study, our analysis has identified many new uncommon and unexplored molecules in PNET or PDAC angiogenesis, such as SCG2 and ISL1 in PNETs, collagens and integrins in PDACs, or APOLD1, GPLD1, and SFRP1 in both PNETs and PDACs to name only a few. While this study has confirmed the importance of VEGF signaling in pancreatic cancer angiogenesis, it is clear that many other players are also involved and that successful targeting of angiogenesis in PDAC will entail targeting several of them simultaneously in the right patients.

5 Methods

5.1 Immunohistochemistry (IHC)

5.1.1 Human tissue microarray (TMA)

A paraffin-embedded hPDAC TMA was obtained from the Tissue Procurement and Distribution core at the Indiana University Simon Cancer Center, and 4 μm sections were prepared. Approval for the acquisition of all human tissue was granted by the Institutional Review Board (IRB) at the Office of Research Administration at Indiana University.

IHC was performed as described [114]. For the CD31 analysis, a CD31 (Abcam) antibody was used at a dilution of 1:200. For the CD31 and SMAD4 analysis, SMAD4 (Leica Biosystems, Buffalo Grove, IL) and CD31 (BD Biosciences, Franklin Lakes, NJ) antibodies were used. Quantitation was performed using positive pixel count in Aperio Imagescope software.

5.1.2 KRC or KPC tumors

IHC was performed as described [114]. In brief, pancreata from KRC or KPC mice were harvested at the indicated time points, fixed in 10% formalin overnight and embedded in paraffin. 4 μm sections were prepared using a HM355S microtome (Thermo Scientific). After deparaffinization and tissue rehydration, antigen retrieval was performed with antigen unmasking solution (Vector Labs, Burlingame, CA) or EDTA. A CD31 (Abcam) antibody was used at a dilution of 1:200, a CK19 (DSHB) antibody was used at a dilution of 1:10, a p-STAT3 antibody was used at a dilution of 1:200, and a p-Histone H3 antibody was used at a dilution of 1:200. Immunohistochemical detection was using biotinylated secondary antibodies, and a NOVA RED detection kit (Vector Labs). Masson's Trichrome (Richard-Allan Scientific) was performed according to manufacturer's recommendations.

For quantification, images were obtained at 20x magnification from 5 different fields using 3 mice using an Olympus BX60 microscope and a QImaging ExiBlue camera. Overall positive pixel intensity was determined using ImageProPlus v7.0 (Media Cybernetics). Quantitation data are presented as mean pixel intensity $\pm$ standard error of the mean (SEM).

5.2 Hierarchical clustering

5.2.1 TCGA angiogenic gene signature

Establishment of signature

The RNA-Seq RSEM [161] normalized reads and the raw count reads from TCGA pancreatic cancer dataset (abbreviated PAAD in TCGA), which has gene expression information on 88 samples from 85 patients: 85 tumor samples and 3 matched normal samples, was downloaded on June 6th, 2014 from http://cancergenome.nih.gov/. This dataset consists of 76 PDAC tumors, 3 colloid (mucinous non-cystic) carcinomas, and 6 samples of unknown histological type. For the analysis, we used all 85 tumor samples, for a total of 85 expression profiles. 580 Human UniProt ids that were directly or indirectly annotated to the GO [162] term angiogenesis (GO:0001525) were mapped to 389 Entrez gene ids via use of the BioMart [163, 164] Bioconductor [165, 166] package, 384 of which had expression values in TCGA dataset.

Hierarchical clustering was performed in R by applying a Pearson correlation distance and average linkage function to the normalized RSEM values of the 384 genes for the 85 tumor samples, and then scaling and graphing the result using the heatmap.2 function of the gplots R package. Because the resulting dendrograms indicated there was a subset of patients with up-regulated angiogenesis genes, we zoomed in on a dendrogram leaf of 129 genes, and then reclustered the data as follows. The normalized RSEM values for the 129 genes for the 85 tumor samples were first centered and scaled in R, and then hierarchical clustering on the rows was done using the Pearson correlation distance and average linkage function while column clustering was done using the Euclidean distance and complete linkage function. After graphing with heatmap.2, the result showed 3 distinct clusters of patients, which we assigned as having a "Strong" (n=10), "Moderate" (n=59), or "Weak" (n=16) angiogenesis signature.

Validation

The RNA-Seq RSEM [161] normalized reads and the raw count reads from TCGA pancreatic cancer dataset (abbreviated PAAD in TCGA), which has gene expression information on 183 samples from 178 patients: 179 tumor samples (2 samples from 1 patient) and 4 matched normal samples, was downloaded on December 31, 2014 from http://cancergenome.nih.gov/. This dataset consists of 135 PDAC tumors, 14 PDAC tumors with varying subtype designations, 4 colloid (mucinous non-cystic) carcinomas,

1 undifferentiated carcinoma, 8 PNETs, and 16 samples of unknown histological type. For the analysis, we only focused on the 135 PDAC tumors and the 8 PNETs, for a total of 143 expression profiles.

Using the previously determined 129 gene angiogenic signature, hierarchical clustering was performed in R by centering and scaling the normalized RSEM values of the 129 genes for the 143 tumor samples, and then clustering the rows using a Pearson correlation distance and average linkage function and the columns using a Euclidean distance and complete linkage function. The centered and scaled expression values were graphed as a heatmap with red representing up-regulated genes and green down-regulated genes in combination with the associated row and column dendrograms using the heatmap.2 function of the gplots R package. The 8 PNET samples all clustered together, and the PDAC tumors were assigned to a "Strong" (n=47), "Moderate" (n=64), or "Weak" (n=24) PDAC angiogenic group based on the remaining clustering results.

5.2.2 TGF-β responsive genes

For the TGF-β profile, 192 Human Genome Organisation (HUGO) gene names annotated to the "TGFB_UP.V1_UP" gene set, which represents genes up-regulated in a panel of epithelial cell lines by TGF-β1 (gene: TGFB1), were obtained from the GSEA Molecular Signatures Database. 190 of these had associated HUGO Gene Nomenclature Committee (HGNC) ids, which were then mapped to 190 Entrez gene ids using the *Homo sapiens* gene_info file available from the National Center for Biotechnology Information (NCBI) FTP site. 2 of the genes that were already a part of the 129 angiogenic signature were removed and another 2 did not have associated TCGA RNA-Seq information, bringing the final list used for clustering to 186 genes. In the clustering, the same samples and parameters were used as in the angiogenesis profile except that the sample columns were not clustered but instead placed in the same order as they appear in the angiogenesis profile. 70 of the 186 TGF-β responsive genes were differentially expressed ("Strong" vs. "Weak", $|FC| \geq 1.5$, FDR < 0.05).

5.2.3 Positive or negative regulation of the inflammatory response

For the inflammatory profiles, 130 or 142 human UniProt ids that were directly or indirectly annotated to the "positive regulation of inflammatory response" (GO:0050729) or the "negative regulation of inflammatory response" (GO:0050728) GO terms, respectively, were mapped to 93 or 92 Entrez gene ids, respectively, via

the use of the BioMart [163, 164] Bioconductor [165, 166] package. Both of these lists had 6 genes that were also a part of the original 129 angiogenic signature, and so these genes were removed, leaving a final list of 87 and 86 genes. 85 out of 87 positive regulators and 81 out of 86 negative regulators had associated TCGA RNA-Seq information. Clustering was performed separately on each list using the same samples and parameters as before except that the sample columns were not clustered, but instead placed in the same order as they appear in the angiogenesis profile. 35 out of the 85 positive regulators and 33 out of the 81 negative regulators were differentially expressed ("Strong" vs. "Weak", $|FC| \geq 1.5$, FDR < 0.05).

5.3 TCGA survival and treatment analysis

Survival or treatment information for PDAC and PNET patients was downloaded on December 31, 2014 from http://cancergenome.nih.gov/. All patients had associated clinical information on days to death or days to last follow-up (censored). Overall survival for the 8 PNET, 34 Stage IIB PDAC, and 15 Stage IIB PDAC patients was plotted using a Kaplan-Meier curve.

5.4 Differential expression

Differential expression analysis between the Strong and the Weak PDAC groups as well as the PNET and Weak PDAC groups was carried out using DESeq [101] on the raw count data. For the full dataset, 5,460 out of 20,531 genes are differentially expressed between the Strong and the Weak PDAC groups ($|FC| \geq 1.5$, FDR < 0.05), with 79 of them belonging to the 129 angiogenic gene signature, while 6,166 out of 20,531 genes are differentially expressed between the PNET and Weak PDAC groups ($|FC| \geq 1.5$, FDR < 0.05), with 50 of them belonging to the 129 angiogenic gene signature.

5.5 Principal Component Analysis (PCA)

PCs of the 129 expression values from the 143 samples were calculated using the prcomp function in R with options set to center and scale the data. 2 PCs account for 38% of the variance while 3 PCs account for 46% of the variance. The first two PCs were graphed using ggplot while the first three PCs were graphed using the plot3d function of the rgl package.

5.6 GeneMANIA

To assess angiogenesis gene interactions, we used GeneMANIA [102]. The angiogenesis genes unique to PNETs (10), unique to the Strong PDAC group (48), or genes that were common to both (31) were analyzed using GeneMANIA's pathway datasets. Any genes that were not directly connected were removed from the resulting network.

5.7 Mutation/copy number analysis

The curated mutation mutation annotation format (MAF) file (v.1.2.0) was downloaded on December 31, 2014 and included information from 98 PDAC cases and 3 PNET cases. The mutation calls are provided by the Broad Institute of MIT and Harvard, a genome sequencing center (GSC) for TCGA, and their pipeline for making the calls has not yet been distributed publicly or published for the pancreatic cancer dataset. Silent mutations were removed. Then, a matrix of genes and samples was built with each gene being coded as 1 (non-silently mutated), 0 (silently mutated or not mutated) or NA (no data available). Therefore, multiple non-silent mutations in a gene would only be counted once per gene. R was used to plot the mutation profiles of the samples in the same order as they appear in the angiogenesis cluster analysis. Significant differences in mutational frequencies were determined using a Fisher's exact test. $P < 0.05$ is considered statistically significant.

PDAC TCGA copy number data (level 4) was downloaded from the April 2, 2015 Broad GDAC Firehose GISTIC analysis run [167, 168]. The all_thresholded.by_genes.txt file was used, which classifies genes as having a copy number of -2 (deep loss, possibly a homozygous deletion), -1 (shallow loss, possibly a heterozygous deletion), 0 (diploid), 1 (low-level amplification), or 2 (high-level amplification). Of the PNET and PDAC samples, all 8 PNETs and 134 of 135 PDACs samples had copy number data. R was used to plot copy number profiles in the same order as in the angiogenesis cluster analysis. For combining SMAD4 mutation and deletion frequency, we used 97 PDAC samples that had both mutation and copy number data, with 40, 38, and 19 samples belonging to the Strong, Moderate, and Weak PDAC groups, respectively. Frequencies of samples with a mutation or deep deletion in SMAD4 were compared among the groups using a Fisher's exact test, with $P < 0.05$ considered significant.

5.8 Ingenuity Pathway Analysis (IPA)

The 79 of 129 differentially expressed angiogenic genes between the Strong and Weak PDAC groups (FC $\geq$ 1.5, FDR $<$ 0.05) was subjected to Ingenuity Pathway Analysis (IPA)'s Upstream Regulator Analysis tool to identify TGF-β as a major upstream regulator of 17 of the 79 genes.

5.9 Protein expression analysis

Normalized RPPA values were downloaded from TCGA PDAC dataset on December 31, 2014 from http://cancergenome.nih.gov. Of the 135 PDAC and 8 PNET samples used in the hierarchical clustering, 85 PDAC and 2 PNET samples had protein expression information. CD31 and SMAD4 protein expression values for the 85 PDAC and 2 PNET samples were used for plotting or calculating the correlation.

5.10 Gene Set Enrichment Analysis (GSEA)

5.10.1 Transplant rejection and inflammatory response gene sets for Strong PDAC vs. Weak PDAC

Using the GSEAPreranked tool, GSEA version 2.2.0 was run on a ranked list of genes that were sorted according to their fold change differences between the Strong and Weak PDAC groups [169, 170]. This analysis identified the transplant rejection and inflammatory response gene sets as being highly enriched.

5.10.2 TCGA angiogenic gene set for Genetically Engineered Mouse Model (GEMM) tumors vs. wild type (WT)

Normalized, log2-transformed array data from the 2 month KRC tumors, 4 month KRC tumors, and 3 month KPC tumors and age matched WT controls were prepared in GSEA format [169]. A custom chip file that mapped probesets from the Agilent SurePrint G3 Mouse GE 8x60K whole mouse genome microarray to HUGO gene symbols was generated. Using version 2.1.0 (KRC and matched WT) or 2.2.0 (KPC and matched WT) of the command line jar application, the array data was compared against the 79 differentially expressed angiogenesis genes (Strong vs. Weak PDAC) from the 129 TCGA angiogenesis gene signature.

5.10.3 TGF-β gene set for GEMM tumors vs. WT or KRC cells vs. KC cells

Normalized, log2-transformed array data from the 2 month KRC tumors, 4 month KRC tumors, KRC cells, KC cells, and 3 month KPC tumors and age matched WT controls were prepared in GSEA format [169]. A custom chip file that mapped probesets from the Agilent SurePrint G3 Mouse GE 8x60K whole mouse genome microarray or the Agilent Whole Mouse Genome 4x44K microarray to HUGO gene symbols was generated. Using version 2.1.0 (KRC and matched WT) or 2.0.13 (KRC or KC cells) of the command line jar application, the array data was compared against the PLASARI_TGFB1_TARGETS_10HR_UP gene set [171], which represents 'Genes up-regulated in mouse embryonic fibroblasts (MEF) cells upon stimulation with TGF-β1 [GeneID=7040] for 10 hours'.

5.11 JAK/STAT heatmap

145 genes involved in JAK/STAT signaling were obtained from the GSEA KEGG_JAK_STAT_SIGNALING_PATHWAY gene set. The differentially expressed FCs and FDRs for these genes were isolated from the differential expression analysis comparing the Strong and Moderate PDAC groups to the Weak PDAC group. 45/145 genes were differentially expressed in at least one of these comparisons ($|FC| >= 1.5$, $FDR < 0.05$) and the FCs were graphed in a heatmap using the heatmap.2 function of the gplots R package with red representing up-regulation, green representing down-regulation, and gray representing not differentially expressed.

5.12 Cell lines and conditioned media (CM)

5.12.1 Human

PANC-1 (CRL-1469) PCCs were from American Type Culture Collection (ATCC). The IUSCC-PC-1 cell line was established from a patient-derived orthotopic xenograft in an athymic mouse [122]. IUSCC-PC-1 cells were authenticated, and confirmed to be human and free of pathogens and other cell types by IDEXX Bioresearch (St. Louis, MO). By sequencing, the cell line harbored a KRAS mutation ($KRAS^{G12D/+}$) but lacked SMAD4 mutations, and readily formed tumors in nude mice. HUVEC (CRL-1730) ECs were from ATCC. PCCs were cultured in Dulbecco's Modified Eagle Medium (DMEM) with 1% antibiotic (100 units/ml penicillin; 100 mg/ml streptomycin) and 5% fetal bovine serum (FBS). HUVECs were cultured in EGM-2 medium (Lonza, Walkersville,

MD). HUVECs were transduced with lentivirus containing JAK1 targeting shRNAs or a non-targeting control shRNA from Thermo Fisher (Waltham, MA) as described [142].

5.12.2 Mouse

KRC cells were generated using standard cell isolation and culture procedures as described [114, 117]. SVEC4–10 ECs were obtained from ATCC (CRL-2181). ECs were cultured in DMEM supplemented with 1% antibiotic (100 units/ml penicillin; 100 mg/ml streptomycin) and 10% FBS. For CM, KRC cells were seeded in 10 cm tissue culture plates (BD Falcon). 72 hours post-serum starvation, media was collected, centrifuged and filtered through a 0.22 μm syringe filter.

5.13 3-dimensional (3D) culture

3D culturing was done as described [114]. PCCs and ECs were fluorescently-labeled before culturing in 3D. PCCs were transduced with an eGFP lentiviral construct (Clontech), and ECs were labeled using the PKH26 red fluorescent cell linker kit per the manufacturer's recommendations (Sigma-Aldrich). 3,000 PCCs or 6,000 ECs were cultured alone or together in 3% matrigel. Two days after plating, and every two days thereafter, cells were treated with control media, media with ruxolitinib [100 nM], media with SB505124 [2 μM], or media with ruxolitinib [100 nM] and SB505124 [2 μM]. The final concentration of DMSO in all experiments was 0.05%. Images were acquired with a Leica DMI3000 inverted microscope outfitted with a DFC300 FX camera. Fluorescence intensity was determined on three independent experiments plated in duplicate using Image Pro Plus v.7 (Media Cybernetics).

5.14 Immunoblotting

5.14.1 Human

Immunoblotting was performed and lysates were prepared as described [114] using CD31 (BD Biosciences), phosphorylated and total SMAD, phosphorylated JAK2 (p-JAK2), PARP (Cell Signaling Technology, Danvers, MA), and p-JAK1, JAK1, JAK2 and ERK2 (gene: MAPK1) (Santa Cruz Biotechnology, Dallas, TX) antibodies. Quantification of band area in each immunoblot was performed using ImageJ software (http://imagej.nih.gov/ij/) from three independent experiments, and quantitation is presented as mean ± SEM.

5.14.2 Mouse

ECs (200,000/well) were seeded in 6-well plates, serum-starved, and media was replaced with control or CM containing SB505124 [2 μM], ruxolitinib [100 nM] or DMSO [0.05%]. Lysates were prepared and immunoblotting was performed as described [114]. For Stat3 knockdown, lysates were prepared from control- and shRNA-transduced cells 48 hours post-seeding. p-SMAD2 (Cell Signaling), p-SMAD3 (Millipore), and SMAD2/3 (Cell Signaling) antibodies were used at dilutions of 1:1000. p-STAT3 and STAT3 antibodies were used at dilutions of 1:2000 and 1:1000, respectively.

5.15 Mice

KRC and KPC mice were generated and maintained as described [114, 119]. For intravital imaging, TRITC conjugated dextran (80 mg/kg) and hoescht (10 mg/kg) were prepared in sterile saline, and injected into the tail vein of anesthetized KRC mice. A lateral incision was made, and the pancreas was exposed and imaged using a Leica TCS SP8 confocal microscope. Mice remained under anesthesia for the entire experiment.

For therapeutic studies, 8 KRC mice or 8 KPC mice were randomized into ruxolitinib (4 mice) or vehicle control (4 mice) groups at postnatal weeks 4 or 12, respectively. For survival studies, 7 KRC mice were randomized into ruxolitinib (4 mice) or vehicle control (3 mice) groups. Ruxolitinib (50 mg/kg) or equal volumes of vehicle (0.5% hydroxypropyl methylcellulose (HPMC)) were administered to mice by daily gavage. This dose is equivalent to or lower than doses used in other studies with this drug [116, 172, 173]. All mice were genotyped twice (pre-weaning and post-necropsy). All mouse studies were approved by the Institutional Care and Use Committee of Indiana University. Log rank Kaplan-Meier survival analysis was used to test for significant differences using Sigma Plot v.11.0 software (Systat Software).

5.16 Orthotopic model

KRC cells (200,000 cells) were injected into the pancreas of 28 (20 males, 8 females) 10-week-old syngeneic mice using KRC1017 and KRC1022-4 cells (10 males, 4 females per cell line). On day 10, mice were randomized to vehicle and SB505124 treatment groups (7 mice per group; 5 males and 2 females in each). Before treatment began, tumors were imaged using Vevo2100 high-resolution ultrasound (VisualSonics). Mice

were injected i.p. daily with vehicle (75% DMSO, 25% saline) or 10 mg/kg SB505124, and 7 days later tumors were imaged. 3D abdominal scans were acquired on days 10 (pretreatment) and 17 (1 week after treatment), and tumor volumes were calculated using Vevo2100 System software. Daily injections continued up to day 50, and mice were sacrificed as they became moribund. All mouse studies were approved by the Institutional Care and Use Committee of Indiana University.

Sigma Plot was used for log-rank survival analysis, and 1 mouse from the SB505124 group was censored from the survival analysis since it died on day 10, shortly after the first injection.

5.17 KRC tumor microarrays

Agilent SurePrint G3 Mouse GE 8x60K whole mouse genome microarrays were hybridized using total RNA from five 2 month-old or four 4 month-old KRC tumors (Cy5-labeled), or five and four age- and sex-matched normal pancreata (Cy3-labeled), respectively. Array analysis of KRC tumors was performed by Miltenyi Biotec. Briefly, array intensity values were extracted, background corrected, LOWESS normalized, quantile normalized, and log2 transformed. Unpaired t-tests with equal variance were used to test log2-normalized data for significant differences. The FDR was controlled by adjusting the P-values using the method of Benjamini and Hochberg [174]. Differentially expressed genes were considered statistically significant using $|FC| >= 2$, $P < 0.01$ for the GO analysis and $FC >= 1.5$, $FDR < 0.05$ otherwise. For comparison to the human TCGA 79 out of 129 gene angiogenic signature ($FC >= 1.5$, $FDR < 0.05$, Strong vs. Weak PDAC), 77 mouse homologs were used, resulting in 13 and 43 concordantly expressed genes ($FC >= 1.5$, $FDR < 0.05$) in the 2 month old or 4 month old KRC tumors as compared to age-matched normal pancreata.

5.18 KPC tumor microarrays

Agilent SurePrint G3 Mouse GE 8x60K whole mouse genome microarrays were hybridized using total RNA from three 3 month-old tumors (Cy5-labeled), or three age- and sex-matched normal pancreata (Cy3-labeled). Array analysis of KRC tumors was performed by Miltenyi Biotec. Briefly, array intensity values were extracted, background corrected, log2 transformed, LOESS normalized, and quantile normalized. Unpaired t-tests with equal variance were used to test log2-normalized data for significant differences. The FDR was controlled by adjusting the P-values using the method of Benjamini and Hochberg [174]. Differentially expressed genes were

considered statistically significant using FC >= 1.5, FDR < 0.05. For comparison to the human TCGA 79 out of 129 gene angiogenic signature (FC >= 1.5, FDR < 0.05, Strong vs. Weak PDAC), 77 mouse homologs were used, resulting in 0 concordantly expressed genes (FC >= 1.5, FDR < 0.05) in the 3 month old KPC tumors as compared to age-matched normal pancreata.

5.19 KRC and KC cell line microarrays

Agilent Whole Mouse Genome 4x44K Microarrays were hybridized using total RNA from 3 different passages of 3 pooled KRC cell lines (3 hybridizations total) (Cy5-labeled), or 3 different passages of 2 pooled KC cell lines (3 samples technically replicated for a total of 6 hybridizations). Array analysis of KRC and KC cell lines was performed by Miltenyi Biotec. Briefly, array intensity values were extracted, background corrected, log2 transformed, LOESS normalized, and quantile normalized. Unpaired t-tests with equal variance were used to test log2-normalized data for significant differences. The FDR was controlled by adjusting the P-values (Ps) using the method of Benjamini and Hochberg [174]. Differentially expressed genes were considered statistically significant using |FC| >= 2, P < 0.01 for the GO analysis and FC >= 1.5, FDR < 0.05 otherwise.

5.20 KRC tumor Gene Ontology (GO)

For each probeset on the array (55,681 probesets), gene annotation information, including the Entrez Gene ID, RefSeq ID, or gene symbol if available, were used to identify the associated Mouse Genome Informatics (MGI) ID (http://www.informatics.jax.org/) or multiple MGI IDs in a few cases of ambiguity. Matches were found for 34,531 probesets representing 25,806 unique MGI IDs.

For the 2 month tumors compared to 2 month WT pancreata, 3,535 differentially expressed probesets were identified (|FC| >= 2, P < 0.01), and 2,550 of these had a matching MGI ID (representing 2,419 unique MGI IDs). For the 4 month tumors compared to 4 month WT pancreata, 6,641 differentially expressed probesets were identified (|FC| >= 2, P < 0.01), and 5,003 of these had a matching MGI ID (representing 4,432 unique MGI IDs).

For each time point, the final unique MGI ID gene list and the 25,806 MGI ID background gene list were uploaded on the Database for Annotation, Visualization and Integrated Discovery (DAVID) site (http://david.abcc.ncifcrf.gov/home.jsp, version 6.7) [175, 176], and an analysis was run using the MGI ID as the identifier. We then

focused on the enriched GO terms [162] in the biological process FAT ontology (which represents a subset of the more specific terms from the ontology). The visualization tool in AmiGO (http://amigo.geneontology.org/visualize?mode=client_amigo) was used to generate the graphical GO graphs.

5.21 KRC vs. KC cell line GO

For each probeset on the array (41,174 probesets), gene annotation information, including the Entrez Gene ID, RefSeq ID, or gene symbol if available, were used to identify the associated MGI ID (http://www.informatics.jax.org/). Matches were found for 34,640 probesets representing 21,247 unique MGI IDs.

For KRC cells compared to KC cells, 2,960 differentially expressed probesets were identified ($|FC| >= 2$, $P < 0.01$), and 2,773 of these had a matching MGI ID (representing 2,206 unique MGI IDs).

The 2,206 MGI ID gene list and the 21,247 MGI ID background gene list were uploaded on the DAVID site (http://david.abcc.ncifcrf.gov/home.jsp, version 6.7) [175, 176], and an analysis was run using the MGI ID as the identifier. We then focused on the enriched GO terms [162] in the biological process FAT ontology (which represents a subset of the more specific GO terms). The visualization tool in AmiGO (http://amigo.geneontology.org/visualize?mode=client_amigo) was used to generate the graphical GO graphs.

5.22 Quantitative Polymerase Chain Reaction (qPCR)

qPCR was performed for the indicated mRNAs using Taqman gene expression assays (Life Technologies) and cDNA prepared from total RNA as described [114, 117]. Actb and Rps6 served as the endogenous controls for cells and tumor tissues, respectively.

5.23 Cell proliferation

Cell proliferation was assessed by MTT [177]. Briefly, ECs (5,000/well) were seeded in 96-well plates, serum starved, and media was replaced with serum-free media (control) or CM from KRC cells. For inhibitor studies, SB505124 [2 μM], ruxolitinib [100 nM] or DMSO [0.05%] were added to control and CM. Stat3 knockdown was performed as described [142] by transducing ECs with two shRNAs that target murine

Stat3 [178] or a non-targeting shRNA control (Thermo Scientific). Proliferation was assessed at 48 hours. The mean of control-treated cells was normalized to 100%, and changes in proliferation were calculated as % control in three independent experiments.

5.24 Migration

Migration was assessed using a Boyden chamber assay. ECs (20,000) were seeded in 8.0 μm cell culture inserts (BD Biosciences) in serum-free media, and placed into 24-well plates containing serum-free media, or CM. For inhibitors, SB505124 [2 μM], ruxolitinib [100 nM] or DMSO [0.05%] were added to the inserts and wells. After 16 hours, cells were fixed in methanol and stained. The total number of cells that migrated was counted.

5.25 Enzyme-linked immunosorbent assay (ELISA)

KRC cells were seeded in 6-well plates (200,000/well). After 24 hours, cells were serum-starved overnight, and treated with control media or TGF-β1 (gene: Tgfb1) [0.5 nM] for 24 hours. CM was prepared, and levels of the indicated cytokines were determined using a Milliplex ELISA kit (Millipore) per the manufacturer's recommendation.

5.26 Luciferase assays

ECs (25,000) were seeded in 24-well culture plates. After 24 hours, ECs were transfected with a STAT3 luciferase reporter (Promega), and Renilla to control for transfection efficiency, using Lipofectamine 2000. After overnight serum starvation, media was replaced with control media or CM for 24 hours, and luciferase assays were performed on three independent experiments as described [114].

6 Supplemental material

6.1 Supplemental tables

Table S1: Expression of 186 TGF-β responsive genes in Strong PDAC and PNET vs. Weak PDAC

Entrez Gene ID	Gene Symbol	Strong PDAC vs. Weak PDAC			PNET vs. Weak PDAC		
		Fold Change	P-value	FDR	Fold Change	P-value	FDR
25841	ABTB2	-1.50	0.001686	0.008159	-8.76	6.63E-13	3.06E-11
23205	ACSBG1	1.23	1	1	24.25	0.175672	0.337868
53616	ADAM22	7.97	3.42E-13	3.01E-11	3.78	0.000637	0.003431
9590	AKAP12	3.79	1.37E-10	5.31E-09	1.62	0.198132	0.368052
286	ANK1	-2.98	0.000112	0.000807	1.22	0.660044	0.812612
23141	ANKLE2	-1.24	0.0763	0.183431	1.13	0.631461	0.790037
94134	ARHGAP12	-1.20	0.180306	0.35276	-1.92	0.006344	0.02383
467	ATF3	-1.16	0.280025	0.485873	-2.58	0.02225	0.066527
54880	BCOR	1.00	0.925665	1	1.70	0.007745	0.028063
8553	BHLHE40	-1.44	0.001574	0.007694	-3.61	5.50E-08	8.81E-07
635	BHMT	-1.27	0.674828	0.850796	1.58	0.677618	0.826618
659	BMPR2	1.93	1.26E-05	0.000121	-1.06	0.710588	0.852558
676	BRDT	3.41	1	1	-2.19	1	1
28984	C13orf15	1.56	0.02266	0.069772	1.90	0.019646	0.060253
126353	C19orf21	-3.93	2.34E-17	7.37E-15	-6.85	9.82E-10	2.30E-08
27042	C1orf107	-1.05	0.693799	0.857321	-2.17	0.001376	0.006637
81626	C1orf14	1.78	1	1	-Inf	1	1
221749	C6orf145	1.13	0.483499	0.704075	-2.07	0.001577	0.007445
203197	C9orf91	1.53	0.006379	0.024712	1.78	0.014934	0.04824
65981	CAPRIN2	-2.34	0.000191	0.001277	-1.61	0.25224	0.438729
838	CASP5	1.26	0.770198	0.901502	-5.72	0.374824	0.58161
79780	CCDC82	1.14	0.518067	0.737443	-1.22	0.480953	0.684663
54520	CCDC93	1.15	0.355736	0.573358	1.34	0.1724	0.332867
9332	CD163	5.32	3.03E-11	1.42E-09	-1.99	0.037955	0.102589
913	CD1E	3.58	9.66E-05	0.000714	-2.72	0.024562	0.072198
10849	CD3EAP	-1.01	0.766337	0.899805	-1.30	0.255079	0.441977
5128	CDK17	1.68	0.001242	0.006311	1.42	0.09233	0.207009
55602	CDKN2AIP	-1.26	0.089821	0.208515	1.10	0.696386	0.841997
1030	CDKN2B	1.82	0.013022	0.044207	-3.29	0.000765	0.004013

PDAC: Pancreatic ductal adenocarcinoma; PNET: Pancreatic neuroendocrine tumor; FDR: False Discovery Rate; 15 genes up-regulated in both Strong PDAC and PNET vs. Weak PDAC; 50 genes up-regulated in Strong PDAC vs. Weak PDAC; 25 genes up-regulated in PNET vs. Weak PDAC; Differential expression cut off: Fold Change >= 1.5, FDR < 0.05

Entrez Gene ID	Gene Symbol	Strong PDAC vs. Weak PDAC			PNET vs. Weak PDAC		
		Fold Change	P-value	FDR	Fold Change	P-value	FDR
50515	CHST11	1.82	0.001907	0.009035	-1.76	0.01087	0.037173
9469	CHST3	1.90	0.000113	0.000811	-1.02	0.710898	0.852776
1160	CKMT2	1.08	0.683904	0.853518	-3.48	0.0181	0.056383
23529	CLCF1	-1.42	0.009147	0.033102	-18.01	1.68E-18	1.96E-16
1307	COL16A1	1.39	0.044775	0.120671	-2.57	0.000189	0.001196
1410	CRYAB	1.57	0.27534	0.480768	3.35	0.038759	0.104317
1436	CSF1R	3.09	2.65E-13	2.47E-11	-1.23	0.247224	0.432026
1454	CSNK1E	-1.38	0.011202	0.039043	-1.04	0.835104	0.947254
1474	CST6	-1.35	0.247021	0.445257	-116.94	8.77E-08	1.33E-06
1490	CTGF	3.33	1.11E-07	1.86E-06	1.03	0.862929	0.967639
1591	CYP24A1	1.09	1	1	-100.23	0.008872	0.031411
56603	CYP26B1	2.77	8.09E-05	0.000614	2.33	0.016291	0.05174
1573	CYP2J2	-2.24	2.89E-06	3.28E-05	-6.82	1.27E-08	2.36E-07
9267	CYTH1	-1.05	0.354144	0.571534	-2.02	0.003228	0.013609
51339	DACT1	2.63	4.39E-09	1.10E-07	-2.28	0.00157	0.007418
1644	DDC	-1.90	0.396732	0.61618	15.03	0.002554	0.011166
25786	DGCR11	-1.14	0.652232	0.839763	-1.74	0.313331	0.512871
10395	DLC1	3.17	6.90E-14	7.65E-12	2.19	0.000228	0.001405
23333	DPY19L1	1.03	1	1	-1.94	0.003275	0.013794
8445	DYRK2	1.28	0.092332	0.212974	-1.09	0.658264	0.811179
1906	EDN1	1.12	0.467069	0.68813	-4.87	3.04E-07	4.03E-06
22936	ELL2	1.79	4.12E-06	4.50E-05	7.23	6.82E-24	2.01E-21
2043	EPHA4	1.03	0.812846	0.929315	1.48	0.217778	0.394668
2114	ETS2	1.10	0.687442	0.85424	-2.05	0.000467	0.002634
2150	F2RL1	-1.65	0.00474	0.01931	-8.60	1.88E-10	5.23E-09
79633	FAT4	5.32	1.58E-20	1.25E-17	2.02	0.007414	0.027068
10979	FERMT2	3.11	1.15E-13	1.17E-11	1.29	0.235036	0.416798
2244	FGB	-1.41	0.724069	0.873385	116.69	0.098781	0.217665
2246	FGF1	1.91	0.194811	0.374355	12.11	4.87E-05	0.000365
54874	FNBP1L	1.10	0.463622	0.684982	1.20	0.381186	0.588152
2297	FOXD1	-2.96	7.67E-05	0.000585	-21.06	6.94E-06	6.49E-05
2295	FOXF2	1.21	0.462769	0.684307	-2.33	0.005274	0.020498
51343	FZR1	-1.78	8.28E-06	8.38E-05	1.28	0.310171	0.509018
4616	GADD45B	1.31	0.244027	0.441464	1.16	0.383587	0.590564
8843	GPR109B	2.24	0.063272	0.15848	-5.38	0.008142	0.029254

PDAC: Pancreatic ductal adenocarcinoma; PNET: Pancreatic neuroendocrine tumor; FDR: False Discovery Rate; 15 genes up-regulated in both Strong PDAC and PNET vs. Weak PDAC; 50 genes up-regulated in Strong PDAC vs. Weak PDAC; 25 genes up-regulated in PNET vs. Weak PDAC; Differential expression cut off: Fold Change >= 1.5, FDR < 0.05

Entrez Gene ID	Gene Symbol	Strong PDAC vs. Weak PDAC			PNET vs. Weak PDAC		
		Fold Change	P-value	FDR	Fold Change	P-value	FDR
3142	HLX	1.21	0.418067	0.638368	-1.25	0.273136	0.463779
3269	HRH1	-1.23	0.078402	0.18734	-4.27	4.77E-08	7.75E-07
9956	HS3ST2	1.95	0.240568	0.43662	-5.09	0.059959	0.147315
3352	HTR1D	-1.06	0.843386	0.949958	-5.50	0.000507	0.002821
3373	HYAL1	-2.82	3.10E-06	3.49E-05	-9.79	1.29E-06	1.45E-05
3399	ID3	1.03	0.898439	0.986619	-1.06	0.584586	0.752716
3589	IL11	1.87	0.48517	0.705724	-4.52	0.219862	0.397423
29949	IL19	-2.29	0.346467	0.563436	-Inf	0.235528	0.417483
9173	IL1RL1	3.88	0.004441	0.01831	1.97	0.26266	0.45084
3667	IRS1	1.30	0.164925	0.330817	-1.55	0.018936	0.058514
3678	ITGA5	1.88	0.00143	0.007113	-1.76	0.025214	0.073721
3694	ITGB6	-1.20	0.196205	0.376223	-156.01	5.74E-19	7.26E-17
58494	JAM2	2.83	2.32E-08	4.76E-07	1.24	0.307727	0.505975
221037	JMJD1C	1.57	0.003792	0.016096	-1.08	0.663027	0.814641
23210	JMJD6	-1.20	0.141488	0.29553	1.21	0.471906	0.676124
3725	JUN	-1.11	0.230011	0.423357	-1.66	0.010102	0.034982
3726	JUNB	-1.75	1.27E-06	1.61E-05	-1.67	0.010997	0.037534
23189	KANK1	1.52	0.013635	0.045944	3.10	3.24E-06	3.28E-05
3783	KCNN4	-3.25	4.45E-15	7.31E-13	-163.87	3.09E-33	3.05E-30
23135	KDM6B	1.21	0.263495	0.46611	1.85	0.005399	0.020896
80759	KHDC1	-1.36	0.302388	0.512847	2.34	0.068656	0.164048
7071	KLF10	1.51	0.008035	0.029789	1.09	0.599354	0.765094
9314	KLF4	-1.66	0.000337	0.002085	-3.89	2.54E-06	2.64E-05
8609	KLF7	2.08	0.000897	0.004785	-1.32	0.200868	0.371979
55323	LARP6	1.09	0.671374	0.849771	1.29	0.355642	0.560123
23592	LEMD3	1.34	0.040008	0.110186	1.27	0.257506	0.444505
3976	LIF	-1.36	0.041359	0.113	-3.12	7.30E-05	0.000522
9388	LIPG	1.82	0.001285	0.006494	-2.10	0.003518	0.014642
29995	LMCD1	1.73	0.001973	0.009297	-1.03	0.801165	0.921573
29967	LRP12	3.39	3.32E-12	2.14E-10	3.33	4.17E-07	5.30E-06
4053	LTBP2	3.07	6.28E-14	7.21E-12	-1.12	0.383343	0.590308
4054	LTBP3	1.12	0.530327	0.747979	1.51	0.038431	0.103591
116372	LYPD1	1.03	0.866997	0.965274	-3.04	0.014884	0.048133
9935	MAFB	2.69	0.008175	0.030182	17.59	1.58E-08	2.86E-07
4216	MAP3K4	1.42	0.014183	0.047443	1.87	0.003287	0.01383

PDAC: Pancreatic ductal adenocarcinoma; PNET: Pancreatic neuroendocrine tumor; FDR: False Discovery Rate; 15 genes up-regulated in both Strong PDAC and PNET vs. Weak PDAC; 50 genes up-regulated in Strong PDAC vs. Weak PDAC; 25 genes up-regulated in PNET vs. Weak PDAC; Differential expression cut off: Fold Change >= 1.5, FDR < 0.05

Entrez Gene ID	Gene Symbol	Strong PDAC vs. Weak PDAC			PNET vs. Weak PDAC		
		Fold Change	P-value	FDR	Fold Change	P-value	FDR
4142	MAS1	1.42	1	1	129.46	0.241457	0.425281
4146	MATN1	1.22	0.978986	1	2.00	0.557309	0.732503
54797	MED18	-1.22	0.335781	0.552403	-1.34	0.375345	0.582188
57591	MKL1	1.06	0.967787	1	-1.60	0.046285	0.120024
22877	MLXIP	1.65	0.000496	0.002906	1.89	0.002791	0.01205
23531	MMD	1.87	9.99E-05	0.000734	1.05	0.880584	0.979094
10205	MPZL2	-1.15	0.368703	0.586358	-12.34	4.50E-12	1.73E-10
9617	MTRF1	-1.38	0.067629	0.167219	-1.27	0.400481	0.606918
4606	MYBPC2	3.79	0.152071	0.311643	-7.54	0.246888	0.43161
9612	NCOR2	-1.17	0.132268	0.280335	1.73	0.011355	0.03845
3340	NDST1	1.87	2.48E-06	2.88E-05	3.53	4.37E-11	1.39E-09
4776	NFATC4	1.04	0.859542	0.959934	1.66	0.168547	0.326941
4803	NGF	1.62	0.27086	0.475285	1.04	0.722244	0.861361
4908	NTF3	1.15	0.882171	0.97594	-1.29	0.852683	0.960022
58495	OVOL2	-3.37	1.75E-12	1.22E-10	-2.35	0.01552	0.049757
400961	PAIP2B	-1.41	0.761897	0.897157	3.31	0.0123	0.04122
5154	PDGFA	-1.67	0.0003	0.001883	-1.31	0.568087	0.739334
5155	PDGFB	1.05	1	1	-1.25	0.25153	0.437865
8572	PDLIM4	-1.04	0.592905	0.797824	1.81	0.134812	0.276712
5209	PFKFB3	1.14	0.837375	0.946192	-1.26	0.279043	0.471457
9767	PHF16	1.15	0.320814	0.535408	-1.10	0.903682	0.995004
23187	PHLDB1	1.51	0.004391	0.018137	-1.88	0.003485	0.014525
5293	PIK3CD	2.81	1.21E-08	2.66E-07	-1.66	0.040039	0.107091
5569	PKIA	1.80	0.007294	0.027533	2.28	0.006303	0.023725
59338	PLEKHA1	-1.13	0.373285	0.591042	-1.27	0.276309	0.467919
56937	PMEPA1	-1.15	0.274573	0.479725	-9.24	6.06E-13	2.83E-11
5376	PMP22	2.19	0.000293	0.001847	-1.47	0.182326	0.347239
5467	PPARD	-1.02	0.628708	0.824119	-2.12	0.00119	0.00587
10848	PPP1R13L	-2.53	1.42E-10	5.51E-09	-5.89	2.83E-09	6.02E-08
5521	PPP2R2B	2.29	0.001532	0.007525	13.74	9.09E-13	4.06E-11
5553	PRG2	-1.68	0.299683	0.509526	-2.08	0.496087	0.69676
79037	PVRIG	2.06	0.095408	0.218622	1.47	0.456456	0.661672
9693	RAPGEF2	1.43	0.015956	0.052179	1.43	0.124769	0.260478
23186	RCOR1	-1.24	0.112413	0.247689	-1.06	0.742573	0.876287
8786	RGS11	-1.46	0.199496	0.380632	6.38	1.66E-05	0.00014

PDAC: Pancreatic ductal adenocarcinoma; PNET: Pancreatic neuroendocrine tumor; FDR: False Discovery Rate; 15 genes up-regulated in both Strong PDAC and PNET vs. Weak PDAC; 50 genes up-regulated in Strong PDAC vs. Weak PDAC; 25 genes up-regulated in PNET vs. Weak PDAC; Differential expression cut off: Fold Change >= 1.5, FDR < 0.05

Entrez Gene ID	Gene Symbol	Strong PDAC vs. Weak PDAC			PNET vs. Weak PDAC		
		Fold Change	P-value	FDR	Fold Change	P-value	FDR
6002	RGS12	-1.94	2.18E-07	3.35E-06	1.20	0.625767	0.786101
388	RHOB	-1.32	0.005838	0.022959	-1.56	0.019829	0.060644
6038	RNASE4	-1.58	0.033794	0.096078	1.73	0.072076	0.170564
376412	RNF126P1	-1.94	0.404669	0.624551	-2.36	0.86816	0.970968
127544	RNF19B	1.01	0.818081	0.932219	-1.18	0.437159	0.643217
6236	RRAD	1.16	0.998934	1	-2.56	0.650931	0.805719
9853	RUSC2	1.11	0.73376	0.879502	1.35	0.41221	0.618671
6274	S100A3	-1.57	0.045352	0.121858	-5.19	0.000364	0.002116
29970	SCHIP1	1.64	0.00758	0.028386	2.28	0.001727	0.008049
23541	SEC14L2	-1.30	0.08198	0.193917	-3.12	0.00024	0.001468
6446	SGK1	2.19	1.45E-08	3.12E-07	-1.82	0.022461	0.067054
8631	SKAP1	-2.36	0.155027	0.316038	3.29	0.103478	0.225697
6498	SKIL	1.99	4.10E-05	0.000338	-3.04	3.11E-06	3.17E-05
10786	SLC17A3	-1.22	0.770785	0.901891	3.82	0.482116	0.685895
1836	SLC26A2	2.44	3.83E-09	9.75E-08	2.37	5.86E-05	0.000428
9057	SLC7A6	1.47	0.01728	0.055779	-1.17	0.51088	0.707316
6578	SLCO2A1	1.53	0.025653	0.076978	1.14	0.625347	0.785874
4091	SMAD6	-2.33	1.92E-07	3.01E-06	-2.97	0.000274	0.001651
54498	SMOX	-2.24	2.85E-08	5.68E-07	-3.86	1.03E-07	1.53E-06
6525	SMTN	1.26	0.710213	0.866357	-2.09	0.315032	0.514662
57154	SMURF1	-1.50	0.000728	0.004008	-1.87	0.014587	0.047364
64750	SMURF2	1.56	0.005722	0.02259	-1.12	0.641038	0.797712
6615	SNAI1	2.11	5.14E-05	0.000412	-1.92	0.016928	0.05343
9306	SOCS6	1.34	0.057184	0.146596	1.66	0.03024	0.085499
8877	SPHK1	-1.35	0.053592	0.139147	-5.92	9.06E-08	1.36E-06
80176	SPSB1	1.73	0.000173	0.001177	-1.81	0.00912	0.032157
23648	SSBP3	-1.32	0.062633	0.157215	1.20	0.185921	0.351489
6781	STC1	2.20	9.74E-07	1.26E-05	2.02	0.003392	0.0142
6862	T	-3.83	0.419899	0.64036	-2.70	1	1
6876	TAGLN	1.83	0.012635	0.043109	-2.38	0.021745	0.065283
23102	TBC1D2B	1.60	0.001821	0.008694	-1.19	0.411877	0.618354
9519	TBPL1	1.08	0.560233	0.772924	1.46	0.109594	0.235857
6926	TBX3	1.90	0.000278	0.001766	1.91	0.040844	0.108845
7942	TFEB	-1.17	0.203398	0.386332	1.35	0.244926	0.429114
7066	THPO	-1.09	1	1	-5.55	0.12764	0.265208

PDAC: Pancreatic ductal adenocarcinoma; PNET: Pancreatic neuroendocrine tumor; FDR: False Discovery Rate; 15 genes up-regulated in both Strong PDAC and PNET vs. Weak PDAC; 50 genes up-regulated in Strong PDAC vs. Weak PDAC; 25 genes up-regulated in PNET vs. Weak PDAC; Differential expression cut off: Fold Change >= 1.5, FDR < 0.05

Entrez Gene ID	Gene Symbol	Strong PDAC vs. Weak PDAC			PNET vs. Weak PDAC		
		Fold Change	P-value	FDR	Fold Change	P-value	FDR
7090	TLE3	-1.18	0.138481	0.290477	-1.25	0.504674	0.703056
79905	TMC7	-2.69	6.89E-11	2.90E-09	-22.60	5.03E-20	7.63E-18
25816	TNFAIP8	1.55	0.012616	0.043051	-6.96	1.44E-11	4.98E-10
84951	TNS4	-1.83	0.010356	0.03666	-2250.70	7.26E-16	5.78E-14
10221	TRIB1	-1.10	0.277087	0.482704	-2.46	0.000124	0.000823
10382	TUBB4	-1.28	0.283641	0.49036	-1.37	0.392716	0.599197
56995	TULP4	1.39	0.026084	0.077982	1.70	0.019603	0.06014
5412	UBL3	1.36	0.020416	0.064146	2.59	7.10E-06	6.61E-05
7481	WNT11	-2.26	0.047416	0.126231	-6.39	0.077876	0.18138
51384	WNT16	-1.76	0.225762	0.417354	-1.34	0.782576	0.907168
7473	WNT3	-1.02	0.931365	1	1.19	0.821232	0.937107
54361	WNT4	1.24	0.589148	0.794771	30.49	6.42E-07	7.81E-06
7476	WNT7A	-2.30	0.000805	0.004364	-94.33	1.26E-11	4.41E-10
81555	YIPF5	1.35	0.024842	0.074982	1.22	0.352082	0.556469
23174	ZCCHC14	1.10	0.562568	0.774584	1.05	0.763676	0.892619
677	ZFP36L1	1.33	0.083793	0.197238	-4.82	5.16E-11	1.62E-09
55279	ZNF654	1.35	0.103117	0.231715	-1.03	0.90664	0.997089

PDAC: Pancreatic ductal adenocarcinoma; PNET: Pancreatic neuroendocrine tumor; FDR: False Discovery Rate; 15 genes up-regulated in both Strong PDAC and PNET vs. Weak PDAC; 50 genes up-regulated in Strong PDAC vs. Weak PDAC; 25 genes up-regulated in PNET vs. Weak PDAC; Differential expression cut off: Fold Change >= 1.5, FDR < 0.05

Table S2: Expression of 85 positive regulators of inflammation in Strong PDAC vs. Weak PDAC

Entrez Gene ID	Gene Symbol	Strong PDAC vs. Weak PDAC		
		Fold Change	P-value	FDR
101	ADAM8	-2.18	1.25E-07	2.07E-06
136	ADORA2B	-1.40	0.327524	0.543411
140	ADORA3	2.78	4.72E-08	8.75E-07
185	AGTR1	2.35	0.000345	0.002126
338699	ANKRD42	1.02	0.898732	0.986776

PDAC: Pancreatic ductal adenocarcinoma; FDR: False Discovery Rate; 28 genes up-regulated in Strong PDAC vs. Weak PDAC; 35 genes differentially expressed in Strong PDAC vs. Weak PDAC (28 up-regulated, 7 down-regulated); Differential expression cut off: |Fold Change| >= 1.5, FDR < 0.05

Entrez Gene ID	Gene Symbol	Strong PDAC vs. Weak PDAC		
		Fold Change	P-value	FDR
6369	CCL24	-6.02	0.265392	0.468215
6348	CCL3	1.78	0.037072	0.103521
1236	CCR7	8.60	0.004296	0.017835
100133941	CD24	-1.23	0.345747	0.562815
940	CD28	8.26	3.22E-11	1.50E-09
961	CD47	1.03	0.832139	0.942403
9575	CLOCK	2.16	1.01E-05	9.99E-05
1268	CNR1	5.38	1.65E-10	6.31E-09
84699	CREB3L3	-2.87	0.401734	0.621051
1520	CTSS	1.11	0.57403	0.783145
6376	CX3CL1	-1.13	0.395828	0.615206
1909	EDNRA	2.53	4.40E-09	1.10E-07
1956	EGFR	1.70	0.00155	0.007595
2161	F12	-6.21	3.35E-15	5.68E-13
2167	FABP4	3.31	0.034416	0.097503
2205	FCER1A	2.66	0.000966	0.005082
2207	FCER1G	1.89	0.000282	0.001785
2867	FFAR2	-1.97	0.450042	0.671311
2865	FFAR3	1.32	0.561418	0.773537
51704	GPRC5B	1.04	0.893443	0.983375
8692	HYAL2	1.21	0.194683	0.374217
3620	IDO1	2.81	0.239865	0.435599
3593	IL12B	3.16	0.334213	0.550746
3600	IL15	1.13	0.696756	0.858676
3605	IL17A	9.42	1	1
27190	IL17B	1.30	0.919437	1
27189	IL17C	-4.67	0.044896	0.120851
112744	IL17F	-2.45	0.649887	0.838644
23765	IL17RA	1.29	0.173192	0.342351
84818	IL17RC	-1.77	2.58E-05	0.000226
3606	IL18	-1.24	0.092931	0.214054
9173	IL1RL1	3.88	0.004441	0.01831
3558	IL2	2.88	0.772575	0.902868
59067	IL21	Inf	1	1

PDAC: Pancreatic ductal adenocarcinoma; FDR: False Discovery Rate; 28 genes up-regulated in Strong PDAC vs. Weak PDAC; 35 genes differentially expressed in Strong PDAC vs. Weak PDAC (28 up-regulated, 7 down-regulated); Differential expression cut off: |Fold Change| >= 1.5, FDR < 0.05

Entrez Gene ID	Gene Symbol	Strong PDAC vs. Weak PDAC		
		Fold Change	P-value	FDR
51561	IL23A	-1.46	0.107447	0.239118
90865	IL33	5.12	1.03E-12	7.78E-11
3569	IL6	4.06	0.008857	0.032238
3572	IL6ST	5.81	9.39E-20	5.49E-17
3673	ITGA2	1.34	0.099583	0.226062
3717	JAK2	1.59	0.008254	0.030425
3818	KLKB1	1.00	0.974636	1
3929	LBP	2.91	0.19577	0.375759
4049	LTA	4.90	0.001887	0.008958
5603	MAPK13	-1.56	0.006447	0.024891
91662	NLRP12	2.60	0.072132	0.175901
4889	NPY5R	1.24	0.701563	0.861658
5008	OSM	1.37	0.371834	0.589543
9180	OSMR	2.27	4.31E-07	6.15E-06
5138	PDE2A	2.81	7.58E-10	2.44E-08
5320	PLA2G2A	1.30	1	1
7941	PLA2G7	2.47	0.021131	0.065952
5733	PTGER3	3.79	3.96E-13	3.43E-11
5734	PTGER4	1.64	0.000637	0.003575
5743	PTGS2	1.47	0.55703	0.770377
6223	RPS19	-2.16	1.32E-07	2.15E-06
6283	S100A12	3.55	0.083594	0.196844
6279	S100A8	-1.00	0.698008	0.85942
6280	S100A9	-1.02	0.764485	0.898862
5054	SERPINE1	3.65	7.38E-07	9.88E-06
8723	SNX4	1.06	0.726897	0.875185
6776	STAT5A	1.13	0.59753	0.801278
6777	STAT5B	1.42	0.022094	0.06837
6863	TAC1	-1.45	0.383751	0.603045
7052	TGM2	1.48	0.099061	0.225149
81793	TLR10	9.80	5.76E-05	0.000455
7097	TLR2	1.83	0.000326	0.002029
7098	TLR3	1.37	0.107796	0.239626
7099	TLR4	3.10	3.33E-11	1.55E-09

PDAC: Pancreatic ductal adenocarcinoma; FDR: False Discovery Rate; 28 genes up-regulated in Strong PDAC vs. Weak PDAC; 35 genes differentially expressed in Strong PDAC vs. Weak PDAC (28 up-regulated, 7 down-regulated); Differential expression cut off: |Fold Change| >= 1.5, FDR < 0.05

Entrez Gene ID	Gene Symbol	Strong PDAC vs. Weak PDAC		
		Fold Change	P-value	FDR
51284	TLR7	4.61	1.05E-11	5.77E-10
54106	TLR9	1.93	0.056105	0.14437
7124	TNF	-1.04	0.568062	0.778033
8792	TNFRSF11A	-1.41	0.168751	0.336384
7132	TNFRSF1A	-1.11	0.349323	0.565869
8600	TNFSF11	-1.59	0.093752	0.215598
7292	TNFSF4	2.06	0.002548	0.011533
10318	TNIP1	-1.28	0.055041	0.142091
6845	VAMP7	1.65	0.000551	0.003168
8673	VAMP8	-2.01	3.11E-07	4.58E-06
7474	WNT5A	1.77	0.00685	0.026145
7784	ZP3	-2.28	1.80E-05	0.000165

PDAC: Pancreatic ductal adenocarcinoma; FDR: False Discovery Rate; 28 genes up-regulated in Strong PDAC vs. Weak PDAC; 35 genes differentially expressed in Strong PDAC vs. Weak PDAC (28 up-regulated, 7 down-regulated); Differential expression cut off: |Fold Change| >= 1.5, FDR < 0.05

Table S3: Expression of 81 negative regulators of inflammation in Strong PDAC vs. Weak PDAC

Entrez Gene ID	Gene Symbol	Strong PDAC vs. Weak PDAC		
		Fold Change	P-value	FDR
29	ABR	-1.02	0.827246	0.938538
54	ACP5	1.29	0.613756	0.813698
100	ADA	1.16	0.487718	0.708096
116	ADCYAP1	3.88	0.001388	0.006933
9370	ADIPOQ	10.99	0.003206	0.013933
134	ADORA1	-1.44	0.347902	0.56478
325	APCS	1.03	0.807491	0.925483
335	APOA1	1.02	1	1

PDAC: Pancreatic ductal adenocarcinoma; FDR: False Discovery Rate; 17 genes down-regulated in Strong PDAC vs. Weak PDAC; 33 genes differentially expressed in Strong PDAC vs. Weak PDAC (16 up-regulated, 17 down-regulated); Differential expression cut off: |Fold Change| >= 1.5, FDR < 0.05

Entrez Gene ID	Gene Symbol	Strong PDAC vs. Weak PDAC		
		Fold Change	P-value	FDR
348	APOE	1.18	0.912798	0.99624
55870	ASH1L	1.38	0.022006	0.068192
613	BCR	-1.51	0.001573	0.007693
114899	C1QTNF3	2.14	0.020014	0.063193
80381	CD276	1.07	0.822491	0.93528
66005	CHID1	-1.45	0.077573	0.185794
1269	CNR2	26.26	0.000343	0.002114
11221	DUSP10	-1.32	0.116857	0.255058
1991	ELANE	-1.02	0.767792	0.900335
90268	FAM105B	1.16	0.368931	0.586627
388581	FAM132A	-3.37	3.10E-05	0.000265
55527	FEM1A	-1.03	1	1
2294	FOXF1	2.12	0.000595	0.003377
50943	FOXP3	4.20	1.38E-06	1.73E-05
2625	GATA3	1.50	0.328561	0.544631
2629	GBA	-1.17	0.335523	0.55207
2693	GHSR	4.83	0.371577	0.589423
2852	GPER	-1.54	0.580602	0.788616
338557	GPR120	-4.11	0.028049	0.082564
2876	GPX1	-1.61	0.000157	0.001084
2877	GPX2	-3.32	9.25E-08	1.60E-06
2950	GSTP1	-2.32	5.91E-11	2.53E-09
3123	HLA-DRB1	2.08	0.000373	0.00227
8870	IER3	-2.53	7.66E-08	1.34E-06
3586	IL10	3.03	0.035074	0.099084
3593	IL12B	3.16	0.334213	0.550746
3558	IL2	2.88	0.772575	0.902868
53833	IL20RB	-1.47	0.330891	0.547291
116379	IL22RA2	1.01	0.799682	0.920372
3559	IL2RA	3.84	3.93E-08	7.47E-07
3565	IL4	1.45	0.97783	1
3630	INS	1.18	0.794523	0.917077
9314	KLF4	-1.66	0.000337	0.002085
3848	KRT1	4.36	0.072277	0.176083

PDAC: Pancreatic ductal adenocarcinoma; FDR: False Discovery Rate; 17 genes down-regulated in Strong PDAC vs. Weak PDAC; 33 genes differentially expressed in Strong PDAC vs. Weak PDAC (16 up-regulated, 17 down-regulated); Differential expression cut off: |Fold Change| >= 1.5, FDR < 0.05

Entrez Gene ID	Gene Symbol	Strong PDAC vs. Weak PDAC		
		Fold Change	P-value	FDR
5598	MAPK7	-1.03	0.579672	0.787785
4210	MEFV	3.99	0.003634	0.015501
284207	METRNL	-1.50	0.000295	0.001854
4598	MVK	-1.87	9.38E-05	0.000697
80762	NDFIP1	1.00	0.721453	0.872355
4790	NFKB1	1.28	0.093579	0.215251
91662	NLRP12	2.60	0.072132	0.175901
114548	NLRP3	3.99	6.42E-09	1.53E-07
79671	NLRX1	-1.24	0.11242	0.247689
64127	NOD2	1.23	0.601968	0.804244
10062	NR1H3	-1.55	0.000785	0.004272
4907	NT5E	-1.10	0.745993	0.886751
55872	PBK	-1.54	0.036326	0.10184
8993	PGLYRP1	1.68	0.967955	1
5467	PPARD	-1.02	0.628708	0.824119
5468	PPARG	-2.82	1.00E-08	2.26E-07
5580	PRKCD	-1.52	0.000383	0.00232
5692	PSMB4	-1.64	0.000331	0.002054
5734	PTGER4	1.64	0.000637	0.003575
5740	PTGIS	2.51	0.032953	0.094137
5771	PTPN2	-1.08	0.566503	0.777092
27342	RABGEF1	1.06	0.659667	0.843973
6223	RPS19	-2.16	1.32E-07	2.15E-06
6288	SAA1	1.56	0.332259	0.548654
55829	SELS	-1.44	0.010148	0.036066
462	SERPINC1	-5.45	0.002483	0.011294
5176	SERPINF1	2.70	3.37E-10	1.17E-08
81858	SHARPIN	-1.92	2.10E-06	2.50E-05
4088	SMAD3	-1.65	1.94E-05	0.000176
9021	SOCS3	1.73	0.004227	0.017615
6693	SPN	3.36	3.34E-10	1.17E-08
7032	TFF2	-1.85	0.215818	0.404138
7128	TNFAIP3	2.69	2.90E-09	7.66E-08
79626	TNFAIP8L2	2.12	0.001088	0.005629

PDAC: Pancreatic ductal adenocarcinoma; FDR: False Discovery Rate; 17 genes down-regulated in Strong PDAC vs. Weak PDAC; 33 genes differentially expressed in Strong PDAC vs. Weak PDAC (16 up-regulated, 17 down-regulated); Differential expression cut off: |Fold Change| >= 1.5, FDR < 0.05

Entrez Gene ID	Gene Symbol	Strong PDAC vs. Weak PDAC		
		Fold Change	P-value	FDR
7132	TNFRSF1A	-1.11	0.349323	0.565869
7133	TNFRSF1B	1.84	0.000111	0.0008
7301	TYRO3	-1.32	0.167036	0.333937
55075	UACA	1.31	0.091579	0.211729
7538	ZFP36	1.06	0.780563	0.908267

PDAC: Pancreatic ductal adenocarcinoma; FDR: False Discovery Rate; 17 genes down-regulated in Strong PDAC vs. Weak PDAC; 33 genes differentially expressed in Strong PDAC vs. Weak PDAC (16 up-regulated, 17 down-regulated); Differential expression cut off: |Fold Change| >= 1.5, FDR < 0.05

Table S4: Expression of 45 JAK/STAT signaling pathway genes in Strong and Moderate PDAC vs. Weak PDAC

Entrez Gene ID	Gene Symbol	Strong PDAC vs. Weak PDAC			Moderate PDAC vs. Weak PDAC		
		Fold Change	P-value	FDR	Fold Change	P-value	FDR
10000	AKT3	3.42	7.12E-15	1.05E-12	2.09	2.91E-07	8.88E-05
867	CBL	1.66	0.003123	0.013644	1.32	0.123839	0.451204
23624	CBLC	-4.26	7.19E-25	2.04E-21	-1.68	6.96E-05	0.004001
1271	CNTFR	1.56	0.664617	0.847142	-4.02	0.001979	0.037008
1438	CSF2RA	2.36	1.49E-05	0.00014	1.28	0.258325	0.660969
1439	CSF2RB	4.98	2.82E-07	4.21E-06	1.96	0.025106	0.181024
1441	CSF3R	2.68	0.000418	0.002506	1.73	0.056468	0.29521
2033	EP300	1.64	0.00059	0.003353	1.32	0.049323	0.272434
2057	EPOR	-1.51	0.011135	0.038858	-1.16	0.264323	0.669341
2690	GHR	4.99	8.99E-06	9.01E-05	1.75	0.047669	0.267402
338376	IFNE	-7.53	0.002234	0.010338	-1.85	0.279327	0.6884
3459	IFNGR1	1.56	0.002345	0.010776	1.26	0.098858	0.399409
3587	IL10RA	3.23	7.52E-11	3.12E-09	1.33	0.119316	0.442423
3594	IL12RB1	1.91	0.014321	0.047841	1.09	0.695597	0.934695
50615	IL21R	3.43	1.10E-05	0.000108	1.66	0.053024	0.285062
3559	IL2RA	3.84	3.93E-08	7.47E-07	1.88	0.012143	0.115874

PDAC: Pancreatic ductal adenocarcinoma; FDR: False Discovery Rate; 44 differentially expressed genes in Strong PDAC vs. Weak PDAC (40 up-regulated, 4 down-regulated); 10 differentially expressed in Moderate PDAC vs. Weak PDAC (8 up-regulated, 2 down-regulated); Differential expression cut off: |Fold Change| >= 1.5, FDR < 0.05

Entrez Gene ID	Gene Symbol	Strong PDAC vs. Weak PDAC			Moderate PDAC vs. Weak PDAC		
		Fold Change	P-value	FDR	Fold Change	P-value	FDR
3560	IL2RB	3.42	4.88E-09	1.19E-07	1.54	0.021141	0.163487
3561	IL2RG	-1.73	0.004305	0.017862	-1.48	0.048387	0.269966
3563	IL3RA	1.58	0.007286	0.027509	1.09	0.525521	0.891302
3569	IL6	4.06	0.008857	0.032238	1.01	0.817692	0.983347
3570	IL6R	2.86	6.32E-05	0.000494	1.41	0.163812	0.526778
3572	IL6ST	5.81	9.39E-20	5.49E-17	2.43	3.26E-07	9.02E-05
3575	IL7R	9.98	9.41E-18	3.66E-15	2.54	0.000195	0.008046
3716	JAK1	1.72	0.000154	0.001067	1.32	0.038427	0.233472
3717	JAK2	1.59	0.008254	0.030425	-1.03	0.649789	0.918528
3718	JAK3	2.25	0.000455	0.002697	1.25	0.353542	0.764938
3952	LEP	7.28	0.014287	0.047744	-2.01	0.381413	0.78991
3953	LEPR	3.87	1.75E-09	4.95E-08	1.86	0.001661	0.033534
3977	LIFR	2.30	2.48E-06	2.87E-05	-1.09	0.715637	0.943575
9180	OSMR	2.27	4.31E-07	6.15E-06	1.86	9.51E-05	0.005001
9063	PIAS2	1.95	0.000441	0.002626	1.23	0.23986	0.638306
5290	PIK3CA	2.24	1.89E-06	2.27E-05	1.65	0.002061	0.037797
5293	PIK3CD	2.81	1.21E-08	2.66E-07	1.60	0.00454	0.062265
5294	PIK3CG	5.16	1.46E-12	1.06E-10	1.96	0.0031	0.049477
5295	PIK3R1	2.41	1.71E-09	4.83E-08	1.41	0.006457	0.076798
8503	PIK3R3	1.79	0.000155	0.001073	1.16	0.293415	0.705203
23533	PIK3R5	3.91	7.50E-13	5.93E-11	1.68	0.003025	0.048665
8835	SOCS2	1.90	5.22E-05	0.000418	-1.03	0.863102	1
9021	SOCS3	1.73	0.004227	0.017615	1.13	0.607341	0.909456
9655	SOCS5	1.82	0.00014	0.00098	1.39	0.02991	0.202197
30837	SOCS7	1.91	0.011688	0.040439	1.39	0.132412	0.467962
6655	SOS2	1.58	0.001599	0.007794	1.29	0.053097	0.285225
10252	SPRY1	2.23	4.05E-08	7.65E-07	1.30	0.040648	0.242245
6772	STAT1	1.56	0.012906	0.043866	1.36	0.068442	0.327722
6775	STAT4	3.22	1.17E-07	1.96E-06	1.21	0.233588	0.631481

PDAC: Pancreatic ductal adenocarcinoma; FDR: False Discovery Rate; 44 differentially expressed genes in Strong PDAC vs. Weak PDAC (40 up-regulated, 4 down-regulated); 10 differentially expressed in Moderate PDAC vs. Weak PDAC (8 up-regulated, 2 down-regulated); Differential expression cut off: |Fold Change| >= 1.5, FDR < 0.05

6.2 Supplemental figures

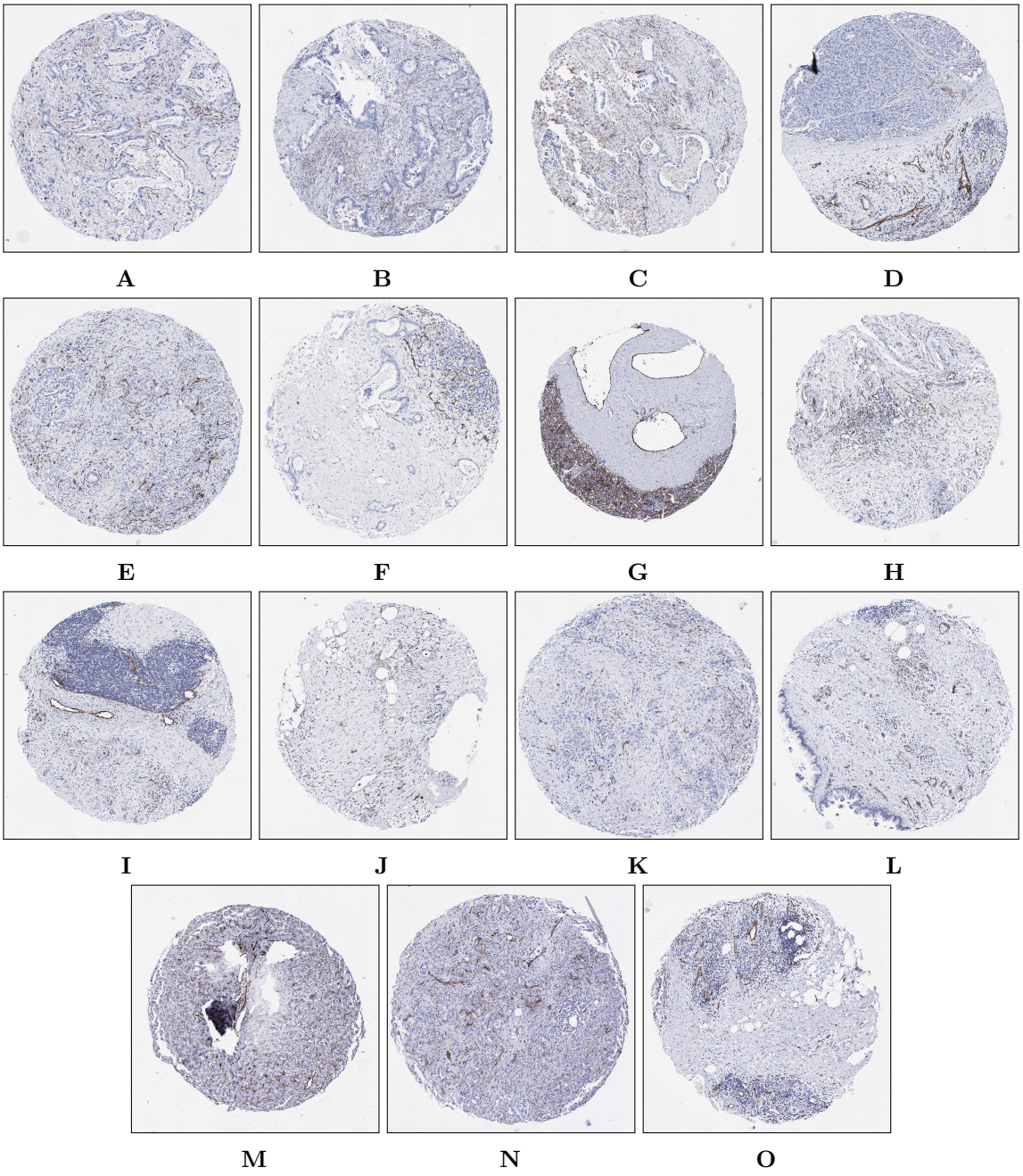

Figure S1: Human PDAC (hPDAC) tissue with strong CD31 (gene: PECAM1) immunoreactivity. (A-O) 28% (15/54) of PDAC tissues had strong CD31 immunoreactivity.

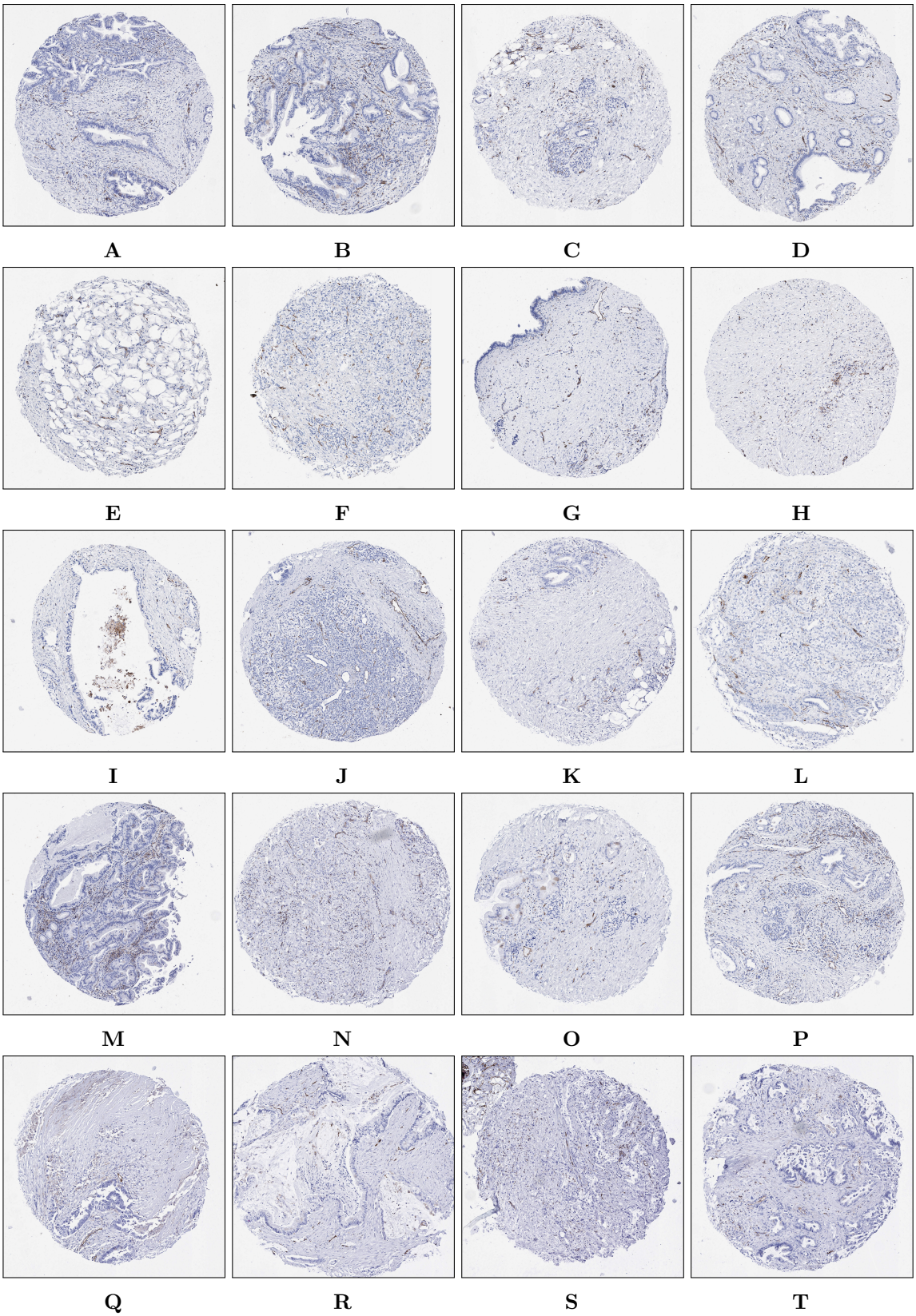

Figure S2: hPDAC tissue with moderate CD31 immunoreactivity. (A-T) 37% (20/54) of PDAC tissues had moderate CD31 immunoreactivity.

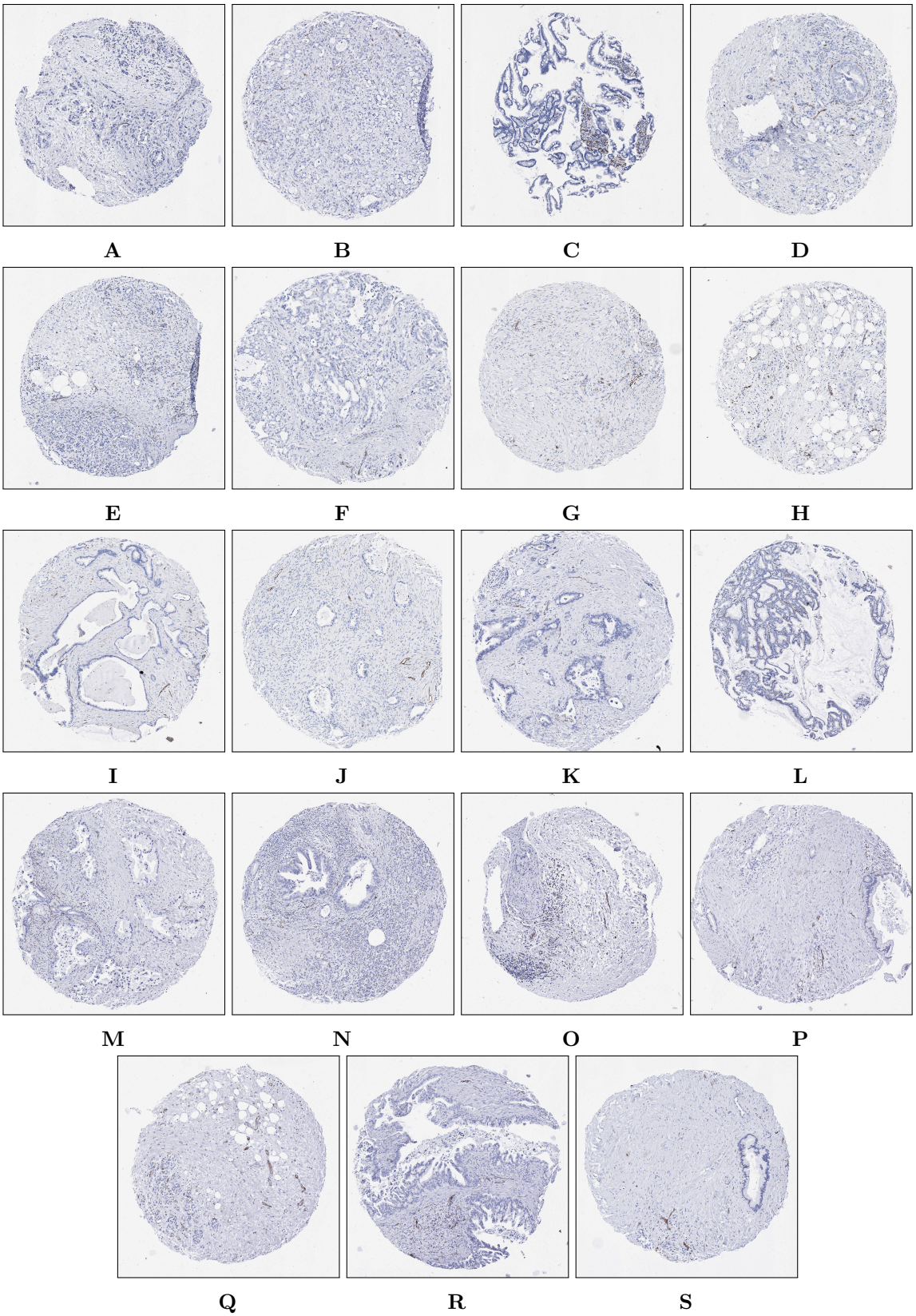

Figure S3: hPDAC tissue with weak CD31 immunoreactivity. (A-S) 35% (19/54) of PDAC tissues had weak CD31 immunoreactivity.

References

[1] Ralph H. Hruban et al. "The Pancreas". In: *Robbins and Cotran Pathologic Basis of Disease*. Ed. by William Schmitt and Rebecca Bruliow. Eighth. Saunders Elsevier, 2010. Chap. The Pancreas.

[2] William E. Fisher et al. "Pancreas". In: *Schwartz's Principles of Surgery*. Ed. by F Brunicardi et al. Tenth. McGraw-Hill Education, 2014. URL: http://accessmedicine.mhmedical.com/content.aspx?bookid=980&Sectionid=59610875.

[3] Barbara Young et al. "Pancreas". In: *Wheater's Functional Histology A Text and Colour Atlas*. Ed. by Inta Ozols and Alison Whitehouse. Fifth. Churchill Livingstone Elsevier, 2006. Chap. Liver and pancreas, pp. 299–301.

[4] Christopher R. Marino and Fred S. Gorelick. "Pancreatic and Salivary Glands". In: *Medical Physiology*. Ed. by Walter F. Boron and Emile L. Boulpaep. Second. Saunders Elsevier, 2009. Chap. Pancreatic and Salivary Glands.

[5] A. L. Mescher and L.C.U. Junqueira. "Pancreas". In: *Junqueira's basic histology: Text and atlas*. Ed. by Michael Weitz and Karen Davis. Twelfth. McGraw Hill Medical, 2010. Chap. Organs Associated with the Digestive Tract, pp. 285–286.

[6] Eugene J. Barrett. "The Endocrine Pancreas". In: *Medical Physiology*. Ed. by Walter F. Boron and Emile L. Boulpaep. Second. Saunders Elsevier, 2009. Chap. The Endocrine Pancreas.

[7] D. Hanahan and J. Folkman. "Patterns and emerging mechanisms of the angiogenic switch during tumorigenesis". In: *Cell* 86.3 (1996), pp. 353–64. URL: http://www.ncbi.nlm.nih.gov/pubmed/8756718.

[8] G. Bergers and L. E. Benjamin. "Tumorigenesis and the angiogenic switch". In: *Nat Rev Cancer* 3.6 (2003), pp. 401–10. DOI: 10.1038/nrc1093. URL: http://www.ncbi.nlm.nih.gov/pubmed/12778130.

[9] H. M. Eilken and R. H. Adams. "Dynamics of endothelial cell behavior in sprouting angiogenesis". In: *Current opinion in cell biology* 22.5 (2010), pp. 617–25. DOI: 10.1016/j.ceb.2010.08.010. URL: http://www.ncbi.nlm.nih.gov/pubmed/20817428.

[10] M. Potente, H. Gerhardt, and P. Carmeliet. "Basic and therapeutic aspects of angiogenesis". In: *Cell* 146.6 (2011), pp. 873–87. DOI: 10.1016/j.cell.2011.08.039. URL: http://www.ncbi.nlm.nih.gov/pubmed/21925313.

[11] A. S. Chung and N. Ferrara. "Developmental and pathological angiogenesis". In: *Annu Rev Cell Dev Biol* 27 (2011), pp. 563–84. DOI: 10.1146/annurev-cellbio-092910-154002. URL: http://www.ncbi.nlm.nih.gov/pubmed/21756109.

[12] D. Hanahan and R. A. Weinberg. "Hallmarks of cancer: the next generation". In: *Cell* 144.5 (2011), pp. 646–74. DOI: 10.1016/j.cell.2011.02.013. URL: http://www.ncbi.nlm.nih.gov/pubmed/21376230.

[13] M. Jeltsch et al. "Receptor tyrosine kinase-mediated angiogenesis". In: *Cold Spring Harb Perspect Biol* 5.9 (2013). DOI: 10.1101/cshperspect.a009183. URL: http://www.ncbi.nlm.nih.gov/pubmed/24003209.

[14] J. Folkman. "Angiogenesis in cancer, vascular, rheumatoid and other disease". In: *Nat Med* 1.1 (1995), pp. 27–31. URL: http://www.ncbi.nlm.nih.gov/pubmed/7584949.

[15] J. Folkman. "Seminars in Medicine of the Beth Israel Hospital, Boston. Clinical applications of research on angiogenesis". In: *The New England journal of medicine* 333.26 (1995), pp. 1757–63. DOI: 10.1056/NEJM199512283332608. URL: http://www.ncbi.nlm.nih.gov/pubmed/7491141.

[16] J. Welti et al. "Recent molecular discoveries in angiogenesis and antiangiogenic therapies in cancer". In: *J Clin Invest* 123.8 (2013), pp. 3190–200. DOI: 10.1172/JCI70212. URL: http://www.ncbi.nlm.nih.gov/pubmed/23908119.

[17] P. Carmeliet and R. K. Jain. "Principles and mechanisms of vessel normalization for cancer and other angiogenic diseases". In: *Nat Rev Drug Discov* 10.6 (2011), pp. 417–27. DOI: 10.1038/nrd3455. URL: http://www.ncbi.nlm.nih.gov/pubmed/21629292.

[18] D. Hanahan and R. A. Weinberg. "The hallmarks of cancer". In: *Cell* 100.1 (2000), pp. 57–70. URL: http://www.ncbi.nlm.nih.gov/pubmed/10647931.

[19] Y. Yang et al. "HIFs, angiogenesis, and cancer". In: *J Cell Biochem* 114.5 (2013), pp. 967–74. DOI: 10.1002/jcb.24438. URL: http://www.ncbi.nlm.nih.gov/pubmed/23225225.

[20] V. Baeriswyl and G. Christofori. "The angiogenic switch in carcinogenesis". In: *Semin Cancer Biol* 19.5 (2009), pp. 329–37. DOI: 10.1016/j.semcancer.2009.05.003. URL: http://www.ncbi.nlm.nih.gov/pubmed/19482086.

[21] P. Saharinen et al. "VEGF and angiopoietin signaling in tumor angiogenesis and metastasis". In: *Trends Mol Med* 17.7 (2011), pp. 347–62. DOI: 10.1016/j.molmed.2011.01.015. URL: http://www.ncbi.nlm.nih.gov/pubmed/21481637.

[22] N. Volkan Adsay, Duangpen Thirabanjasak, and Deniz Altinel. "Pancreatic Cancer". In: *Pancreatic Cancer*. Ed. by Andrew M. Lowy, Steven D. Leach, and Philip A. Philip. M.D. Anderson Solid Tumor Oncology Series. Springer, 2008. Chap. Spectrum of Human Pancreatic Neoplasia, p. 5.

[23] D. P. Ryan, T. S. Hong, and N. Bardeesy. "Pancreatic adenocarcinoma". In: *New England Journal of Medicine* 371.11 (2014), pp. 1039–49. DOI: 10.1056/NEJMra1404198. URL: http://www.ncbi.nlm.nih.gov/pubmed/25207767.

[24] American Cancer Society. "Cancer Facts & Figures". In: Atlanta: American Cancer Society, 2016.

[25] A. Rishi et al. "Pathological and molecular evaluation of pancreatic neoplasms". In: *Seminars in Oncology* 42.1 (2015), pp. 28–39. DOI: 10.1053/j.seminoncol.2014.12.004. URL: http://www.ncbi.nlm.nih.gov/pubmed/25726050.

[26] M. V. Apte et al. "Pancreatic cancer: The microenvironment needs attention too!" In: *Pancreatology* (2015). DOI: 10.1016/j.pan.2015.02.013. URL: http://www.ncbi.nlm.nih.gov/pubmed/25845856.

[27] A. V. Biankin et al. "Pancreatic cancer genomes reveal aberrations in axon guidance pathway genes". In: *Nature* 491.7424 (2012), pp. 399–405. DOI: 10.1038/nature11547. URL: http://www.ncbi.nlm.nih.gov/pubmed/23103869.

[28] N. Waddell et al. "Whole genomes redefine the mutational landscape of pancreatic cancer". In: *Nature* 518.7540 (2015), pp. 495–501. DOI: 10.1038/nature14169. URL: http://www.ncbi.nlm.nih.gov/pubmed/25719666.

[29] The Cancer Genome Atlas Network. *The Cancer Genome Atlas*. Dataset. 2016. URL: http://cancergenome.nih.gov/.

[30] L. Rahib et al. "Projecting cancer incidence and deaths to 2030: the unexpected burden of thyroid, liver, and pancreas cancers in the United States". In: *Cancer Research* 74.11 (2014), pp. 2913–21.

[31] D. P. Ryan, T. S. Hong, and N. Bardeesy. "Pancreatic adenocarcinoma". In: *N Engl J Med* 371.11 (2014), pp. 1039–49. DOI: 10.1056/NEJMra1404198. URL: http://www.ncbi.nlm.nih.gov/pubmed/25207767.

[32] American Cancer Society. "Cancer Facts & Figures". In: Atlanta: American Cancer Society, 2015.

[33] American Cancer Society. "Cancer Facts & Figures". In: Atlanta: American Cancer Society, 2014.

[34] I. Garrido-Laguna and M. Hidalgo. "Pancreatic cancer: from state-of-the-art treatments to promising novel therapies". In: *Nat Rev Clin Oncol* 12.6 (2015), pp. 319–34. DOI: 10.1038/nrclinonc.2015.53. URL: http://www.ncbi.nlm.nih.gov/pubmed/25824606.

[35] K. P. Olive et al. "Inhibition of Hedgehog signaling enhances delivery of chemotherapy in a mouse model of pancreatic cancer". In: *Science* 324.5933 (2009), pp. 1457–61. DOI: 10.1126/science.1171362. URL: http://www.ncbi.nlm.nih.gov/pubmed/19460966.

[36] P. P. Provenzano et al. "Enzymatic targeting of the stroma ablates physical barriers to treatment of pancreatic ductal adenocarcinoma". In: *Cancer Cell* 21.3 (2012), pp. 418–29. DOI: 10.1016/j.ccr.2012.01.007. URL: http://www.ncbi.nlm.nih.gov/pubmed/22439937.

[37] L. Hlatky, P. Hahnfeldt, and J. Folkman. "Clinical application of antiangiogenic therapy: microvessel density, what it does and doesn't tell us". In: *J Natl Cancer Inst* 94.12 (2002), pp. 883–93. URL: http://www.ncbi.nlm.nih.gov/pubmed/12072542.

[38] S. J. Harper and D. O. Bates. "VEGF-A splicing: the key to anti-angiogenic therapeutics?" In: *Nat Rev Cancer* 8.11 (2008), pp. 880–7. DOI: 10.1038/nrc2505. URL: http://www.ncbi.nlm.nih.gov/pubmed/18923433.

[39] S. M. Eswarappa et al. "Programmed translational readthrough generates antiangiogenic VEGF-Ax". In: *Cell* 157.7 (2014), pp. 1605–18. DOI: 10.1016/j.cell.2014.04.033. URL: http://www.ncbi.nlm.nih.gov/pubmed/24949972.

[40] N. Ikeda et al. "Prognostic significance of angiogenesis in human pancreatic cancer". In: *British journal of cancer* 79.9-10 (1999), pp. 1553–63. DOI: 10.1038/sj.bjc.6690248. URL: http://www.ncbi.nlm.nih.gov/pubmed/10188906.

[41] Y. Seo et al. "High expression of vascular endothelial growth factor is associated with liver metastasis and a poor prognosis for patients with ductal pancreatic adenocarcinoma". In: *Cancer* 88.10 (2000), pp. 2239–45. URL: http://www.ncbi.nlm.nih.gov/pubmed/10820344.

[42] J. Itakura et al. "Enhanced expression of vascular endothelial growth factor in human pancreatic cancer correlates with local disease progression". In: *Clin Cancer Res* 3.8 (1997), pp. 1309–16. URL: http://www.ncbi.nlm.nih.gov/pubmed/9815813.

[43] L. M. Ellis et al. "Vessel counts and vascular endothelial growth factor expression in pancreatic adenocarcinoma". In: *Eur J Cancer* 34.3 (1998), pp. 337–40. URL: http://www.ncbi.nlm.nih.gov/pubmed/9640218.

[44] E. Cerami et al. "The cBio cancer genomics portal: an open platform for exploring multidimensional cancer genomics data". In: *Cancer Discov* 2.5 (2012), pp. 401–4. DOI: 10.1158/2159-8290.CD-12-0095. URL: http://www.ncbi.nlm.nih.gov/pubmed/22588877.

[45] J. Gao et al. "Integrative analysis of complex cancer genomics and clinical profiles using the cBioPortal". In: *Sci Signal* 6.269 (2013), pl1. DOI: 10.1126/scisignal.2004088. URL: http://www.ncbi.nlm.nih.gov/pubmed/23550210.

[46] J. Luo et al. "Pancreatic cancer cell-derived vascular endothelial growth factor is biologically active in vitro and enhances tumorigenicity in vivo". In: *International journal of cancer. Journal international du cancer* 92.3 (2001), pp. 361–9. URL: http://www.ncbi.nlm.nih.gov/pubmed/11291072.

[47] H. G. Hotz et al. "Specific targeting of tumor vasculature by diphtheria toxin-vascular endothelial growth factor fusion protein reduces angiogenesis and growth of pancreatic cancer". In: *Journal of gastrointestinal surgery : official journal of the Society for Surgery of the Alimentary Tract* 6.2 (2002), 159–66, discussion 166. URL: http://www.ncbi.nlm.nih.gov/pubmed/11992800.

[48] T. Hoshida et al. "Gene therapy for pancreatic cancer using an adenovirus vector encoding soluble flt-1 vascular endothelial growth factor receptor". In: *Pancreas* 25.2 (2002), pp. 111–21. URL: http://www.ncbi.nlm.nih.gov/pubmed/12142732.

[49] T. Ogawa et al. "Anti-tumor angiogenesis therapy using soluble receptors: enhanced inhibition of tumor growth when soluble fibroblast growth factor receptor-1 is used with soluble vascular endothelial growth factor receptor". In: *Cancer gene therapy* 9.8 (2002), pp. 633–40. DOI: 10.1038/sj.cgt.7700478. URL: http://www.ncbi.nlm.nih.gov/pubmed/12136423.

[50] C. C. Solorzano et al. "Inhibition of growth and metastasis of human pancreatic cancer growing in nude mice by PTK 787/ZK222584, an inhibitor of the vascular endothelial growth factor receptor tyrosine kinases". In: *Cancer Biother Radiopharm* 16.5 (2001), pp. 359–70. DOI: 10.1089/108497801753354267. URL: http://www.ncbi.nlm.nih.gov/pubmed/11776753.

[51] M. Fukasawa and M. Korc. "Vascular endothelial growth factor-trap suppresses tumorigenicity of multiple pancreatic cancer cell lines". In: *Clin Cancer Res* 10.10 (2004), pp. 3327–32. DOI: 10.1158/1078-0432.CCR-03-0820. URL: http://www.ncbi.nlm.nih.gov/pubmed/15161686.

[52] H. L. Kindler et al. "Phase II trial of bevacizumab plus gemcitabine in patients with advanced pancreatic cancer". In: *J Clin Oncol* 23.31 (2005), pp. 8033–40. DOI: 10.1200/JCO.2005.01.9661. URL: http://www.ncbi.nlm.nih.gov/pubmed/16258101.

[53] 3rd Burris H. A. et al. "Improvements in survival and clinical benefit with gemcitabine as first-line therapy for patients with advanced pancreas cancer: a randomized trial". In: *J Clin Oncol* 15.6 (1997), pp. 2403–13. URL: http://www.ncbi.nlm.nih.gov/pubmed/9196156.

[54] A. H. Ko et al. "A phase II study evaluating bevacizumab in combination with fixed-dose rate gemcitabine and low-dose cisplatin for metastatic pancreatic cancer: is an anti-VEGF strategy still applicable?" In: *Investigational new drugs* 26.5 (2008), pp. 463–71. DOI: 10.1007/s10637-008-9127-2. URL: http://www.ncbi.nlm.nih.gov/pubmed/18379729.

[55] M. Javle et al. "Bevacizumab combined with gemcitabine and capecitabine for advanced pancreatic cancer: a phase II study". In: *British journal of cancer* 100.12 (2009), pp. 1842–5. DOI: 10.1038/sj.bjc.6605099. URL: http://www.ncbi.nlm.nih.gov/pubmed/19491904.

[56] C. H. Crane et al. "Phase II study of bevacizumab with concurrent capecitabine and radiation followed by maintenance gemcitabine and bevacizumab for locally advanced pancreatic cancer: Radiation Therapy Oncology Group RTOG 0411". In: *J Clin Oncol* 27.25 (2009), pp. 4096–102. DOI: 10.1200/JCO.2009.21.8529. URL: http://www.ncbi.nlm.nih.gov/pubmed/19636002.

[57] D. Fogelman et al. "Bevacizumab plus gemcitabine and oxaliplatin as first-line therapy for metastatic or locally advanced pancreatic cancer: a phase II trial". In: *Cancer Chemother Pharmacol* 68.6 (2011), pp. 1431–8. DOI: 10.1007/s00280-011-1601-4. URL: http://www.ncbi.nlm.nih.gov/pubmed/21479635.

[58] Jr. Small W. et al. "Phase II trial of full-dose gemcitabine and bevacizumab in combination with attenuated three-dimensional conformal radiotherapy in patients with localized pancreatic cancer". In: *International journal of radiation oncology, biology, physics* 80.2 (2011), pp. 476–82. DOI: 10.1016/j.ijrobp.2010.02.030. URL: http://www.ncbi.nlm.nih.gov/pubmed/20598452.

[59] 2nd Van Buren G. et al. "Phase II study of induction fixed-dose rate gemcitabine and bevacizumab followed by 30 Gy radiotherapy as preoperative treatment for potentially resectable pancreatic adenocarcinoma". In: *Ann Surg Oncol* 20.12 (2013), pp. 3787–93. DOI: 10.1245/s10434-013-3161-9. URL: http://www.ncbi.nlm.nih.gov/pubmed/23904005.

[60] I. A. Astsaturov et al. “Phase II and coagulation cascade biomarker study of bevacizumab with or without docetaxel in patients with previously treated metastatic pancreatic adenocarcinoma”. In: *Am J Clin Oncol* 34.1 (2011), pp. 70–5. DOI: 10.1097/COC.0b013e3181d2734a. URL: http://www.ncbi.nlm.nih.gov/pubmed/20458210.

[61] H. L. Kindler et al. “Gemcitabine plus bevacizumab compared with gemcitabine plus placebo in patients with advanced pancreatic cancer: phase III trial of the Cancer and Leukemia Group B (CALGB 80303)”. In: *J Clin Oncol* 28.22 (2010), pp. 3617–22. DOI: 10.1200/JCO.2010.28.1386. URL: http://www.ncbi.nlm.nih.gov/pubmed/20606091.

[62] H. Q. Xiong and J. L. Abbruzzese. “Epidermal growth factor receptor-targeted therapy for pancreatic cancer”. In: *Semin Oncol* 29.5 Suppl 14 (2002), pp. 31–7. DOI: 10.1053/sonc.2002.35645. URL: http://www.ncbi.nlm.nih.gov/pubmed/12422311.

[63] K. Tobita et al. “Epidermal growth factor receptor expression in human pancreatic cancer: Significance for liver metastasis”. In: *International journal of molecular medicine* 11.3 (2003), pp. 305–9. URL: http://www.ncbi.nlm.nih.gov/pubmed/12579331.

[64] C. Papageorgio and M. C. Perry. “Epidermal growth factor receptor-targeted therapy for pancreatic cancer”. In: *Cancer Invest* 25.7 (2007), pp. 647–57. DOI: 10.1080/07357900701522653. URL: http://www.ncbi.nlm.nih.gov/pubmed/18027154.

[65] R. Longo et al. “Pancreatic cancer: from molecular signature to target therapy”. In: *Crit Rev Oncol Hematol* 68.3 (2008), pp. 197–211. DOI: 10.1016/j.critrevonc.2008.03.003. URL: http://www.ncbi.nlm.nih.gov/pubmed/18436450.

[66] P. A. Philip et al. “Phase III study comparing gemcitabine plus cetuximab versus gemcitabine in patients with advanced pancreatic adenocarcinoma: Southwest Oncology Group-directed intergroup trial S0205”. In: *J Clin Oncol* 28.22 (2010), pp. 3605–10. DOI: 10.1200/JCO.2009.25.7550. URL: http://www.ncbi.nlm.nih.gov/pubmed/20606093.

[67] M. J. Moore et al. “Erlotinib plus gemcitabine compared with gemcitabine alone in patients with advanced pancreatic cancer: a phase III trial of the National Cancer Institute of Canada Clinical Trials Group”. In: *J Clin Oncol* 25.15 (2007), pp. 1960–6. DOI: 10.1200/JCO.2006.07.9525. URL: http://www.ncbi.nlm.nih.gov/pubmed/17452677.

[68] J. P. Spano et al. "Efficacy of gemcitabine plus axitinib compared with gemcitabine alone in patients with advanced pancreatic cancer: an open-label randomised phase II study". In: *Lancet* 371.9630 (2008), pp. 2101–8. DOI: 10.1016/S0140-6736(08)60661-3. URL: http://www.ncbi.nlm.nih.gov/pubmed/18514303.

[69] E. M. O'Reilly et al. "A Cancer and Leukemia Group B phase II study of sunitinib malate in patients with previously treated metastatic pancreatic adenocarcinoma (CALGB 80603)". In: *Oncologist* 15.12 (2010), pp. 1310–9. DOI: 10.1634/theoncologist.2010-0152. URL: http://www.ncbi.nlm.nih.gov/pubmed/21148613.

[70] M. Reni et al. "Maintenance sunitinib or observation in metastatic pancreatic adenocarcinoma: a phase II randomised trial". In: *Eur J Cancer* 49.17 (2013), pp. 3609–15. DOI: 10.1016/j.ejca.2013.06.041. URL: http://www.ncbi.nlm.nih.gov/pubmed/23899530.

[71] A. B. El-Khoueiry et al. "A randomized phase II of gemcitabine and sorafenib versus sorafenib alone in patients with metastatic pancreatic cancer". In: *Investigational new drugs* 30.3 (2012), pp. 1175–83. DOI: 10.1007/s10637-011-9658-9. URL: http://www.ncbi.nlm.nih.gov/pubmed/21424698.

[72] H. L. Kindler et al. "Gemcitabine plus sorafenib in patients with advanced pancreatic cancer: a phase II trial of the University of Chicago Phase II Consortium". In: *Investigational new drugs* 30.1 (2012), pp. 382–6. DOI: 10.1007/s10637-010-9526-z. URL: http://www.ncbi.nlm.nih.gov/pubmed/20803052.

[73] S. Cascinu et al. "Sorafenib does not improve efficacy of chemotherapy in advanced pancreatic cancer: A GISCAD randomized phase II study". In: *Digestive and liver disease : official journal of the Italian Society of Gastroenterology and the Italian Association for the Study of the Liver* 46.2 (2014), pp. 182–6. DOI: 10.1016/j.dld.2013.09.020. URL: http://www.ncbi.nlm.nih.gov/pubmed/24189171.

[74] T. Dragovich et al. "Phase II trial of vatalanib in patients with advanced or metastatic pancreatic adenocarcinoma after first-line gemcitabine therapy (PCRT O4-001)". In: *Cancer Chemother Pharmacol* 74.2 (2014), pp. 379–87. DOI: 10.1007/s00280-014-2499-4. URL: http://www.ncbi.nlm.nih.gov/pubmed/24939212.

[75] E. Van Cutsem et al. "Phase III trial of bevacizumab in combination with gemcitabine and erlotinib in patients with metastatic pancreatic cancer". In: *J Clin Oncol* 27.13 (2009), pp. 2231–7. DOI: 10.1200/JCO.2008.20.0238. URL: http://www.ncbi.nlm.nih.gov/pubmed/19307500.

[76] H. L. Kindler et al. "Axitinib plus gemcitabine versus placebo plus gemcitabine in patients with advanced pancreatic adenocarcinoma: a double-blind randomised phase 3 study". In: *The lancet oncology* 12.3 (2011), pp. 256–62. DOI: 10.1016/S1470-2045(11)70004-3. URL: http://www.ncbi.nlm.nih.gov/pubmed/21306953.

[77] A. Goncalves et al. "BAYPAN study: a double-blind phase III randomized trial comparing gemcitabine plus sorafenib and gemcitabine plus placebo in patients with advanced pancreatic cancer". In: *Annals of oncology : official journal of the European Society for Medical Oncology / ESMO* 23.11 (2012), pp. 2799–805. DOI: 10.1093/annonc/mds135. URL: http://www.ncbi.nlm.nih.gov/pubmed/22771827.

[78] P. Rougier et al. "Randomised, placebo-controlled, double-blind, parallel-group phase III study evaluating aflibercept in patients receiving first-line treatment with gemcitabine for metastatic pancreatic cancer". In: *Eur J Cancer* 49.12 (2013), pp. 2633–42. DOI: 10.1016/j.ejca.2013.04.002. URL: http://www.ncbi.nlm.nih.gov/pubmed/23642329.

[79] H. Yamaue et al. "Randomized phase II/III clinical trial of elpamotide for patients with advanced pancreatic cancer: PEGASUS-PC Study". In: *Cancer Sci* 106.7 (2015), pp. 883–90. DOI: 10.1111/cas.12674. URL: http://www.ncbi.nlm.nih.gov/pubmed/25867139.

[80] C. J. Bruns et al. "Epidermal growth factor receptor blockade with C225 plus gemcitabine results in regression of human pancreatic carcinoma growing orthotopically in nude mice by antiangiogenic mechanisms". In: *Clin Cancer Res* 6.5 (2000), pp. 1936–48. URL: http://www.ncbi.nlm.nih.gov/pubmed/10815919.

[81] M. Korc. "Pathways for aberrant angiogenesis in pancreatic cancer". In: *Molecular cancer* 2 (2003), p. 8. URL: http://www.ncbi.nlm.nih.gov/pubmed/12556241.

[82] J. R. Tonra et al. "Synergistic antitumor effects of combined epidermal growth factor receptor and vascular endothelial growth factor receptor-2 targeted therapy". In: *Clin Cancer Res* 12.7 Pt 1 (2006), pp. 2197–207. DOI: 10.1158/1078-0432.CCR-05-1682. URL: http://www.ncbi.nlm.nih.gov/pubmed/16609035.

[83] A. H. Ko et al. "A phase II study of bevacizumab plus erlotinib for gemcitabine-refractory metastatic pancreatic cancer". In: *Cancer Chemother Pharmacol* 66.6 (2010), pp. 1051–7. DOI: 10.1007/s00280-010-1257-5. URL: http://www.ncbi.nlm.nih.gov/pubmed/20130876.

[84] A. H. Ko et al. "A phase II randomized study of cetuximab and bevacizumab alone or in combination with gemcitabine as first-line therapy for metastatic pancreatic adenocarcinoma". In: *Investigational new drugs* 30.4 (2012), pp. 1597–606. DOI: 10.1007/s10637-011-9691-8. URL: http://www.ncbi.nlm.nih.gov/pubmed/21629990.

[85] D. J. Watkins et al. "The combination of a chemotherapy doublet (gemcitabine and capecitabine) with a biological doublet (bevacizumab and erlotinib) in patients with advanced pancreatic adenocarcinoma. The results of a phase I/II study". In: *Eur J Cancer* 50.8 (2014), pp. 1422–9. DOI: 10.1016/j.ejca.2014.02.003. URL: http://www.ncbi.nlm.nih.gov/pubmed/24613126.

[86] D. B. Cardin et al. "Phase II trial of sorafenib and erlotinib in advanced pancreatic cancer". In: *Cancer Med* 3.3 (2014), pp. 572–9. DOI: 10.1002/cam4.208. URL: http://www.ncbi.nlm.nih.gov/pubmed/24574334.

[87] S. Wada et al. "Rationale for antiangiogenic cancer therapy with vaccination using epitope peptides derived from human vascular endothelial growth factor receptor 2". In: *Cancer Research* 65.11 (2005), pp. 4939–46. DOI: 10.1158/0008-5472.CAN-04-3759. URL: http://www.ncbi.nlm.nih.gov/pubmed/15930316.

[88] J. A. Chan and M. H. Kulke. "Medical Management of Pancreatic Neuroendocrine Tumors: Current and Future Therapy". In: *Surg Oncol Clin N Am* 25.2 (2016), pp. 423–37. DOI: 10.1016/j.soc.2015.11.009. URL: http://www.ncbi.nlm.nih.gov/pubmed/27013373.

[89] A. Chiruvella and D. A. Kooby. "Surgical Management of Pancreatic Neuroendocrine Tumors". In: *Surg Oncol Clin N Am* 25.2 (2016), pp. 401–21. DOI: 10.1016/j.soc.2015.12.002. URL: http://www.ncbi.nlm.nih.gov/pubmed/27013372.

[90] E. A. Collisson et al. "Subtypes of pancreatic ductal adenocarcinoma and their differing responses to therapy". In: *Nature Medicine* 17.4 (2011), pp. 500–3. DOI: 10.1038/nm.2344. URL: http://www.ncbi.nlm.nih.gov/pubmed/21460848.

[91] P. Bailey et al. "Genomic analyses identify molecular subtypes of pancreatic cancer". In: *Nature* (2016). DOI: 10.1038/nature16965. URL: http://www.ncbi.nlm.nih.gov/pubmed/26909576.

[92] V.J. Carey. "Machine Learning Concepts and Tools for Statistical Genomics". In: *Bioinformatics and Computational Biology Solutions Using R and Bioconductor*. Ed. by Robert Gentleman et al. Statistics for Biology and Health. Springer, 2005. Chap. Machine Learning Concepts and Tools for Statistical Genomics.

[93] Inaki Inza et al. “Machine Learning: An Indispensable Tool in Bioinformatics”. In: *Bioinformatics Methods in Clinical Research*. Ed. by Rune Matthiesen. Methods in Molecular Biology. Humana Press, 2010. Chap. Machine Learning: An Indispensable Tool in Bioinformatics.

[94] C. M. Perou et al. “Molecular portraits of human breast tumours”. In: *Nature* 406.6797 (2000), pp. 747–52. DOI: 10.1038/35021093. URL: http://www.ncbi.nlm.nih.gov/pubmed/10963602.

[95] T. Sorlie et al. “Gene expression patterns of breast carcinomas distinguish tumor subclasses with clinical implications”. In: *Proc Natl Acad Sci U S A* 98.19 (2001), pp. 10869–74. DOI: 10.1073/pnas.191367098. URL: http://www.ncbi.nlm.nih.gov/pubmed/11553815.

[96] R. G. Verhaak et al. “Integrated genomic analysis identifies clinically relevant subtypes of glioblastoma characterized by abnormalities in PDGFRA, IDH1, EGFR, and NF1”. In: *Cancer Cell* 17.1 (2010), pp. 98–110. DOI: 10.1016/j.ccr.2009.12.020. URL: http://www.ncbi.nlm.nih.gov/pubmed/20129251.

[97] The Cancer Genome Atlas Research Network. “Integrated genomic analyses of ovarian carcinoma”. In: *Nature* 474.7353 (2011), pp. 609–15. DOI: 10.1038/nature10166. URL: http://www.ncbi.nlm.nih.gov/pubmed/21720365.

[98] The Cancer Genome Atlas Research Network. “Comprehensive molecular portraits of human breast tumours”. In: *Nature* 490.7418 (2012), pp. 61–70. DOI: 10.1038/nature11412. URL: http://www.ncbi.nlm.nih.gov/pubmed/23000897.

[99] V. G. Tusher, R. Tibshirani, and G. Chu. “Significance analysis of microarrays applied to the ionizing radiation response”. In: *Proc Natl Acad Sci U S A* 98.9 (2001), pp. 5116–21. DOI: 10.1073/pnas.091062498. URL: http://www.ncbi.nlm.nih.gov/pubmed/11309499.

[100] A. W. Lowe et al. “Gene expression patterns in pancreatic tumors, cells and tissues”. In: *PLoS One* 2.3 (2007), e323. DOI: 10.1371/journal.pone.0000323. URL: http://www.ncbi.nlm.nih.gov/pubmed/17389914.

[101] S. Anders and W. Huber. “Differential expression analysis for sequence count data”. In: *Genome biology* 11.10 (2010), R106. DOI: 10.1186/gb-2010-11-10-r106. URL: http://www.ncbi.nlm.nih.gov/pubmed/20979621.

[102] D. Warde-Farley et al. “The GeneMANIA prediction server: biological network integration for gene prioritization and predicting gene function”. In: *Nucleic Acids Res* 38.Web Server issue (2010), W214–20. DOI: 10.1093/nar/gkq537. URL: http://www.ncbi.nlm.nih.gov/pubmed/20576703.

[103] W. G. Purschke et al. "Identification and characterization of a mirror-image oligonucleotide that binds and neutralizes sphingosine 1-phosphate, a central mediator of angiogenesis". In: *Biochem J* 462.1 (2014), pp. 153–62. DOI: 10.1042/BJ20131422. URL: http://www.ncbi.nlm.nih.gov/pubmed/24832383.

[104] M. Mori et al. "Promotion of cell spreading and migration by vascular endothelial-protein tyrosine phosphatase (VE-PTP) in cooperation with integrins". In: *J Cell Physiol* 224.1 (2010), pp. 195–204. DOI: 10.1002/jcp.22122. URL: http://www.ncbi.nlm.nih.gov/pubmed/20301196.

[105] S. Jones et al. "Core signaling pathways in human pancreatic cancers revealed by global genomic analyses". In: *Science* 321.5897 (2008), pp. 1801–6. DOI: 10.1126/science.1164368. URL: http://www.ncbi.nlm.nih.gov/pubmed/18772397.

[106] A. K. Witkiewicz et al. "Whole-exome sequencing of pancreatic cancer defines genetic diversity and therapeutic targets". In: *Nat Commun* 6 (2015), p. 6744. DOI: 10.1038/ncomms7744. URL: http://www.ncbi.nlm.nih.gov/pubmed/25855536.

[107] S. A. Hahn et al. "DPC4, a candidate tumor suppressor gene at human chromosome 18q21.1". In: *Science* 271.5247 (1996), pp. 350–3. URL: http://www.ncbi.nlm.nih.gov/pubmed/8553070.

[108] M. Schutte et al. "DPC4 gene in various tumor types". In: *Cancer Res* 56.11 (1996), pp. 2527–30. URL: http://www.ncbi.nlm.nih.gov/pubmed/8653691.

[109] R. E. Wilentz et al. "Immunohistochemical labeling for dpc4 mirrors genetic status in pancreatic adenocarcinomas : a new marker of DPC4 inactivation". In: *Am J Pathol* 156.1 (2000), pp. 37–43. DOI: 10.1016/S0002-9440(10)64703-7. URL: http://www.ncbi.nlm.nih.gov/pubmed/10623651.

[110] M. Schutte et al. "Abrogation of the Rb/p16 tumor-suppressive pathway in virtually all pancreatic carcinomas". In: *Cancer Research* 57.15 (1997), pp. 3126–30. URL: http://www.ncbi.nlm.nih.gov/pubmed/9242437.

[111] C. Greenman et al. "Patterns of somatic mutation in human cancer genomes". In: *Nature* 446.7132 (2007), pp. 153–8. DOI: 10.1038/nature05610. URL: http://www.ncbi.nlm.nih.gov/pubmed/17344846.

[112] M. S. Lawrence et al. "Mutational heterogeneity in cancer and the search for new cancer-associated genes". In: *Nature* 499.7457 (2013), pp. 214–8. DOI: 10.1038/nature12213. URL: http://www.ncbi.nlm.nih.gov/pubmed/23770567.

[113] H. M. Genau et al. "CUL3-KBTBD6/KBTBD7 ubiquitin ligase cooperates with GABARAP proteins to spatially restrict TIAM1-RAC1 signaling". In: *Molecular Cell* 57.6 (2015), pp. 995–1010. DOI: 10.1016/j.molcel.2014.12.040. URL: http://www.ncbi.nlm.nih.gov/pubmed/25684205.

[114] A. J. Gore et al. "Pancreatic cancer-associated retinoblastoma 1 dysfunction enables TGF-beta to promote proliferation". In: *J Clin Invest* 124.1 (2014), pp. 338–52. DOI: 10.1172/JCI71526. URL: http://www.ncbi.nlm.nih.gov/pubmed/24334458.

[115] M. Lieber et al. "Establishment of a continuous tumor-cell line (panc-1) from a human carcinoma of the exocrine pancreas". In: *Int J Cancer* 15.5 (1975), pp. 741–7. URL: http://www.ncbi.nlm.nih.gov/pubmed/1140870.

[116] A. Quintas-Cardama et al. "Preclinical characterization of the selective JAK1/2 inhibitor INCB018424: therapeutic implications for the treatment of myeloproliferative neoplasms". In: *Blood* 115.15 (2010), pp. 3109–17. DOI: 10.1182/blood-2009-04-214957. URL: http://www.ncbi.nlm.nih.gov/pubmed/20130243.

[117] C. Carriere et al. "Deletion of Rb accelerates pancreatic carcinogenesis by oncogenic Kras and impairs senescence in premalignant lesions". In: *Gastroenterology* 141.3 (2011), pp. 1091–101. DOI: 10.1053/j.gastro.2011.05.041. URL: http://www.ncbi.nlm.nih.gov/pubmed/21699781.

[118] Y. Matsuo et al. "K-Ras promotes angiogenesis mediated by immortalized human pancreatic epithelial cells through mitogen-activated protein kinase signaling pathways". In: *Mol Cancer Res* 7.6 (2009), pp. 799–808. DOI: 10.1158/1541-7786.MCR-08-0577. URL: http://www.ncbi.nlm.nih.gov/pubmed/19509115.

[119] S. R. Hingorani et al. "Trp53R172H and KrasG12D cooperate to promote chromosomal instability and widely metastatic pancreatic ductal adenocarcinoma in mice". In: *Cancer Cell* 7.5 (2005), pp. 469–83. DOI: 10.1016/j.ccr.2005.04.023. URL: http://www.ncbi.nlm.nih.gov/pubmed/15894267.

[120] J. P. Morton et al. "Mutant p53 drives metastasis and overcomes growth arrest/senescence in pancreatic cancer". In: *Proceedings of the National Academy of Sciences of the United States of America* 107.1 (2010), pp. 246–51. DOI: 10.1073/pnas.0908428107. URL: http://www.ncbi.nlm.nih.gov/pubmed/20018721.

[121] K. A. O'Connell and M. Edidin. "A mouse lymphoid endothelial cell line immortalized by simian virus 40 binds lymphocytes and retains functional characteristics of normal endothelial cells". In: *J Immunol* 144.2 (1990), pp. 521–5. URL: http://www.ncbi.nlm.nih.gov/pubmed/2153170.

[122] J. Gore et al. "TCGA data and patient-derived orthotopic xenografts highlight pancreatic cancer-associated angiogenesis". In: *Oncotarget* 6.10 (2015), pp. 7504–21. URL: http://www.ncbi.nlm.nih.gov/pubmed/25762644.

[123] J. Bromberg and Jr. Darnell J. E. "The role of STATs in transcriptional control and their impact on cellular function". In: *Oncogene* 19.21 (2000), pp. 2468–73. DOI: 10.1038/sj.onc.1203476. URL: http://www.ncbi.nlm.nih.gov/pubmed/10851045.

[124] H. Yu and R. Jove. "The STATs of cancer–new molecular targets come of age". In: *Nat Rev Cancer* 4.2 (2004), pp. 97–105. DOI: 10.1038/nrc1275. URL: http://www.ncbi.nlm.nih.gov/pubmed/14964307.

[125] J. E. Jung et al. "STAT3 is a potential modulator of HIF-1-mediated VEGF expression in human renal carcinoma cells". In: *FASEB J* 19.10 (2005), pp. 1296–8. DOI: 10.1096/fj.04-3099fje. URL: http://www.ncbi.nlm.nih.gov/pubmed/15919761.

[126] H. Yu, M. Kortylewski, and D. Pardoll. "Crosstalk between cancer and immune cells: role of STAT3 in the tumour microenvironment". In: *Nat Rev Immunol* 7.1 (2007), pp. 41–51. DOI: 10.1038/nri1995. URL: http://www.ncbi.nlm.nih.gov/pubmed/17186030.

[127] J. R. Westphal, D. J. Ruiter, and R. M. De Waal. "Anti-angiogenic treatment of human cancer: pitfalls and promises". In: *International Journal of Cancer* 86.6 (2000), pp. 870–3. URL: http://www.ncbi.nlm.nih.gov/pubmed/10842203.

[128] C. Whipple and M. Korc. "Targeting angiogenesis in pancreatic cancer: rationale and pitfalls". In: *Langenbecks Arch Surg* 393.6 (2008), pp. 901–10. DOI: 10.1007/s00423-008-0280-z. URL: http://www.ncbi.nlm.nih.gov/pubmed/18210149.

[129] A. Eberhard et al. "Heterogeneity of angiogenesis and blood vessel maturation in human tumors: implications for antiangiogenic tumor therapies". In: *Cancer Res* 60.5 (2000), pp. 1388–93. URL: http://www.ncbi.nlm.nih.gov/pubmed/10728704.

[130] D. Greenbaum et al. "Comparing protein abundance and mRNA expression levels on a genomic scale". In: *Genome Biol* 4.9 (2003), p. 117. DOI: 10.1186/gb-2003-4-9-117. URL: http://www.ncbi.nlm.nih.gov/pubmed/12952525.

[131] D. Ansari et al. "The role of quantitative mass spectrometry in the discovery of pancreatic cancer biomarkers for translational science". In: *J Transl Med* 12 (2014), p. 87. DOI: 10.1186/1479-5876-12-87. URL: http://www.ncbi.nlm.nih.gov/pubmed/24708694.

[132] D. Britton et al. "Quantification of pancreatic cancer proteome and phosphorylome: indicates molecular events likely contributing to cancer and activity of drug targets". In: *PLoS One* 9.3 (2014), e90948. DOI: 10.1371/journal.pone.0090948. URL: http://www.ncbi.nlm.nih.gov/pubmed/24670416.

[133] J. K. Thomas et al. "Pancreatic Cancer Database: an integrative resource for pancreatic cancer". In: *Cancer Biol Ther* 15.8 (2014), pp. 963–7. DOI: 10.4161/cbt.29188. URL: http://www.ncbi.nlm.nih.gov/pubmed/24839966.

[134] L. Zanotti et al. "Diagnostic tests based on gene expression profile in breast cancer: from background to clinical use". In: *Tumour Biol* 35.9 (2014), pp. 8461–70. DOI: 10.1007/s13277-014-2366-2. URL: http://www.ncbi.nlm.nih.gov/pubmed/25048969.

[135] L. N. Harris et al. "Use of Biomarkers to Guide Decisions on Adjuvant Systemic Therapy for Women With Early-Stage Invasive Breast Cancer: American Society of Clinical Oncology Clinical Practice Guideline". In: *J Clin Oncol* 34.10 (2016), pp. 1134–50. DOI: 10.1200/JCO.2015.65.2289. URL: http://www.ncbi.nlm.nih.gov/pubmed/26858339.

[136] J. Y. Scoazec. "Angiogenesis in neuroendocrine tumors: therapeutic applications". In: *Neuroendocrinology* 97.1 (2013), pp. 45–56. DOI: 10.1159/000338371. URL: http://www.ncbi.nlm.nih.gov/pubmed/22538258.

[137] Y. Jiao et al. "DAXX/ATRX, MEN1, and mTOR pathway genes are frequently altered in pancreatic neuroendocrine tumors". In: *Science* 331.6021 (2011), pp. 1199–203. DOI: 10.1126/science.1200609. URL: http://www.ncbi.nlm.nih.gov/pubmed/21252315.

[138] A. M. Schmitt et al. "Islet 1 (Isl1) expression is a reliable marker for pancreatic endocrine tumors and their metastases". In: *Am J Surg Pathol* 32.3 (2008), pp. 420–5. DOI: 10.1097/PAS.0b013e318158a397. URL: http://www.ncbi.nlm.nih.gov/pubmed/18300808.

[139] J. L. Kopp et al. "Identification of Sox9-dependent acinar-to-ductal reprogramming as the principal mechanism for initiation of pancreatic ductal adenocarcinoma". In: *Cancer Cell* 22.6 (2012), pp. 737–50. DOI: 10.1016/j.ccr.2012.10.025. URL: http://www.ncbi.nlm.nih.gov/pubmed/23201164.

[140] B. Leitner et al. "Formation and sequence analysis of secretoneurin, a neuropeptide derived from secretogranin II, in mammalian, bird, reptile, amphibian and fish brains". In: *Neurosci Lett* 248.2 (1998), pp. 105–8. URL: http://www.ncbi.nlm.nih.gov/pubmed/9654353.

[141] R. Kirchmair et al. "The neuropeptide secretoneurin acts as a direct angiogenic cytokine in vitro and in vivo". In: *Circulation* 109.6 (2004), pp. 777–83. DOI: 10.1161/01.CIR.0000112574.07422.C1. URL: http://www.ncbi.nlm.nih.gov/pubmed/14970115.

[142] F. Liu et al. "DUSP1 is a novel target for enhancing pancreatic cancer cell sensitivity to gemcitabine". In: *PLoS One* 9.1 (2014), e84982. DOI: 10.1371/journal.pone.0084982. URL: http://www.ncbi.nlm.nih.gov/pubmed/24409315.

[143] J. B. Regard et al. "Verge: a novel vascular early response gene". In: *J Neurosci* 24.16 (2004), pp. 4092–103. DOI: 10.1523/JNEUROSCI.4252-03.2004. URL: http://www.ncbi.nlm.nih.gov/pubmed/15102925.

[144] K. Watanabe et al. "Growth factor induction of Cripto-1 shedding by glycosylphosphatidylinositol-phospholipase D and enhancement of endothelial cell migration". In: *Journal of Biological Chemistry* 282.43 (2007), pp. 31643–55. DOI: 10.1074/jbc.M702713200. URL: http://www.ncbi.nlm.nih.gov/pubmed/17720976.

[145] J. S. Esser et al. "Fibroblast growth factor signaling pathway in endothelial cells is activated by BMPER to promote angiogenesis". In: *Arterioscler Thromb Vasc Biol* 35.2 (2015), pp. 358–67. DOI: 10.1161/ATVBAHA.114.304345. URL: http://www.ncbi.nlm.nih.gov/pubmed/25503991.

[146] P. Dufourcq et al. "FrzA, a secreted frizzled related protein, induced angiogenic response". In: *Circulation* 106.24 (2002), pp. 3097–103. URL: http://www.ncbi.nlm.nih.gov/pubmed/12473558.

[147] A. Bottos et al. "The synaptic proteins neurexins and neuroligins are widely expressed in the vascular system and contribute to its functions". In: *Proc Natl Acad Sci U S A* 106.49 (2009), pp. 20782–7. DOI: 10.1073/pnas.0809510106. URL: http://www.ncbi.nlm.nih.gov/pubmed/19926856.

[148] A. Rissone et al. "The synaptic proteins beta-neurexin and neuroligin synergize with extracellular matrix-binding vascular endothelial growth factor a during zebrafish vascular development". In: *Arterioscler Thromb Vasc Biol* 32.7 (2012), pp. 1563–72. DOI: 10.1161/ATVBAHA.111.243006. URL: http://www.ncbi.nlm.nih.gov/pubmed/22516065.

[149] S. Graziano et al. "A peptide from the extracellular region of the synaptic protein alpha Neurexin stimulates angiogenesis and the vascular specific tyrosine kinase Tie2". In: *Biochem Biophys Res Commun* 432.4 (2013), pp. 574–9. DOI: 10.1016/j.bbrc.2013.02.045. URL: http://www.ncbi.nlm.nih.gov/pubmed/23485462.

[150] V. M. Bedell et al. "roundabout4 is essential for angiogenesis in vivo". In: *Proc Natl Acad Sci U S A* 102.18 (2005), pp. 6373–8. DOI: 10.1073/pnas.0408318102. URL: http://www.ncbi.nlm.nih.gov/pubmed/15849270.

[151] A. Eichmann, T. Makinen, and K. Alitalo. "Neural guidance molecules regulate vascular remodeling and vessel navigation". In: *Genes Dev* 19.9 (2005), pp. 1013–21. DOI: 10.1101/gad.1305405. URL: http://www.ncbi.nlm.nih.gov/pubmed/15879551.

[152] B. Naimi et al. “Down-regulation of (IIIb) and (IIIc) isoforms of fibroblast growth factor receptor 2 (FGFR2) is associated with malignant progression in human prostate”. In: *Prostate* 52.3 (2002), pp. 245–52. DOI: 10.1002/pros.10104. URL: http://www.ncbi.nlm.nih.gov/pubmed/12111699.

[153] B. A. Foster et al. “Enforced expression of FGF-7 promotes epithelial hyperplasia whereas a dominant negative FGFR2iiib promotes the emergence of neuroendocrine phenotype in prostate glands of transgenic mice”. In: *Differentiation* 70.9-10 (2002), pp. 624–32. DOI: 10.1046/j.1432-0436.2002.700915.x. URL: http://www.ncbi.nlm.nih.gov/pubmed/12492503.

[154] C. D. Hu, R. Choo, and J. Huang. “Neuroendocrine differentiation in prostate cancer: a mechanism of radioresistance and treatment failure”. In: *Front Oncol* 5 (2015), p. 90. DOI: 10.3389/fonc.2015.00090. URL: http://www.ncbi.nlm.nih.gov/pubmed/25927031.

[155] C. J. Avraamides, B. Garmy-Susini, and J. A. Varner. “Integrins in angiogenesis and lymphangiogenesis”. In: *Nat Rev Cancer* 8.8 (2008), pp. 604–17. DOI: 10.1038/nrc2353. URL: http://www.ncbi.nlm.nih.gov/pubmed/18497750.

[156] P. Foubert and J. A. Varner. “Integrins in tumor angiogenesis and lymphangiogenesis”. In: *Methods in Molecular Biology* 757 (2012), pp. 471–86. DOI: 10.1007/978-1-61779-166-6_27. URL: http://www.ncbi.nlm.nih.gov/pubmed/21909928.

[157] M. Vallon and M. Essler. “Proteolytically processed soluble tumor endothelial marker (TEM) 5 mediates endothelial cell survival during angiogenesis by linking integrin alpha(v)beta3 to glycosaminoglycans”. In: *J Biol Chem* 281.45 (2006), pp. 34179–88. DOI: 10.1074/jbc.M605291200. URL: http://www.ncbi.nlm.nih.gov/pubmed/16982628.

[158] M. J. Truty and R. Urrutia. “Basics of TGF-beta and pancreatic cancer”. In: *Pancreatology* 7.5-6 (2007), pp. 423–35. DOI: 10.1159/000108959. URL: http://www.ncbi.nlm.nih.gov/pubmed/17898532.

[159] C. Neuzillet et al. “Targeting the TGFbeta pathway for cancer therapy”. In: *Pharmacol Ther* 147 (2015), pp. 22–31. DOI: 10.1016/j.pharmthera.2014.11.001. URL: http://www.ncbi.nlm.nih.gov/pubmed/25444759.

[160] K. Mittal, J. Ebos, and B. Rini. “Angiogenesis and the tumor microenvironment: vascular endothelial growth factor and beyond”. In: *Semin Oncol* 41.2 (2014), pp. 235–51. DOI: 10.1053/j.seminoncol.2014.02.007. URL: http://www.ncbi.nlm.nih.gov/pubmed/24787295.

[161] B. Li and C. N. Dewey. "RSEM: accurate transcript quantification from RNA-Seq data with or without a reference genome". In: *BMC bioinformatics* 12 (2011), p. 323. DOI: 10.1186/1471-2105-12-323. URL: http://www.ncbi.nlm.nih.gov/pubmed/21816040.

[162] M. Ashburner et al. "Gene ontology: tool for the unification of biology. The Gene Ontology Consortium". In: *Nat Genet* 25.1 (2000), pp. 25–9. DOI: 10.1038/75556. URL: http://www.ncbi.nlm.nih.gov/pubmed/10802651.

[163] S. Durinck et al. "BioMart and Bioconductor: a powerful link between biological databases and microarray data analysis". In: *Bioinformatics* 21.16 (2005), pp. 3439–40. DOI: 10.1093/bioinformatics/bti525. URL: http://www.ncbi.nlm.nih.gov/pubmed/16082012.

[164] S. Durinck et al. "Mapping identifiers for the integration of genomic datasets with the R/Bioconductor package biomaRt". In: *Nat Protoc* 4.8 (2009), pp. 1184–91. DOI: 10.1038/nprot.2009.97. URL: http://www.ncbi.nlm.nih.gov/pubmed/19617889.

[165] R. C. Gentleman et al. "Bioconductor: open software development for computational biology and bioinformatics". In: *Genome biology* 5.10 (2004), R80. DOI: 10.1186/gb-2004-5-10-r80. URL: http://www.ncbi.nlm.nih.gov/pubmed/15461798.

[166] M. Reimers and V. J. Carey. "Bioconductor: an open source framework for bioinformatics and computational biology". In: *Methods in enzymology* 411 (2006), pp. 119–34. DOI: 10.1016/S0076-6879(06)11008-3. URL: http://www.ncbi.nlm.nih.gov/pubmed/16939789.

[167] Broad Institute TCGA Genome Data Analysis Center. "SNP6 Copy number analysis (GISTIC2)". In: *Broad Institute of MIT and Harvard* (2015). DOI: 10.7908/C18S4P1Q.

[168] C. H. Mermel et al. "GISTIC2.0 facilitates sensitive and confident localization of the targets of focal somatic copy-number alteration in human cancers". In: *Genome biology* 12.4 (2011), R41. DOI: 10.1186/gb-2011-12-4-r41. URL: http://www.ncbi.nlm.nih.gov/pubmed/21527027.

[169] A. Subramanian et al. "Gene set enrichment analysis: a knowledge-based approach for interpreting genome-wide expression profiles". In: *Proc Natl Acad Sci U S A* 102.43 (2005), pp. 15545–50. DOI: 10.1073/pnas.0506580102. URL: http://www.ncbi.nlm.nih.gov/pubmed/16199517.

[170] V. K. Mootha et al. “PGC-1alpha-responsive genes involved in oxidative phosphorylation are coordinately downregulated in human diabetes”. In: *Nature Genetics* 34.3 (2003), pp. 267–73. DOI: 10.1038/ng1180. URL: http://www.ncbi.nlm.nih.gov/pubmed/12808457.

[171] G. Plasari et al. “Nuclear factor I-C links platelet-derived growth factor and transforming growth factor beta1 signaling to skin wound healing progression”. In: *Mol Cell Biol* 29.22 (2009), pp. 6006–17. DOI: 10.1128/MCB.01921-08. URL: http://www.ncbi.nlm.nih.gov/pubmed/19752192.

[172] A. Heine et al. “The JAK-inhibitor ruxolitinib impairs dendritic cell function in vitro and in vivo”. In: *Blood* 122.7 (2013), pp. 1192–202. DOI: 10.1182/blood-2013-03-484642. URL: http://www.ncbi.nlm.nih.gov/pubmed/23770777.

[173] P. Tsirigotis et al. “Treatment of Experimental Candida Sepsis with a Janus Kinase Inhibitor Controls Inflammation and Prolongs Survival”. In: *Antimicrob Agents Chemother* 59.12 (2015), pp. 7367–73. DOI: 10.1128/AAC.01533-15. URL: http://www.ncbi.nlm.nih.gov/pubmed/26369979.

[174] Y. Benjamini and Y. Hochberg. “Controlling the False Discovery Rate - a Practical and Powerful Approach to Multiple Testing”. In: *Journal of the Royal Statistical Society Series B-Methodological* 57.1 (1995), pp. 289–300. URL: %3CGo%20to%20ISI%3E://A1995QE45300017.

[175] W. Huang da, B. T. Sherman, and R. A. Lempicki. “Systematic and integrative analysis of large gene lists using DAVID bioinformatics resources”. In: *Nat Protoc* 4.1 (2009), pp. 44–57. DOI: 10.1038/nprot.2008.211. URL: http://www.ncbi.nlm.nih.gov/pubmed/19131956.

[176] W. Huang da, B. T. Sherman, and R. A. Lempicki. “Bioinformatics enrichment tools: paths toward the comprehensive functional analysis of large gene lists”. In: *Nucleic Acids Res* 37.1 (2009), pp. 1–13. DOI: 10.1093/nar/gkn923. URL: http://www.ncbi.nlm.nih.gov/pubmed/19033363.

[177] D. Neupane and M. Korc. “14-3-3sigma Modulates pancreatic cancer cell survival and invasiveness”. In: *Clinical Cancer Research* 14.23 (2008), pp. 7614–23. DOI: 10.1158/1078-0432.CCR-08-1366. URL: http://www.ncbi.nlm.nih.gov/pubmed/19047086.

[178] R. B. Corcoran et al. “STAT3 plays a critical role in KRAS-induced pancreatic tumorigenesis”. In: *Cancer Research* 71.14 (2011), pp. 5020–9. DOI: 10.1158/0008-5472.CAN-11-0908. URL: http://www.ncbi.nlm.nih.gov/pubmed/21586612.

CURRICULUM VITAE

Kelly E. Craven

Education

Indiana University, Indianapolis, IN — Aug 2010 – May 2018
- MD
- PhD in Biochemistry & Molecular Biology
- Minor in Cancer Biology
- Certificate in the Business of Life Sciences

Indiana University, Bloomington, IN — Aug 2001 – May 2005
- BS in Biology with High Distinction
- BS in Computer Science with High Distinction
- Minors: Mathematics, Chemistry

Employment

Indiana University School of Medicine, Indianapolis, IN
- PhD Student, Department of Biochemistry & Molecular Biology — Jan 2013 – Jun 2016
  - Advisor: Murray Korc, MD
- Graduate Rotation Student, Department of Medical & Molecular Genetics — Oct 2012 – Dec 2012
  - Advisor: Bryan P. Schneider, MD
- Graduate Rotation Student, Department of Biochemistry & Molecular Biology — Jul 2012 – Sep 2012
  - Advisor: Murray Korc, MD
- Graduate Rotation Student, Department of Biochemistry & Molecular Biology — Jun 2012 – Jul 2012
  - Advisor: Harikrishna Nakshatri, BVSc, PhD

University of Texas MD Anderson Cancer Center – Department of Leukemia, Houston, TX
- Medical Student Researcher — May 2011 – Aug 2011
  - Advisor: Michael Andreeff, MD, PhD

Eli Lilly & Company – Lilly Research Laboratories R&D IT – Discovery Informatics, Indianapolis, IN
- Senior Analyst — Mar 2008 – Jul 2010
- Analyst — Jun 2005 – Mar 2008

Publications

- Gore, J., Imasuen-Williams, I.E., Conteh, A.M., **Craven K.E.**, Cheng, M., & Korc, M. (2016) Combined targeting of TGF-beta, EGFR and HER2 suppresses lymphangiogenesis and metastasis in a pancreatic cancer model. Cancer Letters, 379(1), 143-153.

- **Craven, K.E.**, Gore, J., & Korc, M. (2016). Overview of pre-clinical and clinical studies targeting angiogenesis in pancreatic ductal adenocarcinoma. Cancer Letters.

- **Craven, K. E.**, Gore, J., Wilson, J. L., & Korc, M. (2016). Angiogenic gene signature in human pancreatic cancer correlates with TGF-beta and inflammatory transcriptomes. Oncotarget, 7(1), 323-341.

- Palam, L. R., Gore, J., **Craven, K. E.**, Wilson, J. L., & Korc, M. (2015). Integrated stress response is critical for gemcitabine resistance in pancreatic ductal adenocarcinoma. Cell Death Dis, 6, e1913.

- Burnett, R. M., **Craven, K. E.**, Krishnamurthy, P., Goswami, C. P., Badve, S., Crooks, P., Mathews, W. P., Bhat-Nakshatri, P., & Nakshatri, H. (2015). Organ-specific adaptive signaling pathway activation in metastatic breast cancer cells. Oncotarget, 6(14), 12682-12696.

- Gore, J., **Craven, K. E.**, Wilson, J. L., Cote, G. A., Cheng, M., Nguyen, H. V., Cramer, H. M., Sherman, S., & Korc, M. (2015). TCGA data and patient-derived orthotopic xenografts highlight pancreatic cancer-associated angiogenesis. Oncotarget, 6(10), 7504-7521.

- Gore, A. J., Deitz, S. L., Palam, L. R., **Craven, K. E.**, & Korc, M. (2014). Pancreatic cancer-associated retinoblastoma 1 dysfunction enables TGF-beta to promote proliferation. Journal of Clinical Investigation, 124(1), 338-352.

- Li, S., Zhang, H. Y., Hu, C. C., Lawrence, F., **Gallagher, K. E.**, Surapaneni, A., Estrem, S. T., Calley, J. N., Varga, G., Dow, E. R., & Chen, Y. (2008). Assessment of diet-induced obese rats as an obesity model by comparative functional genomics. Obesity (Silver Spring), 16(4), 811-818.

Academic and Professional Honors

- Extramural Funding
  - Ruth L. Kirschstein National Research Service Award Individual Predoctoral MD/PhD Fellowship (F30) — Jul 2015 – Jul 2019
  - Indiana University Medical Scientist Training Program — Jan 2012 – May 2018

- Indiana University Melvin and Bren Simon Cancer Center
  - Travel Award — Mar 2016
  - Cancer Biology Training Program — Aug 2013 – Jul 2014

- Indiana University–Purdue University Indianapolis
  - Graduate Office Travel Fellowship Award — Mar 2016
  - Graduate – Professional Educational Travel Grant — Mar 2015

- American Association for Cancer Research
  - Woman in Cancer Research Scholar Award — Feb 2016
  - Associate Member Council-led Program Committee Member — Apr 2015 – Apr 2016

- Eli Lilly & Company
  - Global Lilly IT Solution Achievement Award — 2010
  - Regional Lilly IT Solution Achievement Award — 2008
  - Lilly Research Laboratories President's Award — 2006

Conference Presentations

- **Craven, K.E.**, Gore, J., Wilson, J.L., Korc, M. (2016) An angiogenesis gene signature points to active TGF-beta/JAK signaling pathways in a subset of human pancreatic ductal adenocarcinoma cancer patients that are distinct from pathways in pancreatic neuroendocrine tumors. **Abstract for poster presentation**, American Association for Cancer Research, New Orleans, LA.

- Gore, J., **Craven, K.E.**, Wilson, J.L., Korc, M. (2015) Angiogenic Signature Points to JAK/STAT and TGF-beta as Therapeutic Targets in Pancreatic Cancer. **Abstract**, American Pancreatic Association, San Diego, CA.

- **Craven, K.E.**, Gore, J., Wilson, J.L., Korc, M. (2015) Tackling Anti-Angiogenic Therapy Failure in Pancreatic Ductal Adenocarcinoma. **Abstract for poster presentation**, National MD/PhD Student Conference, Keystone, CO.

- Gore, J., **Craven, K.E.**, Wilson, J.L., Korc, M. (2015) TGF-beta promotes angiogenesis in an RB-deficient, Kras-driven mouse model of pancreatic cancer. **Abstract**, American Association for Cancer Research, Philadelphia, PA.

- **Craven, K.E.**, Gore, J., Wilson, J.L., Korc, M. (2015) Tackling Anti-Angiogenic Therapy Failure in Pancreatic Ductal Adenocarcinoma. **Abstract for poster presentation**, American Physician Scientists Association, Chicago, IL.

- Ruvolo PP, Ruvolo VR, Zeng Z, Qui Y, Zhou L, **Gallagher KE**, Konopleva M, Kornblau SM, Andreeff M. (2011) The PP2A Subunit B55α Suppresses Survival Signaling in Acute Myeloid Leukemia Cells. **Abstract**, American Society of Hematology Annual Meeting and Exposition, San Diego, CA.

- Webster Y, **Gallagher KE**, McAhren S. (2009) Google Maps for Innovation. **Abstract for poster presentation**, Lilly Scientific Expo, Indianapolis, IN.

- **Gallagher KE**, McAhren S, Lin Y, Kumar A, Dow ER. (2007) Expression Pipeline. **Abstract for poster presentation**, Lilly Scientific Expo, Indianapolis, IN.

Professional Society Memberships

- American Physician Scientists Association
- American Society of Clinical Oncology
- American Society for Clinical Pathology
- American Association for Cancer Research
- American College of Physicians
- Phi Beta Kappa

Bench Skills

Cell culture (2D and 3D), DNA, RNA, and protein isolation, immunoblotting, immunohistochemistry, immunoprecipitation, qPCR, PCR, cloning, site-directed mutagenesis, CRISPR, shRNA, siRNA, reporter assays (invasion, migration, clonogenic, luciferase), flow cytometry, transfection/transduction

Technical Skills

Languages: R, Perl, JavaScript, C#/C++/C, Java, Shell Scripting, XML/HTML (CSS), SQL
Databases: Oracle, MySQL
Tools: RStudio, Partek, TIBCO Spotfire, Pipeline Pilot, Emacs, Visual Studio, Eclipse, GitHub, CVS, SVN
Operating Systems: Windows, Linux/Unix